Distribution Agreement

In presenting this thesis or dissertation as a partial fulfillment of the requirements for an advanced degree from Emory University, I hereby grant to Emory University and its agents the non-exclusive license to archive, make accessible, and display my thesis or dissertation in whole or in part in all forms of media, now or hereafter known, including display on the world wide web. I understand that I may select some access restrictions as part of the online submission of this thesis or dissertation. I retain all ownership rights to the copyright of the thesis or dissertation. I also retain the right to use in future works (such as articles or books) all or part of this thesis or dissertation.

Signature:

_____ _____

Justin Edward Pye Date

Glass Transition and Physical Aging Behavior of Thin Free-Standing and Supported Polystyrene Films

By

Justin Edward Pye
Doctor of Philosophy

Physics

_____
Connie B. Roth
Advisor

_____
David Bucknall
Committee Member

_____
Fereydoon Family
Committee Member

_____
Sergei Urazhdin
Committee Member

_____
Eric Weeks
Committee Member

Accepted:

_____
Lisa A. Tedesco, Ph.D.
Dean of the James T. Laney School of Graduate Studies

_____
Date

Glass Transition and Physical Aging Behavior of Thin Free-Standing and Supported Polystyrene Films

By

Justin Edward Pye
B.Sc., Carnegie Mellon University, 2008

Advisor: Connie B. Roth, PhD

An abstract of
A dissertation submitted to the Faculty of the
James T. Laney School of Graduate Studies of Emory University
in partial fulfillment of the requirements for the degree of
Doctor of Philosophy
in Physics
2014

Abstract

Glass Transition and Physical Aging Behavior of
Thin Free-Standing and Supported Polystyrene Films
By Justin Edward Pye

In this dissertation, I have explored the glass transition and physical aging of thin and ultrathin polystyrene (PS) films held in both the supported and free-standing state with ellipsometry. We measured the physical aging rate of supported PS films as a function of aging temperature and film thickness, find a reduced aging rate for the ultrathin films at all aging temperatures. These results have shown that the enhanced mobility at the free surface known to be responsible for glass transition temperature (T_g) reductions in supported and free-standing films also causes reductions in the physical aging rate for supported films. The distance from the surface at which dynamics are perturbed from bulk values grows as the temperature is reduced.

We also measured the T_g of ultrathin high molecular weight (MW) free-standing PS films and report the first observation of two T_gs in ultrathin high MW free-standing films. We believe these two T_gs are caused by two different but simultaneous mechanisms of T_g reduction. The lower transition is MW dependent and has previously been observed, while the upper transition is MW independent, has not been seen before in these films, and matches the T_g reduction previously measured in low MW free-standing films. Physical aging measurements on films held between the two transitions demonstrate that the upper transition is an actual glass transition. Additionally, by measuring the thermal expansion of these films above, below, and between the two transitions, we find that the majority of the film (~90%) solidifies at the upper transition while only ~10% of the film remains mobile until freezing out at the second transition.

In addition to these free surface based confinement effects, the physical aging rate of thin (500 nm thick) free-standing PS films can be reduced by nearly a factor of two when the stress applied during the quench is reduced. This stress is due to the thermal expansion mismatch between the film and the frame. Finally, the background, theory, and data needed to perform a complete thermoviscoelastic calculation of this stress is described and shown to be a significantly non-trivial task.

Glass Transition and Physical Aging Behavior of Thin Free-Standing and Supported Polystyrene Films

By

Justin Edward Pye
B.Sc., Carnegie Mellon University, 2008

Advisor: Connie B. Roth, PhD

A dissertation submitted to the Faculty of the
James T. Laney School of Graduate Studies of Emory University
in partial fulfillment of the requirements for the degree of
Doctor of Philosophy
in Physics
2014

Acknowledgements

The support and help I have received the past several years on the road to my PhD has been instrumental in my continuance and success. There is far more than I can cover with the thanks it deserves within this acknowledgement section, but I will try my best.

It is without saying that none of this would have happened were it not for my phenomenal advisor, Connie Roth. From taking me in as a research assistant before I knew where I was going, to helping me realize that wherever it was I was going to go, getting a PhD is part of that plan, you have provided me all the support I could hope for in the pursuit of this PhD. Nearly every conversation we had resulted with me coming away wiser than before in physics, in science, in writing, in presenting, in academia, in career planning. The room may have been empty when I arrived, but I am immensely grateful to have been involved in the building of the great Roth Polymer Physics Lab! I am especially thankful for the tireless work you put in these past several months on dissertation edits and flexibility that Ethan demanded.

My committee members, David Bucknall, Eric Weeks, Fereydoon Family, and Sergei Urazhdin, all get a big thank you for working with me to get everything done to graduate, and that it is done to a high standard. With the miracle of getting five professors to agree to meet on the first date and time I proposed getting dashed by the miracle of my son coming two weeks early, I thank you for being flexible and supportive of my attempt to graduate and take care of a Ethan at the same time.

Most of the work in this dissertation would also not have been possible without the help of the machine shop staff, Cody Anderson and Horace Dale. You took our design for the free-standing heater and turned it into reality and were willing to help me

at a moment's notice with whatever weird widget I needed to make. Additional thanks go out to Jon Carr and Josh Savory for assistance with building the heater controllers and to Josh for all the other random problems and electrical demons you helped solve.

The physics department staff has always been of the highest quality and I am sure my time at Emory would not have been quite as smooth if it were not for their help. Connie Copeland, Paulette Evans, and Calvin Jackson made sure all the details were taken care of and I'm sure have saved me from many catastrophes with their excellent administration abilities. I thank Jason Boss and Art Kleyman for keeping the computers going despite my best efforts to turn them into a mess.

The time I have spent with all of the various members of the Roth lab will be remembered well. A great amount of perspective was gained and time saved from discussions with Laura Gray about what's important (or not) in life and research. Much to the chagrin of anyone at the bar with us, I have immensely enjoyed being able to have serious research conversations with Roman Baglay at any time of night or state of inebriation. I hope I was a good influence on the undergraduates (Kate, Andy, Daniel, Katy, Phil, etc.) I mentored in full or limited capacity along the way.

The friends I have found along the way will always be remembered, even if our paths only crossed for a short time. I learned a great many things and had a great time at trivia (mostly from Trent Brunson and Nafees Kahn), adult trivia (thanks to Meghan Kohne, Roman Baglay, Wesley Robertson, and his crew), and (including things we may not have wanted to learn) playing Cards Against Humanity with everyone. I should also call out Kazem Edmond for his contagious enthusiasm for science and technology, Laura Gray for being a great friend from nearly the beginning and keeping me grounded,

Roman Baglay and Meghan Kohne for keeping me young, Neil Anthony and Adonis Bovell for getting me to join and eventually run the Young Emory Physicists group, and everyone else (Jakub, Carla, Ken, Andy, …) that I had such a great time with.

My parents were a vital part of what got me to this point. You have always supported me in my studies and encouraged my scientific interests. Mom, you and the Shaw clan have given me the greatest accomplishment of humanity, the ability to stand up for others that can't stand up for themselves and to fight for human rights. Dad, your advice on work, life, and career is always excellent, even if it takes me far too long to follow it. Sean, I may not have been the best older brother growing up, but I now always enjoy our time together. I will try to get myself back into shape to keep up with you in whatever is our next family vacation adventure, never give up your great active outdoor life. To grow up in such an encouraging and loving family has probably been one of the greatest influences on the person I am today.

To my wife, Jessica. I don't think anything I can write here would do justice to how much you mean to me. To say that we have grown up together is the least that can be said about how I have improved by having you as my partner in life. You have helped me along a path to success, awoken the work ethic and determination within me, kept me light hearted and smiling, and of course giving me the greatest gift one could ever give. To have a baby while you were pursuing a PhD yourself and I was chained to my desk to finish my own is an triumph beyond compare. Ethan, you are a lot of work, but provide joy that is unmatched in my life. Your smile (the only resemblance to me yet :D) is the happiest thing in the world.

To everyone I have met along the way, thank you.

Table of Contents

List of Figures

List of Tables

Chapter 1
Introduction

1.1 Polymer Basics

This dissertation is about the properties of thin films of glassy polymers, as measured by ellipsometry. As such, I will give brief backgrounds on polymers, glasses, confinement, and ellipsometry in this chapter, starting with polymers in this section. Polymers have been produced synthetically for nearly a century and comprise a large part of the global manufacturing economy.[1] Natural polymers, though not identified as polymers until much later, have been in use for millennia in paper and practically all of human civilization counting the cellulose and lignin in wood.[2]

A polymer is a long chain molecule comprised of many smaller, repeated units called monomers. Polymers typically contain thousands of repeat units and molecular weights (MW) reaching millions of g/mol. The average length of the chain can be more than a micron long, but is typically coiled up such that its size is best described by the radius of gyration R_g that can reach tens of nanometers. These huge length and size scales, molecularly speaking, lead to many interesting and unique properties of polymers including strong viscoelasticity, and complex solution and blend phase behavior. An even more vast array of behaviors can be obtained if modifications are made to the structure of the polymer (branches, stars, brushes, etc.), various repeat units are combined in a single chain as copolymers (two or more blocks, random, graft, etc. copolymers), or more complex monomers are used (polyelectrolytes, semiconducting polymers, liquid

crystal polymers, etc.).[1] For this dissertation, we will stick with simple, linear polystyrene chains.

The long chain aspect of polymers gives them one of the most significant features of polymer behavior: their strong viscoelastic response. A material is viscoelastic when it behaves like a solid on one time scale and like a liquid on another.[3] This occurs when the material contains a relaxation time similar to the relevant experimental time scale. When a material is deformed for a time much less than its relaxation time, all of the deformation is elastically stored and the energy of deformation can be recovered. When the deformation time is longer that the relaxation time, the material relaxes the stress due to the deformation such that the deformation energy is converted to internal heat energy.

A high MW polymer melt has several regimes of relaxation leading to a rather complex viscoelastic response to deformations as sketched in Figure 1.1. At short time scales, elastic behavior is encountered before the individual segments of the chain begin to relax among their neighbors with relaxation time τ_{seg}. As the individual segments and longer sections of the chain begin to relax, some of the deformation is relaxed and some energy is dissipated. For chain sections of moderate size, the motion can be described by Brownian diffusion of beads connected by springs in the Rouse model. The segmental and Rouse mode relaxations are apparent in the large decrease of modulus that occurs in Figure 1.1 after the segmental relaxation time τ_{seg}. However, entanglements with the other chains in the melt soon restrict overall chain motion at times longer than τ_e, like a giant snake not being able to "diffuse" through a forest due to the trees blocking its path. τ_e is the time corresponding to the Rouse mode of the average length of chain found between entanglements.

The network of entanglements impinging on a single chain defines a "tube" that it must escape before large scale motion occurs. To escape the tube, reptation occurs in which the chain moves forward and backward along the length of the tube, creating a new tube as it goes, until none of the original tube is left at τ_{rep}, defined as the reptation time. For times between τ_e and τ_{rep}, the response of the material to deformations is primarily due to stretching of the chain sections between the entanglements. This stretching is an elastic response that leads to the large region of elastic-like behavior between τ_e and τ_{rep} often called the rubbery plateau where the modulus is almost constant in time and most of the deformation energy is stored rather than dissipated. The release of the initial constraints on the chain at τ_{rep} allows the chains to finally flow large distances, giving viscous behavior. As would be expected, this process is very slow and the time it takes to escape the tube, the reptation time τ_{rep}, controls the viscosity and increases with the molecular weight to the 3.4 power.[4]

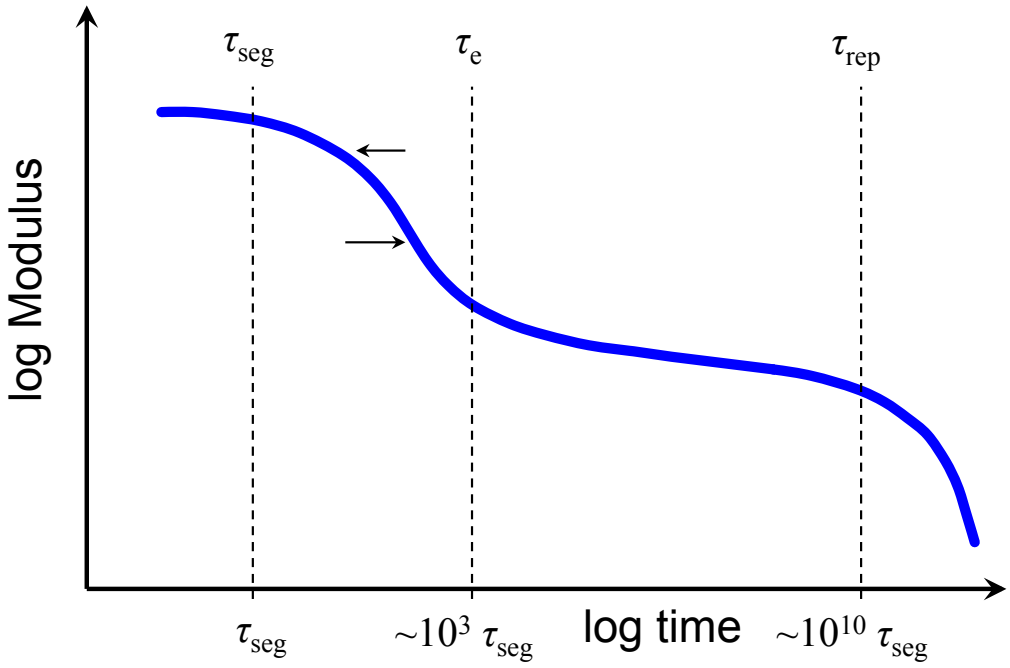

Figure 1.1: Construction of log modulus *vs*. log time master curve. Each of the partial curves represents data taken at a different temperature with the uppermost curve collected at the lowest temperature and the lowermost curve collected at the highest temperature. To build the master curve, curves are shifted horizontally along the log time axis until they are all superimposed. The reptation time τ_{rep} depends on the MW of the polymer and is illustrated here for a relatively large MW of order 1,000 kg/mol.

The complete span of time scales from the segmental relaxation time to the reptation time can reach 12 or more orders of magnitude for high MW polymers.[4] The time a polymer spends in the elastic regime between the time entanglements are first felt, τ_e, and the reptation time, τ_{rep}, can also extend across more than five orders of magnitude in time. This expansive rubbery plateau is part of the reason polymers make up the vast majority of confinement measurements. Thin polymer films on non-attractive substrates or held free-standing are in a metastable state, allowing annealing and glass transition temperature measurements to take place before dewetting can occur.

The time dependence of polymer behavior is very strongly temperature dependent. From the very short segmental relaxation times, or at temperatures below the glass

transition temperature described below, to the rubbery plateau, the modulus decreases by more than three orders of magnitude. This very strong dependence of the modulus on time and temperature, further discussed below, underlines the importance of considering the time and temperature scales of an experiment or application. In many polymer systems a change in temperature has been found to be equivalent to a change in experimental time-scale such that if two experimental measurements are performed at different temperatures and plotted on a log time scale as in Figure 1.1, then a simple shift along the log time axis will overlap the data. This behavior and procedure is referred to as time-temperature superposition (tTS). Experimentally, this is extraordinarily useful such that a plot like Figure 1.1 that covers more than 10 orders of magnitude in time, far larger than the range of any technique, can be gathered simply by collecting data at different temperatures and then building a master curve by shifting the timescales until all of the data overlap.

The remarkable ability to apply this tTS scaling and build such master curves is called thermorheological simplicity, and is based on all relaxation times having the same temperature dependence.[3] In the typical calculations used in the Rouse and reptation models alluded to above, all of the relaxations can be thought of as hierarchical by including a single friction factor for the movement of short sections of the chains. Thus, thermorheological simplicity is satisfied since there is only one parameter that depends on temperature. This description makes a fairly strong statement that dynamics separated by ~10 orders of magnitude in time are controlled by the same underlying temperature dependence. It was found already in 1965 by Plazek that even in polystyrene the temperature dependence of the viscosity was different from the recoverable viscoelastic

temperature dependence.[5] Thus, while tTS is quite useful, its blanket application should be cautioned against, particularly when the terminal flow and glassy behavior are compared.

1.2 Glass Transition

1.2.1 Fundamentals of the Glass Transition

When a material is cooled down faster than it can crystallize or its structure is too irregular, as most polymers are, its dynamics continue to slow down until at some point segmental dynamics are arrested and it becomes a solid, regardless of whether the molecules are in the most energetically favorable arrangement. This solid is a glass, comprising an important class of materials both practically and theoretically. Amazingly, the solidification occurs without any obvious change in structure such that the molecular structure in the glass is nearly indistinguishable from the structure in the liquid state.

Even though it is not yet clear if the glass transition (T_g) is a true phase transition,[6–8] it is similar in appearance to a second order transition. T_g is commonly measured by observing a change in slope of volume V or enthalpy H as a function of temperature. T_g is also apparent in the derivatives as a (somewhat broad) step change in the thermal expansion α or heat capacity C_p as sketched in Figure 1.2. T_g occurs when the molecular rearrangements required to reach equilibrium become slower than the rate at which the temperature is being changed. This means that T_g is cooling rate dependent. Although experimentally T_g manifests as a non-equilibrium, rate dependent transition, it is not yet clear whether there is an underlying thermodynamic ideal glass transition that could be reached with an infinitely slow cooling rate.[6–8] Below T_g, the system is in a

non-equilibrium state and has many of the interesting properties that one expects to see in non-equilibrium systems such as memory effects and aging (discussed below).

Furthermore, there is no single well-accepted theoretical framework to explain both the properties of materials in the glassy state and that of materials between the glass transition temperature (T_g) and (real or theoretical) crystallization temperature, called the supercooled region.[9] The change in dynamics as a system approaches the glass transition from above is also quite remarkable. Over a relatively small temperature range, the viscosity increases smoothly up to 10^{12} Pa s, compared to the viscosity of water at 10^{-3} Pa s. Near T_g the dynamics are so sensitive to temperature that a change of only a few degrees can change the time scale and viscosity by an order of magnitude.[10] These dramatic changes in dynamics are sometimes explained in terms of a cooperative process by which several units (segments, molecules, colloids, etc.) must move in a cooperative fashion for any significant motion to occur.[11] The degree of cooperativity is often described with the size or number of units in a cooperative rearrangement. This cooperative motion also leads to the proposal of another striking feature of glassy dynamics. Dynamic heterogeneity is the idea that the dynamics in a material near T_g is heterogeneous in both space and time.[12] In the view of dynamic heterogeneity, one region of a sample may relax faster than average during one time period, but be equal to or slower than average during another time period. This behavior is directly observed in simulations[13] and supercooled colloidal systems[11,14] but has so far only been indirectly inferred from experiments on molecular and polymeric glasses.[15]

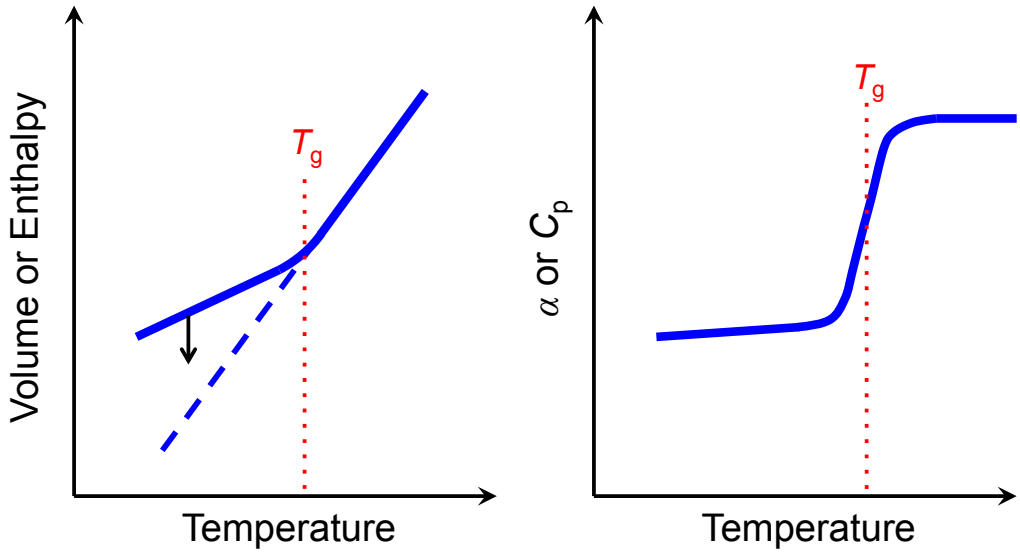

Figure 1.2: Sketches of typical T_g measurements. Left: Volume or enthalpy *vs.* temperature of a material passing through T_g. T_g is identified by the change in slope. The dashed line is the extrapolation of the equilibrium liquid line to lower temperatures. Physical aging of a glass occurs through reduction in volume and enthalpy towards equilibrium as represented by the black arrow. Right: Thermal expansion or specific heat *vs*. temperature of a material passing through T_g. T_g is often identified as the middle of the step change.

1.2.2 Measurement of T_g with Ellipsometry

In this dissertation we use ellipsometry to measure the glass transition temperature of our polymer films. Ellipsometry is a powerful non-destructive optical technique that has existed since the 19th century.[16] In an ellipsometric measurement, light with a known polarization state is reflected off of or transmitted through a sample after which the polarization state of the light is measured. The change in polarization can then be compared to an optical model of the sample. The name ellipsometry derives from the general state of elliptically polarized light used in the technique. Elliptically polarized light has a phase and magnitude difference between the orthogonal polarization components such that the electric field vector traces out an ellipse. The fundamental parameter measured in ellipsometry is the complex reflectivity ratio $\rho = r_p/r_s = \tan(\Psi)e^{i\Delta}$

where r_p and r_s are amplitude reflectivities of reflected light polarized parallel (p) and perpendicular (s) to the plane of incidence, tan(Ψ) is the amplitude ratio of the p and s polarizations, i is the imaginary unit, and Δ is the phase shift between the polarizations.[16] The same equation is valid in transmission with the transmission amplitudes used instead of the reflection amplitudes.

In practice, the polarization state is set up before the sample by passing light through a polarizer and a quarter wave plate (compensator) to generate elliptically polarized light and another polarizer (often called the analyzer) to analyze the resulting reflected polarization. Instruments often have one or more of these elements rotating which generates a time varying signal that can be used to calculate Ψ and Δ. The ellipsometer we have in our lab, a J.A. Woollam M-2000D, has a rotating compensator and with a broad spectrum light source and CCD detector that can simultaneously measure Ψ and Δ for 500 wavelengths from 193 – 2000 nm in less than a second. For the extreme precision measurements of Chapter 3 and Chapter 5, longer averaging times are required. The multi-wavelength rotating compensator design means that sensitivity is the same across all values of Ψ and Δ and allows the wavelength dependent index of refraction to be determined. Several hundreds of data points are used to match a model with only a handful of fitting parameters leading to a very robust measurement.

To determine the glass transition temperature of thin polymer films we measure the film thickness as a function of temperature as schematized in Figure 1.2. This is done for films supported on silicon wafers (with native oxide layer) in the reflection geometry and for free-standing films held by rigid frames in the transmission geometry. T_g can then be determined from the change in slope in such a thickness *vs*. temperature curve.

Alternatively, the thermal expansion can be calculated by numerically differentiating the thickness *vs*. temperature data, and T_g determined from the midpoint in the step change. For very thin films, calculation of the thermal expansion becomes quite difficult as the already significant noise in the thickness data is amplified by the differentiation.[17] To still obtain reliable measures of thermal expansion in such a case, the data are usually averaged or the thermal expansions are determined from the slope of a linear fit to the thickness *vs*. temperature data.

1.2.3 Physical Aging

Glasses are inherently non-equilibrium systems whose properties evolve with time and as such are entirely history dependent. The slow evolution of a glass towards its ideal equilibrium state is called physical aging. As physical aging occurs, a material experiences an increase in density, modulus, and brittleness and a decrease in enthalpy and gas permeability among other effects.[18] In the schematic diagram of Figure 1.2, physical aging is a slow progression from the glassy line towards the equilibrium line, though equilibrium can only be reached very near T_g over reasonable time scales. Physical aging is initiated by taking a sample that is in equilibrium (typically well above T_g) and quenching it quickly to some lower temperature in which it is no longer in equilibrium (i.e., below T_g). The typical physical aging response is sketched in Figure 1.3. At short times there sometimes is an initial plateau where the sample evolves very slowly.[19,20] This plateau is followed by a long region in time where the properties change in a logarithmic fashion. Finally, the equilibrium plateau is reached at very long aging times. In practice equilibrium can only be reached within a few degrees of T_g after days of aging.[21] The length of the initial plateau becomes shorter as the aging temperature is

brought closer to T_g and the quench rate is increased[19] such that in this dissertation the plateau is not visible except for the lowest aging temperatures.

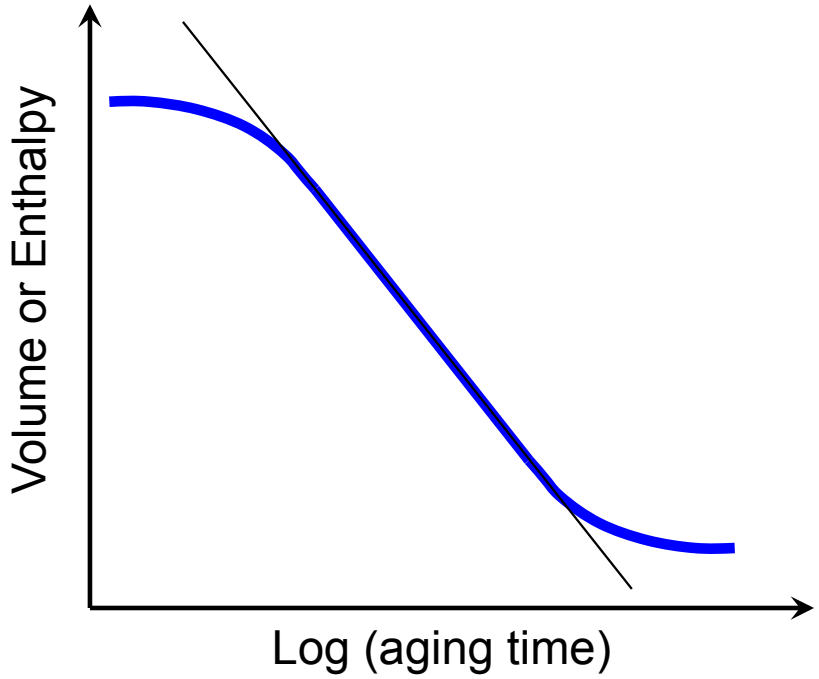

Figure 1.3: Sketch of typical physical aging behavior. At short times an initial plateau is observed where little change occurs. In the intermediate region, the volume and enthalpy decrease linearly with logarithmic time. At very long times, equilibrium may be reached. However, equilibrium is typically only reachable within a few degrees of T_g, even after several days of aging time.

Physical aging can be measured directly by observing the change in properties over time or in a recovery type measurement. Direct measurement of physical aging is commonly a dilatometric or relaxation time measurement. Dilatometric measurements involve determining the sample volume, density, or thickness in the case of thin films as a function of aging time. Thermodynamic measurements of physical aging can also be done with differential scanning calorimetry (DSC).[18,21] As a sample is aged it loses enthalpy as it moves towards equilibrium. When it is heated back through T_g, the enthalpy is recovered and the enthalpy loss that occurred during aging can be determined

from the difference in areas under the heat capacity *vs*. temperature curves for the aged and unaged sample. This recovery type of measurement does not require the sample to be continuously monitored during the aging process, but it does require a different sample or measurement for every aging time.

Mechanical measurements can also be used to determine an aging rate. In these types of measurements, short stress relaxation or creep measurements are performed as a function of aging time to determine the evolution of modulus or compliance.[22] These types of mechanical aging measurements were the focus of pioneering work on physical aging by Struik from 1962 to 1976.[22] Struik defined the aging rate as $\beta = -\partial(V/V_\infty)/\partial(\log t)$ where V_∞ is the volume achieved at equilibrium. This definition describes the rate at which the sample moves towards equilibrium and can conveniently be determined from the slope of volume *vs*. log time in the middle region of Figure 1.3. It is found that the aging rate as a function of aging temperature exhibits a peak.[19,22,23] This peak occurs due to competing effects between the driving force, based on the distance from equilibrium, and the mobility, which varies with temperature.[19,20] As the temperature is reduced, the driving force becomes stronger, but the mobility decreases.

Our lab has previously developed a streamlined ellipsometry procedure to determine the aging rates of polymer films to match the definition provided by Struik.[23] In this paper, extensive tests were performed of various definitions of the aging rate and aging measurement length to find a reliable and efficient procedure to characterize the aging rate of thin films with ellipsometry. Polystyrene (PS) films supported on silicon wafers in a glass petri dish were annealed at T_g + 20 K for 20 minutes in a vacuum oven to remove any previous thermal history. Films were then quenched to room temperature

by placing them (in their glass petri dish) on a large room temperature aluminum block. The films were then transferred onto the ellipsometer hot stage that had been equilibrated at the aging temperature and the film thickness and index of refraction were measured as a function of aging time.

Various analogous equations to Struik's original definition of the physical aging rate were used by Baker *et al*. to fit the data.[23] These variations are alternatively based on the film thickness h, the index of refraction n, and the Lorentz-Lorenz parameter $L = (n^2 - 1)/(n^2 + 2)$. For the film thickness based definition, data were normalized with either the extrapolated equilibrium thickness h_∞ or the initial film thickness h_0 at the start of the aging run. Baker *et al*. found that the physical aging rates calculated using the film thickness, normalized with either h_∞ or h_0, or the index of refraction gave identical aging rates within experimental error at aging temperatures from 307 – 367 K (T_g – 63 K to T_g – 3 K). The Lorentz-Lorenz calculation produced aging rates slightly lower than the other methods. Since the first three definitions produced the same aging rates, the film thickness based definition in which the normalized film thickness h_0 is set to be the thickness at an aging time of 10 min was chosen as the best method:[23]

$$\beta = -\frac{1}{h_0}\frac{\partial h}{\partial(\log t)} \tag{1.1}$$

Using Eq. 1.1, the physical aging rate is identified as the slope of the normalized film thickness h/h_0 *vs.* log(time) data as shown in Figure 1.4, reproduced from Chapter 3 (Ref. 24), and calculated from a linear fit with a fixed point at $h/h_0 = 1$ and $t_{age} = 10$ min.

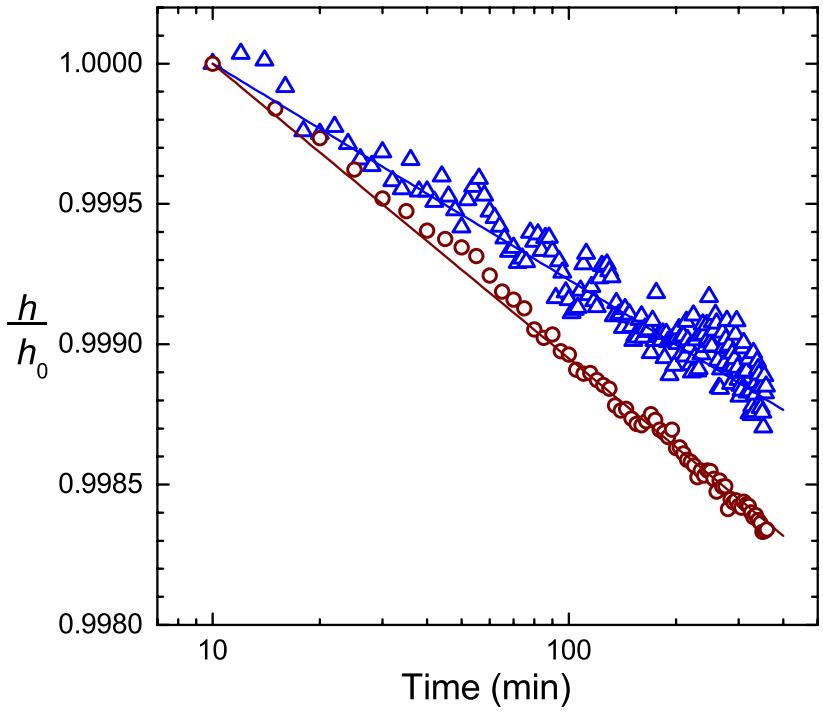

Figure 1.4: Normalized film thickness h/h_0 as a function of logarithmic aging time for polystyrene films aged at 338 K. Dark red circles are data from a 2300 nm thick film and blue triangles are data from a 29 nm thick film. Solid lines are fits of the data to Eq. 1.1. Physical aging data and figure are reproduced from Chapter 3 (Ref. 24).

Baker *et al.*[23] also tested a range of aging times from 2 – 24 hours to develop an aging protocol to efficiently characterize physical aging rates in thin polymer films. The initial plateau in aging response where the film changes very little with time can affect the calculated aging rates if the total aging time is not long enough.[18] It was found that for aging temperatures near and above the peak in aging rate at ~330 K, the calculated aging rate from all aging times is identical within the uncertainty of the measurement. For lower temperatures, there is a slight decrease in measured aging rate as the aging time is reduced, but that the deviation is similar to the uncertainty in the measurements. An aging time of 6 h was found to give a good compromise that allows significant experimental efficiency.

1.3 Confinement

As we push technology and materials to ever increasing limits, interfaces are playing a more important role. Film thickness and feature widths are reaching below 100 nm in photolithography,[25] nanocomposite filler surface areas are reaching hundreds of square meters per gram,[26] and systems composed almost entirely of polymer-polymer interfaces[27] are currently being produced. With these advances it is becoming industrially necessary to understand the effect of polymer-air, polymer-substrate, and polymer-polymer interfaces. Fundamentally, there is still significant understanding and agreement missing from theories on the glass transition.[6,8,9] Confinement effects have the potential to probe fundamental length scales of glasses.[28]

1.3.1 T_g Reductions in Ultrathin Supported PS films

The industrial and scientific impacts have been recognized from the very first studies of confinement effects on the glass transition.[29,30] In 1991, Jackson and McKenna studied the organic liquids o-terphenyl and benzyl alcohol confined within nanopores using differential scanning calorimetry (DSC).[29] They found reductions in T_g of 18 and 7 K for o-terphenyl and benzyl alcohol in 4 nm nanopores. The first study of T_g in thin polymer films followed in 1994 by Keddie, Jones, and Cory who measured T_g as a function of film thickness for polystyrene (PS) on hydrogen passivated silicon wafers with ellipsometry.[30] Reductions in T_g of 30 K and factor of two increases in the glassy thermal expansion were found for 15 nm thick films. T_g as a function of thickness was found to follow a semi-empirical equation:

$$T_g(h) = T_g^{bulk}\left[1 - \left(\frac{A}{h}\right)^{\delta}\right] \tag{1.2}$$

with a characteristic length A = (3.2 ± 0.6) nm and exponent δ = 1.8 ± 0.2. Surprisingly, the film thickness at which T_g starts to deviate from the bulk value, ~40 nm, is much larger than the ~3 nm cooperativity length scales found near T_g in experiments.[31] These and subsequent measurements have determined that there is no molecular weight (MW) dependence of the T_g reductions in PS films supported on silicon from 5,000 g/mol to 3,000,000 g/mol.[32,33]

Keddie, Jones, and Cory[30] interpreted their results with a layer model that has been quite popular since then.[34–36] It was proposed that at the free surface of a polymer film there is a reduced requirement for the cooperativity commonly believed to be important in glassy dynamics.[9,28] This reduction in constraints would lead to a region of enhanced mobility with a lower glass transition temperature. The film can then be approximated by a surface layer with a lower T_g (or no T_g such that it is always in the liquid state) and a bulk layer with properties given by the bulk polymer. The film average T_g of such a two-layer model is either set as a weighted average of the layer T_gs[35,36] or found from an apparent change in slope in total film thickness *vs*. temperature calculated from the thermal expansion of the individual layers.[34,37,38] The layer model has also been successfully used in measurements of dynamics such as viscosity determined from embedding of nanoparticles into the surface of the film,[39–42] thermal capillary wave evolution,[43,44] and capillary leveling,[45] as well as rotational reorientation measurements of dye molecules.[46] In situations where there may be an attractive interaction between the polymer and the substrate, or an adsorbed layer is suspected, an additional substrate layer is often added to the layer model that typically has more glassy properties.[34,47]

The layer model is appealing and relatively easy to use, but is not likely to be a realistic picture of the dynamics of thin films. It is more likely that there is a smooth change in dynamics from the free surface (or substrate) into the film, eventually recovering bulk dynamics far from the interface. A discrete layer model seems even less likely when one considers the many orders of magnitude difference in relaxation times that would exist between a liquid-like surface layer and a bulk layer. The first direct experimental measurement of a gradient in dynamics came in 2003 from multilayer fluorescence measurements by Ellison and Torkelson.[48] By covalently labeling polymer chains with a dye that had previously been shown to be sensitive to T_g[49,50] and building a multilayer sample in which only one thin layer is labeled, they were able to measure the T_g of a thin layer at the free surface as a function of that layer thickness. They found that the T_g was reduced by 32 K in a 14 nm layer at the free surface and that a significant T_g reduction persisted to tens of nanometers away from the surface. This gradient in dynamics is also supported by results from simulations of polymer films.[28,51,52]

1.3.2 T_g Reductions in Ultrathin Free-Standing Polymer Films

In an effort to remove any potential substrate related effect, measurements have also been performed on free-standing polymer films. Surprisingly, the results are actually more complicated. Forrest *et al*.[35] and Mattsson *et al*.[36] measured "low MW" free-standing PS films with M_w < 368 kg/mol, finding that $T_g(h)$ follows the same functional form as Eq. 1.2 but with T_g roughly equivalent to that measured for supported films of half the film thickness.[35,36] They were not too surprised by this result since free-standing films have two free surfaces compared to one in a supported film.[36] However, for "high MW" free-standing PS films with M_w > 575 kg/mol, a much more interesting behavior

was found.[36,53–55] T_g depends very strongly on MW and $T_g(h)$ decreases linearly with film thickness. There is no smooth transition to T_g^{bulk}, instead a cutoff thickness exists below which the T_g reduction is seen. Both this cutoff thickness and the slope of $T_g(h)$ depend on MW. Amazingly, the linear fits of $T_g(h)$ for different MW all intersect at a single temperature and film thickness.[55] This fact allows all of the data to be collapsed with a single expression able to represent the thickness and MW dependence of T_g for all free-standing films with $M_w \geq 575$ kg/mol that exhibit a T_g reduction:[55]

$$T_g - T_g^* = b \ln(M_W/M_w^*)\,(h - h^*) \tag{1.3}$$

where T_g^* = (423 ± 2) K and h^* = (103 ± 1) nm define the point where all of the linear fits to the high MW free-standing data in Figure 1.5 intersect, M_w^* = (69 ± 4) kg/mol is the M_w at which there would be no T_g reduction for a film of any thickness, and b = (0.70 ± 0.02) K/nm characterizes the overall strength of the T_g reduction. As is evident in Eq. 1.3, the MW dependence of the T_g reduction is surprisingly not proportional to $M_w^{1/2}$, or equivalently R_g, but is well characterized by a logarithmic dependence.

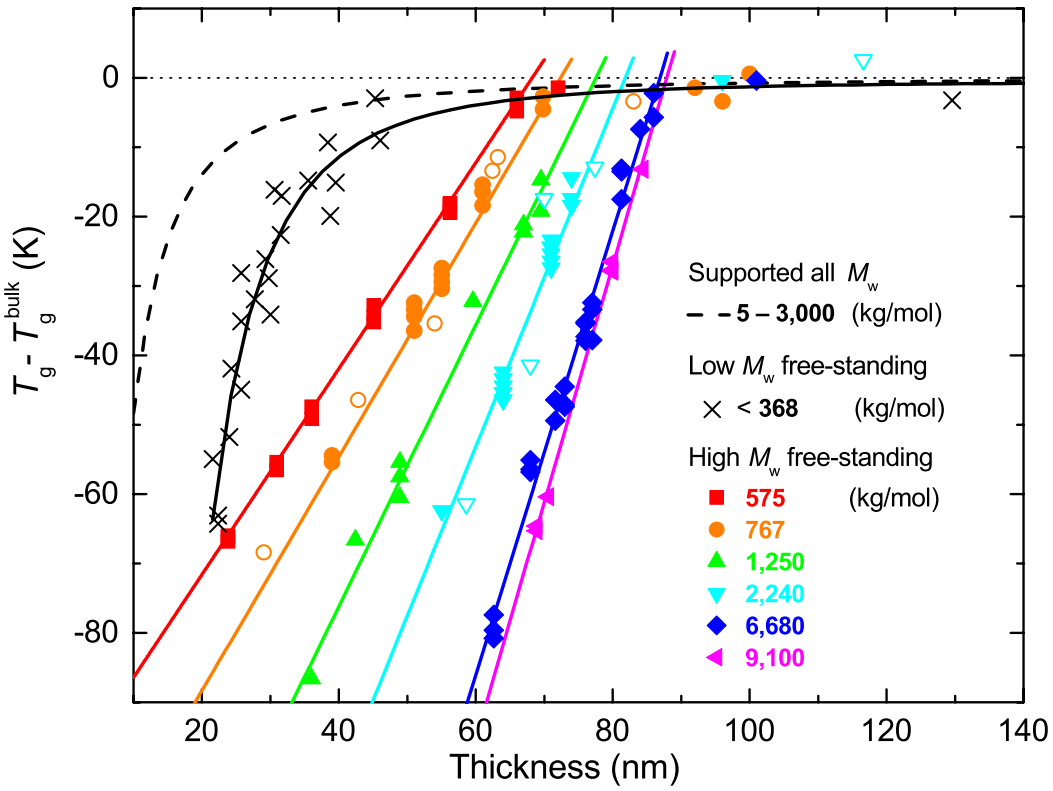

Figure 1.5: T_g reduction as a function of film thickness for PS films of varying geometry and MW. The T_g reduction for supported PS films of all MW is represented by the curved dashed line using Eq. 1.2. Data for free-standing PS films with $M_w \leq 368$ kg/mol are shown with ×s and fit with Eq. 1.2 as the thick solid curved line. Data for high MW free-standing PS films are shown as colored symbols with M_w given in the figure legend. Open symbols of all MW and ×s are from Ref. 36 and closed symbols are from Ref. 55.

Similar measurements performed on free-standing PMMA films showed the same type of behavior as free-standing PS films with $T_g(h)$ characterized by Eq. 1.2 for low MW ($M_w = 159$ kg/mol) films and $T_g(h, M_w)$ characterized by Eq. 1.3 for high MW ($M_w \geq 509$ kg/mol) films.[56,57] The $T_g^* = (T_g^{bulk} \pm 2)$ K ($T_g^{bulk} = 383$ or 388 K depending on slight variations in tacticity for the atactic PMMA used), $M_w^* = (236 \pm 25)$ kg/mol, and $b = (0.21 \pm 0.01)$ K/nm values found to fit the PMMA data with Eq. 1.3[57] are significantly different than the values listed in the previous paragraph found to fit the PS data. However, $h^* = (96 \pm 8)$ nm for the PMMA data is nearly identical to that found to fit the PS data, suggesting that this ~100 nm length scale may be universal to high MW T_g

reductions. Nevertheless, the relative strength of the T_g reductions, characterized by the b parameter, for free-standing PMMA films is less than 1/3 that for free-standing PS films. A proposed reason for the smaller T_g reduction in high MW free-standing PMMA films is the anomalously strong coupling of the backbone α-relaxation and side-group β-relaxation that exists in PMMA.[57] Unfortunately, T_g^* and M_w^* for both PS and PMMA defy explanation.

The scaling collapse of the T_g reductions in high MW free-standing polymer films discussed above was done with data collected by ellipsometry.[54,56–58] However, the earliest data on free-standing films and that for low MW films was collected using Brillouin light scattering (BLS).[35,36,53,54] These huge MW dependent T_g reductions seen in ultrathin high MW free-standing polymer films has since been confirmed with dielectric spectroscopy,[59,60] Raman spectroscopy,[61] X-ray reflectivity,[62] and fluorescence.[63,64] Interestingly, T_g extracted from nanobubble creep measurements on high MW PS films by O'Connell *et al*. seems to match more closely with the T_g reductions of low MW PS films than the T_g reduction predicted for their high MW (M_w = 994 kg/mol).[65]

1.4 Outline of Dissertation

This dissertation is broken into six chapters and an appendix encompassing the work completed while pursuing a PhD at Emory University.

1.4.1 Chapter Descriptions

Chapter 2 describes the results of glass transition temperature measurements on ultrathin high MW free-standing PS films over an extended temperature range. We report the first measurement of two glass transitions in ultrathin high MW free-standing

PS films. The lower transition is MW dependent and matches the previously reported T_g in these high MW free-standing PS films, while the upper transition, not before seen in these films, matches the previously reported T_g in *low* MW free-standing PS films. The nature of these two transitions is discussed in view of previous measurements on free-standing films. A version of this chapter was published as:

> Pye, J. E.; Roth, C. B. Two Simultaneous Mechanisms Causing Glass Transition Temperature Reductions in High Molecular Weight Freestanding Polymer Films as Measured by Transmission Ellipsometry. *Phys. Rev. Lett.* **2011**, *107*, 235701.

In Chapter 3 we present physical aging measurements of supported polystyrene films as a function of film thickness and aging temperature. These results provide the first report that the temperature dependent length scale characterizing the depth to which enhanced dynamics propagate into a PS film from the free surface is the same for both reductions in the physical aging rate and T_g. This evidence is from both a layer model and gradient model fit to physical aging rate measurements of supported PS films as a function of film thickness at an aging temperature of 338 K and as a function of aging temperature for 30 nm thick films. The length scale found to represent the depth to which the free surface effect perturbs the dynamics from the bulk value was shown to increase as temperature is reduced. A version of this chapter was published as:

> Pye, J. E.; Rohald, K. A.; Baker, E. A.; Roth, C. B. Physical Aging in Ultrathin Polystyrene Films: Evidence of a Gradient in Dynamics at the Free Surface and Its Connection to the Glass Transition Temperature Reductions. *Macromolecules* **2010**, *43*, 8296–8303.

Chapter 4 demonstrates a method to perform *in situ* physical aging measurements on free-standing polymer films with ellipsometry. The results demonstrate that the physical aging rate is strongly affected by the thermal expansion mismatch between the free-standing polymer film and the rigid frame. By varying the material of the rigid

frame and the resulting stress applied to the film from the thermal quench used to initiate aging measurements, we observe a change in aging rate by nearly a factor of two. A higher thermal expansion mismatch and thus stress result in a higher aging rate. The implications of this result and the film thickness independent aging rate of films from 200 – 1800 nm in thickness in terms of the free volume diffusion model is discussed. A version of this chapter was published as:

> Pye, J. E.; Roth, C. B. Physical Aging of Polymer Films Quenched and Measured Free-Standing via Ellipsometry: Controlling Stress Imparted by Thermal Expansion Mismatch between Film and Support. *Macromolecules* **2013**, *46*, 9455–9463.

In Chapter 5, we investigate the nature of the two transitions in ultrathin high MW free-standing PS films reported in Chapter 2 (Ref. 66) by determining the thermal expansion above, between, and below the two transitions, and performing physical aging measurements between and below both transitions. We find that most of the thermal expansion change occurs at the upper transition and that physical aging does occur between the two transitions, indicating that the upper transition accounts for the solidification of the majority of the film and is an actual glass transition.

The Appendix describes the background, theory, and data needed to perform the thermoviscoelastic calculation of stress developed in a film quenched through T_g due to thermal expansion mismatch between the film and the support. This calculation applies to both supported and free-standing films. The physics and math required for this calculation includes an understanding of the different modes of deformation and resulting moduli, viscoelasticity, and time-temperature superposition. These are formulated in terms of the reduced time ξ, with the Boltzmann superposition principle and Laplace transform used to solve viscoelastic problems. The literature data required to perform

such a calculation and the transformations required to combine data from different experimental conditions are described.

1.4.2 Additional Work not Included in this Dissertation

In addition to the work described in this thesis, I helped develop a modified fluorescence method to measure T_g in thin fluorescently labeled polymer films.[67] The temperature dependent fluorescence of pyrene dye, either doped into the film or covalently bonded to the polymer, was shown to be sensitive to T_g in polystyrene more than 10 years ago.[48,50] In these measurements the film is held at a constant temperature, starting well above T_g, and the fluorescence spectrum or intensity at a particular wavelength(s) is collected. The temperature is then iteratively stepped down, allowed to equilibrate, and then another fluorescence measurement is made. This procedure is repeated until enough data has been collected to determine T_g from the change in slope of intensity *vs*. temperature.

To improve the amount of data collected and allow the measurement to be automated, I developed a temperature ramping procedure. The fluorescence emission intensity at a single wavelength just off of the first emission peak of pyrene is measured for 3 seconds every 30 seconds while the sample is cooled at 1 K/min. The advantages of this ramping method include minimization of photobleaching by reducing the sample illumination time, collection of more than ten times the number of data points for a given temperature range, and complete automation of the data collection portion of the T_g measurement. Developing this ramping method took significant effort to find the excitation and emission wavelengths, bandpasses, illumination time, frequency of data

collection, and sample orientation in the fluorometer that gave the greatest sensitivity to T_g with the least amount of photobleaching.

This modified fluorescence ramping method was subsequently used by Roman Baglay in our lab to measure the T_g of a thin pyrene labeled PS layer supported on a thick layer of poly(n-butyl methacrylate) (PnBMA) as a function of the PS layer thickness.[67] He found a 25 – 30 K reduction in T_g for films 84 nm thick, much larger than the T_g reductions seen in PS films on silicon as described in Section 1.3.1. Phil Rauscher performed physical aging measurements using ellipsometry on films with identical geometry and found that the aging rate of the PS layer did not change down to a PS layer thickness of 84 nm.[67] This strong dichotomy between physical aging rate and T_g as a function of PS layer thickness appears to be distinctly different than my results on single layer PS films in Chapter 3 (Ref. 24) These results and discussion of these differences were recently published as:

> Rauscher, P. M.; Pye, J. E.; Baglay, R. R.; Roth, C. B. Effect of Adjacent Rubbery Layers on the Physical Aging of Glassy Polymers. *Macromolecules* **2013**, *46*, 9806–9817.

Chapter 2

Dual T_gs in Ultrathin Free-Standing Polystyrene Films

A version of this chapter was published as Pye, J. E.; Roth, C. B., *Physical Review Letters*, *107*, 235701, **2011**.

2.1 Introduction

In polymer systems, reductions in T_g observed with decreasing film thickness h can be classified into two qualitatively different behaviors.[36,57,68] Supported films,[30,33,48,69,70] and freestanding films of low molecular weight (MW) chains,[36,57] exhibit decreases in T_g that follow an empirical relation:[30] $T_g(h) = T_g^{bulk}\,[1 - (A/h)^{\delta}]$. T_g reductions of ~25 K for 15 nm thick polystyrene (PS) films supported on silica are typical, with no MW dependence observed in supported films for M_n ranging between 5 and 3000 kg/mol.[33] Low MW (M_w < 368 kg/mol) freestanding PS films show qualitatively the same $T_g(h)$ reduction as supported films, but the presence of two free surfaces results in T_g reductions that are essentially the same as that of a supported film with half the film thickness (h/2).[36] Originally proposed by Keddie, Jones, and Cory, this functional form was based on the notion that some region of the film near the free surface would experience faster dynamics.[30] This initial assumption has since been experimentally confirmed,[48] with results indicating a gradient in dynamics emanating from the free surface that extends several tens of nanometers into the material, and appears to be correlated with cooperative motion.[24,33,36] This gradient in dynamics manifests itself as a broadening of the glass transition with decreasing film thickness, and its effects have been linked to

other properties such as changes in physical aging rate[24,71] and modulus[72] with decreasing film thickness. There is no chain connectivity associated with this mechanism and similar effects are seen in colloidal systems[73] and small molecules.[74–76] The most promising theoretical model for this behavior is a percolation model proposed by Long and Lequeux[77] that has since been further refined for thin films[78] and polymer nanocomposites.[79]

In contrast, high MW freestanding films exhibit a qualitatively different behavior with a MW dependent linear reduction in T_g below some critical thickness h_0: $T_g(h) = T_g^{bulk} - \alpha (h_0 - h)$, for $h < h_0$.[36,53–57,68] The slope α of the linear decrease, as well as h_0, both depend on MW, and the transition itself always appears sharp. T_g reductions as large as 85 K have been measured for 35 nm thick freestanding films of PS (M_w = 1250 kg/mol).[55] This mechanism clearly depends on chain connectivity, but no direct correlation with chain size has yet been found.[68] The only theoretical model that has been proposed for this behavior is the suggestion by de Gennes of a possible "sliding mode" available to chain segments occurring between mobile surface layers that could impart faster dynamics from the free surface deeper into the film,[80,81] though a recent multilayer fluorescence experiment generated some evidence against this model.[64]

This strong qualitative difference between the two observed $T_g(h)$ dependencies has led some to propose that two separate mechanisms could be responsible for this behavior.[36,57,77] In fact, Long and Lequeux suggested that the "… de Gennes sliding effect, which applies for large polymer chains, and our proposed mechanism are compatible and can take place simultaneously…".[77] Here, we report the first experimental evidence of two separate mechanisms occurring simultaneously in high

MW freestanding films. Using transmission ellipsometry to measure the thermal expansion of high MW freestanding PS films over an extended temperature range, we have observed two separate and distinct glass transitions acting simultaneously within high MW freestanding PS films of M_w = 934 and 2257 kg/mol. Both T_gs are reduced from the bulk value. The lower transition is linear in $T_g(h)$ and shows the anticipated MW dependence previously observed in these films.[36,53–55,59,61–64] The upper transition, not previously seen in these films, is much stronger and follows the Keddie, Jones and Cory functional form[30] with $T_g(h)$ values in agreement with that expected for low MW freestanding PS films.[36] We envision these dual T_gs as reflecting two separate population dynamics within the film resulting from two separate mechanisms simultaneously imparting enhanced mobility from the free surface deeper into the material.

2.2 Experimental

High MW polystyrene with weight average molecular weight M_w = 934 kg/mol and polydispersity M_w/M_n = 1.14, or M_w = 2257 kg/mol and M_w/M_n = 1.17, were dissolved in toluene and spin-coated onto freshly cleaved mica. Samples were vacuum annealed at ~405 K (> T_g^{bulk} + 30 K) for at least 16 h, followed by a slow cool (<0.5 K/min) to room temperature. Although there have been renewed concerns regarding whether such annealing is sufficient,[82] we note that our procedure is comparable to the annealing protocol used in the original studies and previously deemed to be sufficient.[36,53–55,68] Films were subsequently floated onto stainless steel sample holders to create freestanding films across a 5 mm opening. Pieces from the same film were also floated onto silicon for film thickness determination by reflection mode using multiple angles of incidence. The absolute, room temperature (298 K) film thickness of each

freestanding film was determined from the corresponding film on silicon, or the thickness at 298 K was measured or extrapolated from the first cooling ramp of the freestanding film, which was found to match the thickness of its corresponding supported film to 1%.

Transmission ellipsometry measurements were performed on the free-standing films using a J.A. Woollam M-2000 ellipsometer with a custom-built, windowless heat cell. Measurements of Ψ and Δ as a function of wavelength λ were collected every 24 s while ramping at 0.5 K/min. Each data point corresponds to an average of $\Psi(\lambda)$ and $\Delta(\lambda)$ over 20 s, during which the temperature varies by <0.2 K. The temperature for a given data point was taken to be the midpoint of the temperature range over which it was collected. The $\Psi(\lambda)$ and $\Delta(\lambda)$ data at each temperature were fit for λ = 400–1000 nm to a layer model consisting of a transparent Cauchy layer, $n(\lambda) = A + B/\lambda^2$, with ambient on both sides. The freestanding films were held at an angle of incidence of ~45°, with the precise angle of incidence for each film determined to within ±0.05° by fitting the film thickness and angle of incidence, while holding the index of refraction fixed at the bulk value, to the $\Psi(\lambda)$ and $\Delta(\lambda)$ data at 378 K where the films are flat and free of wrinkles. The angle of incidence was then held fixed while the thickness $h(T)$ and index $n(T)$ were fit for the entire temperature range. The bulk value of $n(\lambda)$ at 378 K was determined by measuring a thick (>150 nm) film over multiple angles of incidence and fitting the thickness and index of refraction simultaneously to all angles using the Multi Sample Analysis fitting routine in CompleteEASE. The thickness *vs.* temperature data shown in this chapter were further averaged by using a nine point Savitzky-Golay smoothing algorithm, which corresponds to a smoothing window of 1.8 K. In addition, for clarity only every fourth data point is displayed.

Temperature ramps consisted of an initial heat to 383 K (391 K for bulk films) to remove wrinkles and obtain flat films, followed by multiple ramps at 0.5 K/min. Typically the temperature was ramped several times through the lower T_g, with a limited number of ramps through the higher temperature T_g where hole formation is more prevalent.[83,84] The T_g values were determined by fitting each transition independently to the same functional form used by Dalnoki-Veress *et al.*:[55]

$$h(T) = w\left(\frac{M-G}{2}\right)\ln\left[\cosh\left(\frac{T-T_g}{w}\right)\right] + \left(T - T_g\right)\left(\frac{M+G}{2}\right) + c \qquad (2.1)$$

where w is the width of the transition, M and G are the slopes of the melt and glassy regions respectively, and c is the thickness of the film at T_g. The width of the transition was fixed to 2 K for the lower temperature T_g (following Ref. 55) and 10 K for the higher temperature T_g, representative of the larger breadth associated with this mechanism.[70] The T_g of the film was taken as the weighted average of typically 4–7 ramps for the lower T_g and 2–4 ramps for the upper T_g. We also fit the upper transition using the more common method of finding the intercept of two linear fits above and below the transition.[30,36,48,53,54,56,57,63,64,70] Because of the limited range of data in the temperature region between the two transitions, the "glassy" line of the upper transition was extracted from the "liquid" line of the lower transition as determined by the fit to Eq. 2.1. This is appropriate since the region between the two T_gs represents both the "glassy" line for the upper T_g and the "liquid" line for the lower T_g, thus ensuring that these lines have the same slope. This method resulted in T_g values that were comparable to the first fitting method. The error for the measured T_g values were calculated based on a weighted standard error from multiple temperature ramps, where the weights are the standard errors in the T_g fits for each temperature ramp. For the weaker lower T_g, typically 4–7

ramps were measured, while for the stronger upper T_g, typically only 2– 4 ramps were measured because hole formation was more of a concern at the higher temperatures. The bulk value of T_g, T_g^{bulk} = 373 ± 2 K, was determined from the average of films with thicknesses >150 nm.

2.3 Results and Discussion

Figure 2.1 graphs the thickness-temperature profiles for three representative freestanding films of PS with M_w = 934 kg/mol for thicknesses of 166.5, 54.7, and 33.3 nm, all measured on cooling. The thickest film has only a single bulk T_g = 370 ± 2 K, while the thinnest films exhibit two reduced glass transitions of T_g = 364 ± 2 and 338 ± 3 K for the 54.7 nm thick film and T_g = 351 ± 3 and 308 ± 3 K for the 33.3 nm thick film. The lines shown in the figure are drawn to correspond to the slopes obtained from the fitting equation with the lines extended beyond the transition to indicate where they cross.

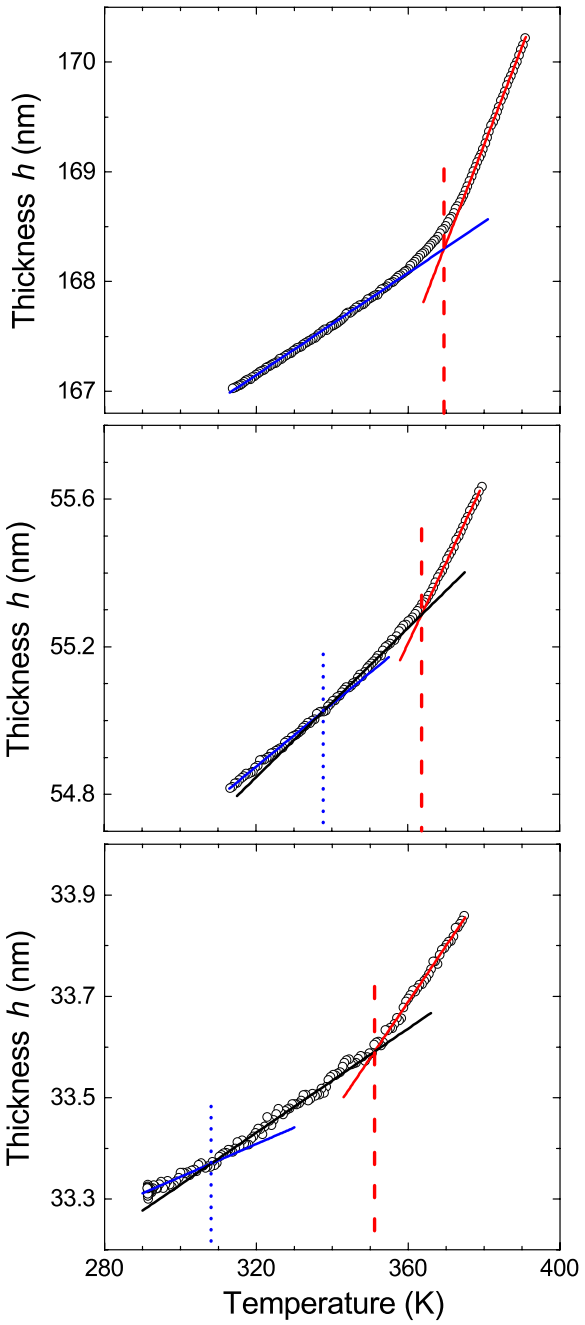

Figure 2.1: Film thickness as a function of temperature for three high MW (Mw = 934 kg/mol) PS freestanding films of thicknesses 166.5, 54.7, and 33.3 nm. The vertical dashed lines indicate the measured T_g of 370 ± 2 K for the bulk 166.5 nm thick film, and the two reduced T_gs for the thinner films: 364 ± 2 and 338 ± 3 K for the 54.7 nm thick film, and 351 ± 3 and 308 ± 3 K for the 33.3 nm thick film. The fit lines are described in the text.

Figure 2.2 shows both the index of refraction $n(T)$ and the film thickness $h(T)$ as a function of temperature for a (a) 33.3 nm thick freestanding PS film of M_w = 934 kg/mol

and a (b) 53.2 nm thick freestanding PS film of M_w = 2257 kg/mol. These data demonstrate that the two reduced T_gs occur at the same temperature in both the thickness and index of refraction for both high MWs measured. The index of refraction plotted in the figure is for a wavelength of 632.8 nm corresponding to a HeNe laser.

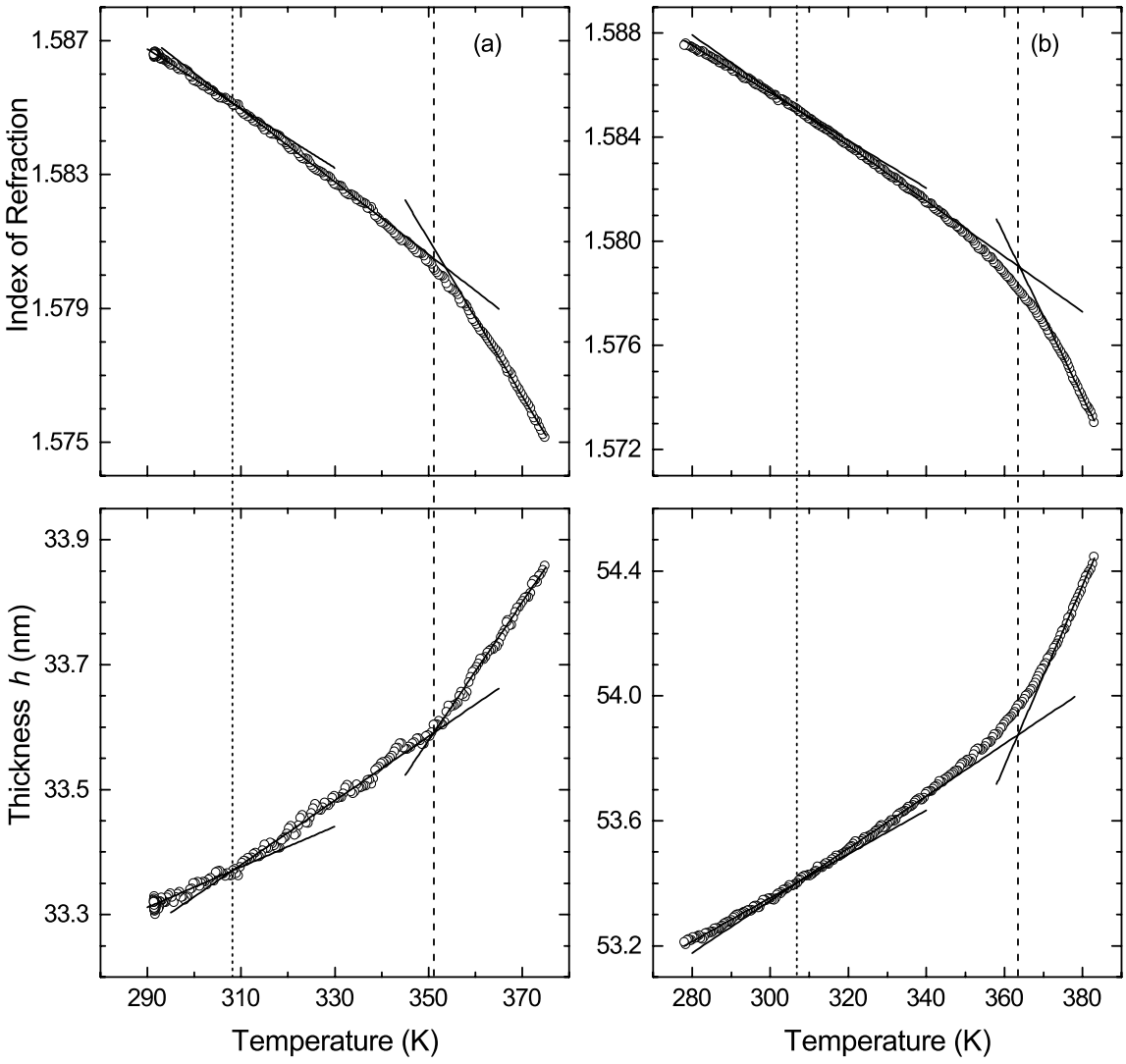

Figure 2.2: Temperature dependence of the index of refraction $n(T)$ and film thickness $h(T)$ for freestanding PS films of (a) M_w = 934 kg/mol with a 33.3 nm thick film showing two reduced T_gs at 308 ± 3 and 351 ± 3 K, and (b) M_w = 2257 kg/mol with a 53.2 nm thick film giving reduced T_gs of 307±3 and 363±3K.

To clearly demonstrate that the upper T_g is independent of MW while the lower T_g is strongly MW dependent, two films of similar film thickness (~55 nm) but different

MW are shown in Figure 2.3. The upper transitions are within error for the two MW with T_g = 364 ± 2 K for the 54.7 nm, M_w = 934 kg/mol film and T_g = 363 ±3 K for the 53.2 nm, M_w = 2257 kg/mol film. However, the lower T_gs are separated by more than 30 K with T_g = 338 ± 2 K for the 54.7 nm, M_w = 934 kg/mol film and T_g = 307 ±3 K for the 53.2 nm, M_w = 2257 kg/mol film.

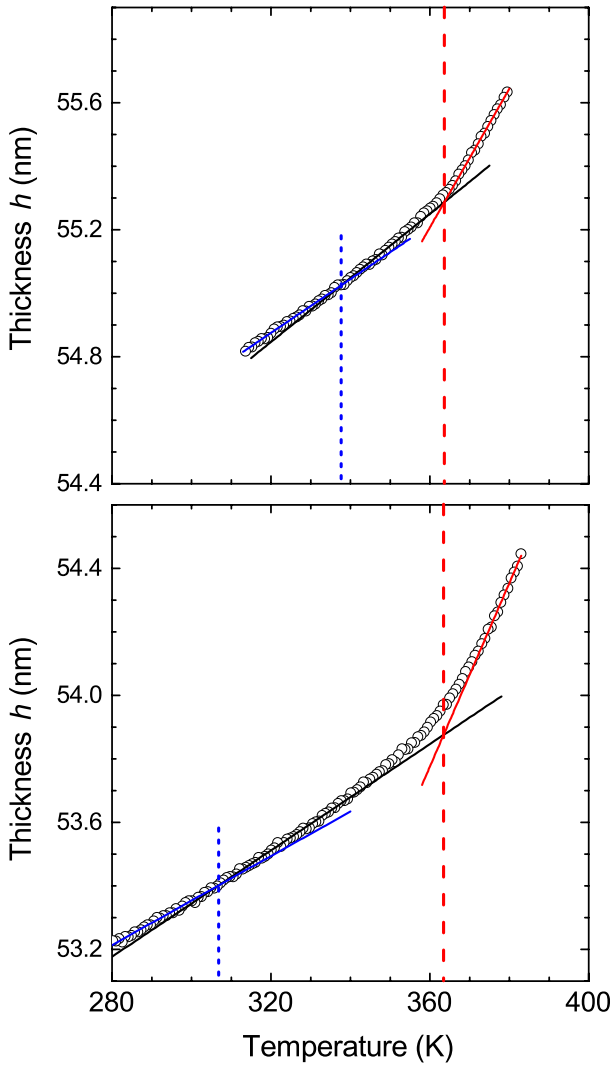

Figure 2.3: Comparison of thickness *vs*. temperature for two films of similar thickness but different MW. a) 54.7 nm, 934 kg/mol film showing two reduced T_gs at 338 ± 3 and 364 ± 2 K. b) 53.2 nm, Mw = 2257 kg/mol film showing two reduced T_gs at 307 ± 3 and 363 ± 3 K. The upper T_g in both films is nearly identical while the lower T_g is different by more than 30 K in the two samples of different MW.

Figure 2.4 plots all of our measured T_g values relative to T_g^{bulk} as a function of film thickness for both MWs, M_w = 934 (triangles) and 2257 (squares) kg/mol. There are two reduced T_gs for each individual thin film with h < 70 nm. The lines and curves in the figure are not fits, but represent the existing literature data for freestanding PS films. The solid black lines represent the expected $T_g(h)$ data for the two MWs, calculated for M_w = 934 and 2257 kg/mol based on the scaling analysis provided by Dalnoki-Veress *et al*. in Ref. 55. We note that the empirical scaling used by Dalnoki-Veress *et al*.[55] to collapse these MW dependent T_g reductions only scales with the *weight-average*-MW (M_w), and not the *number-average*-MW (M_n), suggesting a connection to chain length for this mechanism. The dashed curve is a fit of the Keddie, Jones, and Cory functional form to the low MW freestanding PS film $T_g(h)$ data by Mattsson *et al*..[36] Our data for the lower T_g values exhibit a MW dependence and are in excellent agreement with the anticipated high MW $T_g(h)$ data from Ref. 55 that have been previously[36,53,54,59,61–64] and subsequently[58] observed in these films. While the upper T_g values, corresponding to the much stronger transition not previously observed in these films, are in excellent agreement with the $T_g(h)$ reductions from Ref. 36 previously observed for only low MW freestanding PS films. We have highlighted as solid symbols, the two T_gs measured for a single film of M_w = 934 kg/mol that is 32.9 nm thick, T_g = 353 ± 1.0 K and 294 ± 4.5 K, and for a single film of M_w = 2257 kg/mol that is 53.2 nm thick, T_g = 370 ± 1.5 K and 310 ± 2.0 K. For both films, the two independent, reduced T_gs are separated by nearly 60 K.

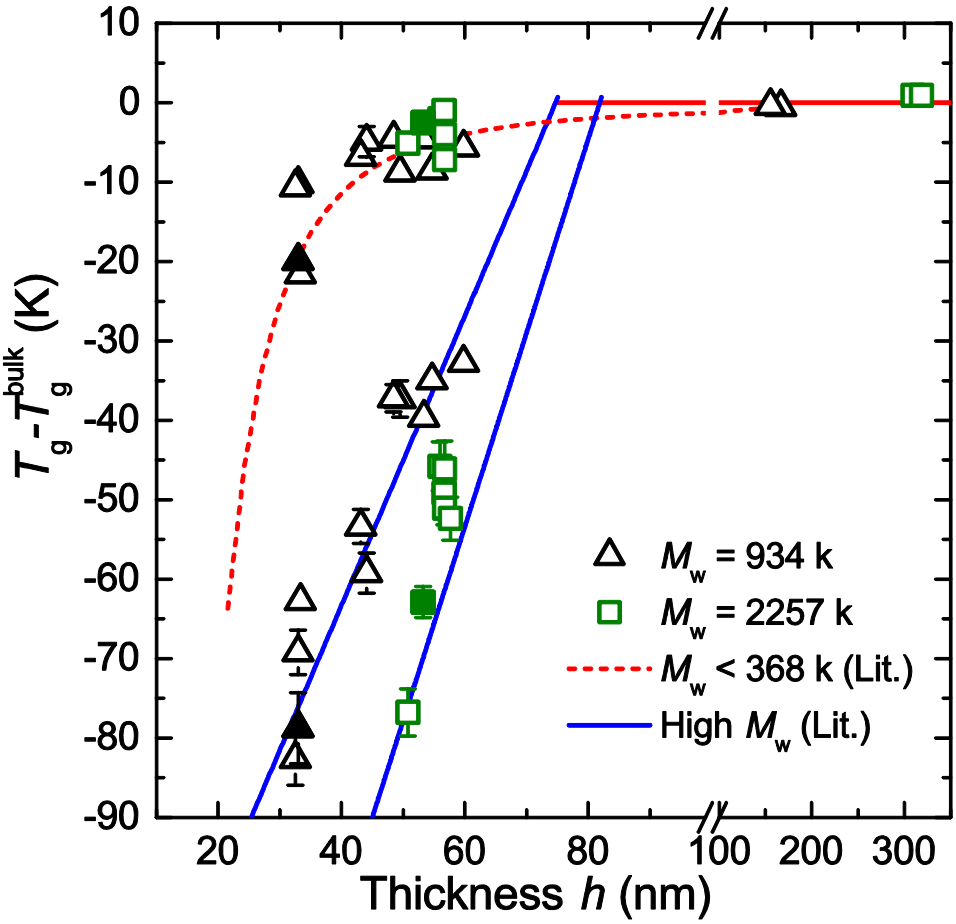

Figure 2.4: $T_g - T_g^{bulk}$ as a function of film thickness for high MW freestanding PS films, M_w = 934 (black triangles) and 2257 (green squares) kg/mol. Two reduced T_gs for each ultrathin film < 70 nm thick are shown; the error is the size of the symbols or smaller except where shown. Highlighted as solid symbols are the two T_gs, separated by nearly 60 K, measured for a single film: solid triangles correspond to a 32.9 nm thick film of M_w = 934 kg/mol, with T_g = 353 ± 1.0 K and 294 ± 4.5 K, and solid squares correspond to a 53.2 nm thick film of M_w = 2257 kg/mol, with T_g = 370 ± 1.5 K and 310 ± 2.0 K. The solid blue lines represents the anticipated $T_g(h)$ for our MW, calculated for M_w = 934 and 2257 kg/mol based on the scaling analysis provided by Dalnoki-Veress *et al*. in Ref. 55. The dashed red curve is a fit of the Keddie, Jones, and Cory functional form to the low MW freestanding PS film $T_g(h)$ data by Mattsson *et al*..[36]

For both MWs, the lower transition (which is quite weak and narrow) is in excellent agreement with the anticipated MW dependent T_gs for these films based on the original work,[36,53–55] and since verified by others,[59,61–64] for high MW freestanding films. However for all films, we unmistakably observe a much stronger upper T_g that is broader. Based on the change in slope, i.e., thermal expansion coefficient of the material, we

determine that upon cooling from the melt to the glass, the majority of the film (~90%) solidifies at the upper transition, while only a small fraction (~10%) remains mobile to much lower temperatures, solidifying at the lower transition. These two T_gs do not simply correspond to values representing the free surface and interior of the film. The free surface region is represented in the breadth of the upper transition that follows the Keddie, Jones and Cory functional form,[30] and has been previously correlated with a gradient in dynamics originating from the free surface that encompasses both the free surface region and the interior of the film.[24,36,48,64] This reasoning is most clearly supported by the layer model analysis of Ref. 36 where the reduced $T_g(h)$ observed in low MW freestanding films, which is in quantitative agreement with our upper transition, was interpreted as corresponding to a measured average of a reduced surface T_g and a bulk-like interior film T_g. Further support is obtained from recent fluorescence anisotropy measurements on freestanding films by Paeng and Ediger, which observed two dynamical populations in the segmental dynamics in ultrathin freestanding films, both found to be independent of MW.[46] They attributed the faster population as corresponding to the free surface region. However, all their measurements on high MW films were at temperatures significantly above that where the lower, MW dependent transition occurs. Thus, their measurements would not have been sensitive to dynamics associated with the mechanism corresponding to the lower transition. The breadth of the upper transition corresponds to the solidification of ~90% of the film (matrix), while the lower MW dependent transition represents some smaller ~10% fraction of the material with extremely fast dynamics. At present, we cannot provide information as to the location of this faster population within the film, but the cause of this very fast population is related to the chain connectivity of

the polymer resulting in faster dynamics for higher MWs. In addition, the narrow temperature range associated with this transition suggests a rather homogeneous dynamical population.

Our results measuring two independent, reduced glass transitions in ultrathin high MW freestanding polymer films, a strong upper transition with no MW dependence and a much weaker lower transition with a distinct MW dependence, represent the first experimental evidence of two separate mechanisms acting *simultaneously* to impart enhanced dynamics to these nanoconfined films. Previous studies have only observed a single glass transition,[36,53–55,59,61–64,85] with the lower (weaker) transition being the "accepted" T_g for high MW freestanding films. [36,53–55,59,61–64] However, there are a few studies that have observed dynamics consistent with the presence of the upper transition in high MW films.[46,60,65,85,86] Svanberg used broadband dielectric spectroscopy to measure the α-relaxation (T_g) of high MW (M_w = 767k) freestanding PS films surrounded by ethylene glycol.[85] Surprisingly, the film thickness dependence of the α-relaxation was found to follow the $T_g(h)$ dependence of the upper transition consistent with low MW freestanding films. The nanobubble inflation method of O'Connell and McKenna,[65,87] which measures the overall compliance of the film, also obtained $T_g(h)$ values for high MW (M_w = 994 kg/mol) freestanding PS films consistent with the upper transition.[65] More recently, Napolitano and Wübbenhorst observed in high MW (M_w = 932k) freestanding films evidence of a gradient in dynamics typically associated with the broad T_g that follows the Keddie, Jones and Cory function form.[60] In addition, the recent fluorescence anisotropy measurements of Paeng and Ediger,[46,86,88] which measure the rotational reorientation time of dyes known to be sensitive to the segmental dynamics,

observed faster segmental dynamics attributed to the free surface in high MW (M_w = 1014 and 8991 kg/mol) freestanding PS films within the temperature range of the upper transition. It appears likely that the discrepancies between studies are caused by the various experimental techniques being sensitive to different dynamical populations with the film.[69,70] Interestingly, Baljon *et al*. has carried out molecular dynamics simulations on exceedingly thin low MW freestanding films, and found that $T_g(h)$ followed the high MW behavior of the lower transition when the film thickness was comparable to the chain size.[89]

The next most obvious question is "why have no previous studies on high MW freestanding films measured two simultaneous glass transitions?" The original BLS studies measured T_g on heating collecting data every 5–6 K and requiring 5–50 min at each temperature to obtain good signal-to-noise, with longer times needed at elevated temperatures as the intensity of the lowest longitudinal mode, S_0, decreased.[53,54] Hole formation becomes a significant concern when the film is held for extended periods of time near bulk T_g.[83] Thus, the original BLS measurements collected data on heating until the film was eventually destroyed due to hole formation and growth. In many instances, it seems likely that only a few data points would have been taken around the temperatures where a second transition would be expected. It appears that in most subsequent studies,[36,55,59,61–64] the authors focused their measurements on the narrow temperature range of interest around the anticipated transition temperature. In particular, this seems to be the case in the ellipsometry measurements by Dalnoki-Veress *et al*.,[55] which most closely match the measurements of the present study, based on their description of the

experimental procedure used. This includes measurements made by the Dalnoki-Veress group[58] after our results of two glass transitions in free-standing films were published.[66]

One exception is the Raman spectroscopy studies by Liem *et al*.,[61] which did collect measurements on high MW freestanding PS films at higher temperatures where a second transition might be anticipated. However, these studies focused on the Raman spectra of PS at ~1100 cm^{-1} which may be coupled to the vibrations corresponding to only one of the mechanisms. Similarly, the fluorescence intensity studies of Kim and Torkelson,[63,64] which measure the presence of only a single sharp transition in high MW freestanding PS films consistent with the lower MW dependent transition, appear to be biased towards the fastest dynamics. These authors have previously demonstrated that their fluorescence technique is primarily sensitive to the faster part of the glass transition distribution in supported PS films,[70] which exhibit a broad transition as observed by ellipsometry.[17] Thus, a similar bias by this technique towards the fastest mechanism is likely contributing in the freestanding measurements.

In the available literature, there exists only one dataset published that is clearly contradictory to our findings. Figure 2 from Mattsson, Forrest, and Börjesson[36] shows BLS data of the frequency shift of the S_0 mode as a function of temperature for a high MW (M_w = 767k) PS film of film thickness 46.6 nm. A reduced T_g of ~330 K is observed and measurements were extended to just above bulk T_g, a full 50 K above the reduced T_g. According to our findings, such a film should experience a second transition at ~355 K. However, Figure 2 of Ref. 36 clearly demonstrates that no second transition is observed. As BLS has been used to measure T_g reductions corresponding to both mechanisms,[36,53,54] this is puzzling. It may be possible that the frequency shift associated

with the lowest longitudinal S_0 mode is only sensitive to a single transition within the material, that a particular phonon mode may be coupled to only one of the mechanisms causing T_g reductions at a time, and that the break (or "kink") in compliance measured by this phonon mode is dominated by the fastest process therefore indicating only a single softening temperature

2.4 Summary

To date, no single theory has been able to capture the two qualitatively different $T_g(h)$ dependences.[37,77,78,80,81,90] Our results indicate that two separate mechanisms can propagate enhanced mobility from the free surface into the film simultaneously. Thus, we recommend that future theories incorporate more than one mechanism to explain the observed phenomena. We note that our results do not directly support any of the existing mechanisms that theorists have suggested for either the upper or lower transition.[37,77,78,80,81,90] Here, we simply articulate the experimental observations of both transitions that should be incorporated into future theoretical efforts. The upper transition appears to be present in *all* films, with $T_g(h)$ following the Keddie, Jones and Cory functional form. This mechanism acts uniformly across the entire free surface of the film causing a gradient in enhanced dynamics with depth that transitions to bulk-like dynamics across a length scale of several tens of nanometers.[24,36,48,64] This mechanism appears to control the dynamics of the majority of the film, effectively forming the matrix that dictates the compliance[65,87] and hole formation[83,84] properties. In contrast, the lower transition with a linear, MW dependent $T_g(h)$ appears to only be present in high MW freestanding films resulting in a small fraction of the material exhibiting extremely fast dynamics.

Chapter 3

Physical Aging in Ultrathin Supported Polystyrene Films

A version of this chapter was published as Pye, J. E.; Rohald, K. A.; Baker, E. A.; Roth, C. B. *Macromolecules* **2010**, *43*, 8296–8303.
http://pubs.acs.org/articlesonrequest/AOR-R9QUtaYUSsBmf6njiD9E

3.1 Introduction

In the twenty years since confinement effects on polymers were first reported, there has been much work exploring the deviations from bulk behavior of the glass transition temperature (T_g) and associated properties such as physical aging, diffusion, and modulus.[20,30,48,68–70,72,74,76,87,91–95] In recent years, a number of studies have investigated correlations between changes in physical aging rate, and time to reach equilibrium, with deviations of T_g in confined systems.[20,49,71,96–111] By definition, structural relaxation can only occur below T_g; thus, one would anticipate properties associated with physical aging to correlate with deviations in T_g. In some studies,[71,97–99,104,105] this has been found to be the case. However, most puzzling are studies, primarily from the gas permeation community, that indicate the length scale (film thickness) at which deviations in the physical aging rate occur can be much larger than the length scale at which deviations in T_g occur.[106–111] These results suggest that there are likely additional factors which influence the physical aging behavior beyond those that influence T_g in confined systems. These additional factors are explored more in Chapter 4 while a recent general review of physical aging studies in confined systems was given by Priestley in Ref. 20; thus, we highlight here only those studies pertinent to our

discussion. In the present chapter, we focus on changes in physical aging rates occurring near an interface on the length scale of tens of nanometers, which we believe are associated with corresponding changes in T_g. Our lab has also observed changes in physical aging rates at much larger, hundreds of nanometers, length scale for films quenched in a free-standing state.[112,113] We proposed that this effect is caused by stress being developed in the film during the thermal quench, which is thickness dependent in certain geometries.[112,113] The details of these results and this interpretation are contained in Chapter 4.

The majority of the investigations into the behavior of nanoconfined systems have focused on the glass transition. The deviations in T_g appear to be primarily associated with interfacial effects perturbing the dynamics rather than simply finite confinement of the material to nanometer-sized dimensions.[48,93,94,114–117] These interfacial effects are believed to lead to a gradient in dynamics emanating from the perturbing interface, with the material eventually returning to bulk-like behavior sufficiently far from the interface. The observations that a free surface can impart enhanced dynamics or that hydrogen bonding at a substrate interface can reduce mobility are not particularly surprising. What seems to defy understanding is the strength and depth of the perturbation in dynamics. In some cases, shifts in T_g of many tens of degrees have been observed[68,69,94] with interfacial perturbations propagating up to tens to hundreds of nanometers from the interface.[20,48,117]

That a gradient in enhanced dynamics could exist near a free surface was originally proposed by Keddie, Jones, and Cory,[30] who developed a semi-empirical fitting function, $T_g(h) = T_g^{bulk} [1 - (A/h)^{\delta}]$, for their T_g reductions in supported polystyrene (PS) films based on the idea of a liquid-like layer near the free surface. They assumed that the

length scale characterizing the mobile free surface layer exhibited a power law divergence at bulk T_g with the reduced film $T_g(h)$ occurring when this length scale became equal to that of the film thickness h. Others have modeled this variation in dynamics with depth using various layer models,[34–36,118] with some proposing a different functional form for the thickness dependent T_g reductions, $T_g(h) = T_g^{bulk} / (1 + h_0/h)$.[51,118–120] However, it was not until nearly a decade after the initial observations of T_g reductions in thin polymer films that Ellison and Torkelson[48] developed a unique fluorescence technique that could demonstrate experimentally that a gradient in T_g did exist near the free surface of PS. Surprisingly, these fluorescence multilayer measurements found that bulk-like dynamics are not recovered until 30-40 nm from the interface,[48] a depth significantly larger than anticipated. Recent computer simulations by Baschnagel and coworkers[51,120] have also observed a gradient in dynamics near the free surface, and theoretical efforts by Lipson and Milner[78] have modified Long and Lequeux's percolation model[77] to model a variation in T_g with depth due to free surface and substrate interactions. What causes the enhanced dynamics at a free surface to propagate to depths of several tens of nanometers from the interface is perhaps the most complex unresolved issue associated with confinement.

Although a length scale of tens of nanometers in polymer systems immediately conjures ideas of chain size and radius of gyration (R_g), T_g reductions in supported PS films have been tested and found to be unequivocally independent of molecular weight (MW).[32,33,92,121] The same T_g reductions for a given film thickness h are observed for PS films with MWs both above and below the critical MW for entanglement, and for R_g values comparable and much less than the film thickness. What seems to influence the

$T_g(h)$ behavior is the size and flexibility of the monomer unit and associated side group,[33,116,121,122] which suggests that cooperative segmental dynamics plays a role in this phenomenon. This cooperative motion idea is supported by a layer model analysis by Forrest and Mattsson[35,36] that fit their MW independent $T_g(h)$ reductions for low MW free-standing films using a layer model that allowed the thickness of the free-surface layer $\xi(T)$ with enhanced dynamics to vary with temperature in a manner similar to that anticipated for the size of the cooperatively rearranging region (CRR). A similar temperature dependence for the length scale quantifying the range of deviations in dynamics near the free surface was observed in computer simulations by Baschnagel and coworkers.[120] Studies have also demonstrated that T_g nanoconfinement effects can be reduced or completely eliminated by the addition of plasticizers,[52,123,124] which has been attributed to the plasticizer molecules reducing the cooperative nature of the dynamics.[52,123] However, careful studies by Torkelson and coworkers[33] and Vogt and coworkers[122] have yet to find a direct correspondence between T_g reductions in confined systems and the size of CRR.

Some physical aging studies have also found evidence for a gradient in dynamics occurring near a perturbing interface. Most notably, fluorescence multilayer measurements by Priestley, Torkelson, and coworkers[71] have shown a gradient in physical aging rate similar to that observed for T_g at both the free surface and substrate interface. However, their studies suggest that the length scale over which such perturbations propagate into the film may be larger than that observed for T_g changes.[71] Kawana and Jones[97] used ellipsometry to measure the overshoot of the expansivity-temperature curve (upon heating at 2 K/min) of ultrathin PS films that had been aged for

7 days at either 343 or 353 K. Studies of 10-200 nm thick films supported on silicon found no physical aging for 10 nm thick films that were aged below bulk T_g but above the reduced T_g of the film (consistent with observations made by fluroescence[98]). The authors interpreted the reduced intensity of the relaxation peak for thinner films as arising from the presence of a liquid-like layer at the free surface of order 10 nm, but they hypothesized that local structural relaxation would be depth dependent reflecting the gradient in T_g present in these films. Recent studies by Rowe *et al*.[104,105] have observed correlations between physical aging measured using gas permeation and T_g reductions for ultrathin polysulfone (PSF) films, and found that the size of free volume elements were different in the near surface region than in the interior of the film. In contrast, Koh and Simon,[99] who have used differential scanning calorimetry (DSC) to measure the enthalpy overshoots of stacked PS films for aging times out to 1000 min at temperatures down to T_g-15K, found that the physical aging rate of PS films at a fixed aging temperature decreased with decreasing film thickness, and that this decrease was consistent with a simple shift in the temperature dependence of the physical aging rate caused by a shift in T_g. The authors also investigated the time to reach equilibrium at a few degrees below T_g and found that thinner films reach equilibrium more quickly. This stacked film DSC technique has also been used by the Cangialosi, Boucher, Alegria, and Colmonero group, giving similar decreases in equilibration times for thinner films.[125]

In the present chapter, we have used a newly developed streamlined ellipsometry technique[23] to measure the temperature dependence of the physical aging rate of ultrathin supported PS films. The physical aging rate is determined from time dependent measurements of the film thickness quantifying the increase in average film density

during aging. A comparison of the temperature dependence of the aging rate between thick (2430 nm) and thin (29 nm) films reveals that the aging rate for the thinner films are not simply shifted to lower temperatures corresponding to the shift in the average T_g of these films. Instead, the physical aging rates are reduced at nearly all aging temperatures for PS films <100 nm thick. We find these results to be consistent with a gradient in dynamics present at the free surface, i.e., that the rate of structural relaxation varies with distance from the free surface. The temperature dependence of the reduced physical aging rates have been analyzed using a popular two-layer model, from which we extract a temperature dependent liquid-like layer at the free surface (of order 10 nm) that characterizes the depth dependence of the gradient in dynamics. We find the temperature dependence of this length scale to be very similar to that previously found to describe the film thickness dependent T_g reductions in these films, strongly suggesting that the enhanced dynamics at the free surface are responsible for both effects. In addition, we have analyzed our data in terms of a more realistic continuous distribution (gradient) in dynamics. In both the two-layer model and gradient model, we observe that the length scale that describes the depth to which the enhanced dynamics at the free surface propagate into the film grows with decreasing temperature bringing renewed support to the idea that the mechanism controlling this behavior involves cooperative motion of the segmental units.

3.2 Experimental

Polystyrene (Sigma-Aldrich secondary standard) with M_w = 245,000 g/mol, M_w/M_n = 2.0, as determined by GPC relative to PS standards,[23] was dissolved in toluene at concentrations from 1-15 wt%. PS films with thicknesses from 29 to 2700 nm were

formed by spin coating at 500–3000 rpm onto silicon substrates (~500 μm thick) that were precut into 2 cm square pieces. All supported PS films were subsequently annealed under vacuum at 393 K for at least 12 h to remove residual solvent and ensure a uniform sample history. Some of the thickest films (~2500 nm) were annealed under vacuum for up to 48 h, but these films produced identical experimental results to those obtained with films annealed for only 12 h. No evidence of dewetting was observed after annealing for any of the thick or thin PS films. The glass transition temperature for the PS used was 374 K as measured by DSC (T_g onset at 10 K/min on second heat after cooling at 20 K/min)[23] and 370 ± 2 K as measured by ellipsometry (T_g from film thickness on cooling at 1 K/min) based on an average of five samples ~2500 nm in thickness.

At the start of each physical aging measurement, the PS films supported on silicon were annealed in a glass petri dish above T_g at 403 K for 25-30 min to equilibrate the sample and erase all previous thermal history. The films were thermally quenched by removing them from the oven and placing the glass petri dish in thermal contact with a room temperature aluminum block for 60 s. This ensured a rapid (50 K/min), reproducible temperature quench of the sample through T_g. More recent work in our lab has shown that a faster quench leads to a faster physical aging rate, with the effect plateauing at high cooling rates.[113] The quenching protocol in this chapter provides consistent results, but a more explicitly controlled quench, ideally at a higher cooling rate, may be warranted in future work. Following the quench, the sample was immediately transferred to the ellipsometer hot stage (Instec heater) that was preset and stabilized (for ~30 min) at the desired aging temperature. The sample was quickly aligned on the ellipsometer (Woollam M-2000) and data collection initiated. Continuous measurements

of the ellipsometric angles Ψ and Δ as a function of wavelength λ at an angle of incidence of 65° were collected (averaging over a 30 s period) every 2 min for 360 min. The film thickness h and index of refraction n(λ) of the polymer film were determined by fitting the Ψ□λ□ and Δ□λ□ values for λ = 400–1000 nm to a layer model comprised of the polymer film, modeled as a Cauchy layer with $n(\lambda) = A + B/\lambda^2 + C/\lambda^4$, atop a silicon substrate with a 2 nm native oxide layer. The silicon substrate is modeled using a temperature dependent reference model included in the ellipsometry software package (CompleteEASE).

3.3 Results and Discussion

Physical aging rates β were calculated by plotting the normalized film thickness h/h_0 as a function of the logarithm of the aging time, as depicted in Figure 3.1. The value of h_0 corresponds to the thickness at an aging time of 10 min, when it is ensured that the sample has reached thermal equilibrium with the aging temperature. The slope of the linear decrease in film thickness as a function of the logarithm of the aging time characteristic of physical aging is evaluated by a single parameter fit with the data forced to pass through the first data point corresponding to an aging time of 10 min:[23]

$$\beta = \frac{-1}{h_0}\frac{dh}{d\log t} \tag{3.1}$$

Figure 3.1 shows data for a 2300 nm thick film with β = 10.5 x 10^{-4} and a 29 nm thick film with β = 7.7 x 10^{-4} aged at 338 K for 360 min. We have previously explored the use of different aging times and found that the physical aging rates obtained from data collected for 360 min are within experimental error of those obtained from data collected for 24 h of aging.[23]

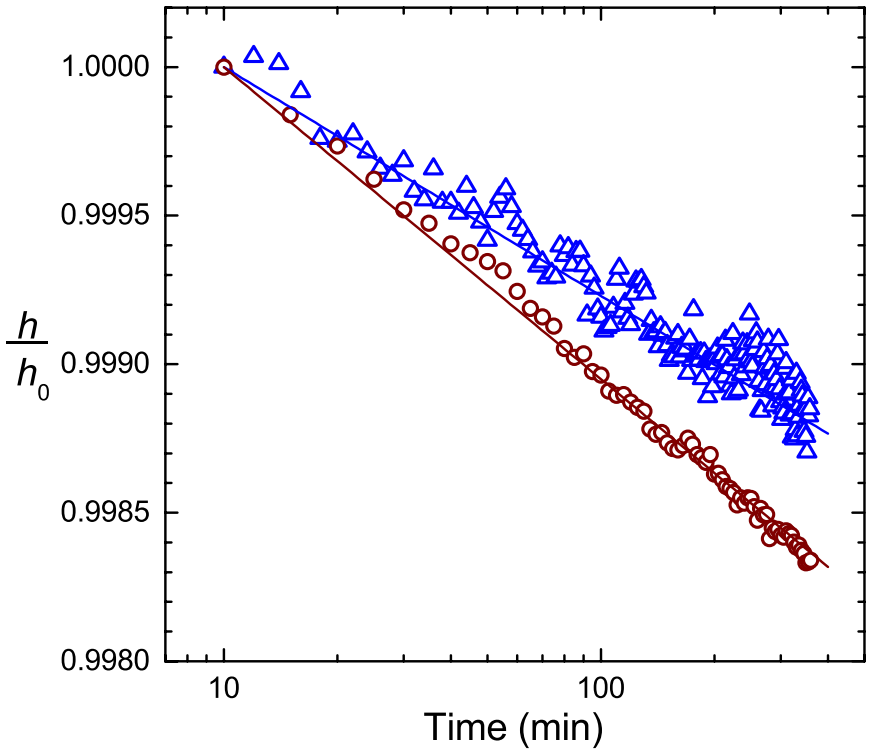

Figure 3.1: Normalized film thickness h/h_0, as a function of the logarithm of the aging time. Circles are data from a 2300 nm thick PS film with the best fit line corresponding to an aging rate β = 10.5 x 10^{-4}, and the triangles are data from a 29 nm thick PS film with a best fit aging rate of β = 7.7 x 10^{-4}.

Figure 3.2 examines the effect of film thickness on the physical aging rate of PS films supported on silicon. In this figure, all of the data have been collected at an aging temperature of 338 K corresponding to the peak in the temperature dependence of our measured aging rate for ~2500 nm thick films (plotted in Figure 3.3). Using ellipsometry, the thickest films we are able to reliably measure are ~2500 nm. For thicknesses beyond this, the oscillations in the Ψ and Δ data as a function of wavelength, and the difficulty associated with producing optically flat samples, degrades the fit to the layer model. The thinnest films we can reliably measure are ~30 nm. At this thickness the total change in film thickness over the entire 360 min aging run is < 0.1 nm (~0.3% change in film thickness). We recognize this change in thickness with aging time is exceedingly small

and that one might question the reliability of such a measurement. However, each data point shown in Figure 3.2 is an average of multiple measurements over 2-6 samples (more for the thinner films). In addition, we have performed control experiments on 30 nm thick films held above T_g in the equilibrium state and find that the measured film thickness is stable to within 0.011 nm over the course of the 360 min measurement, corresponding to a change in overall film thickness of <0.04%. Below ~30 nm, the difficulties associated with the inability of ellipsometry to independently resolve[16,126] h and n make the aging measurement problematic.

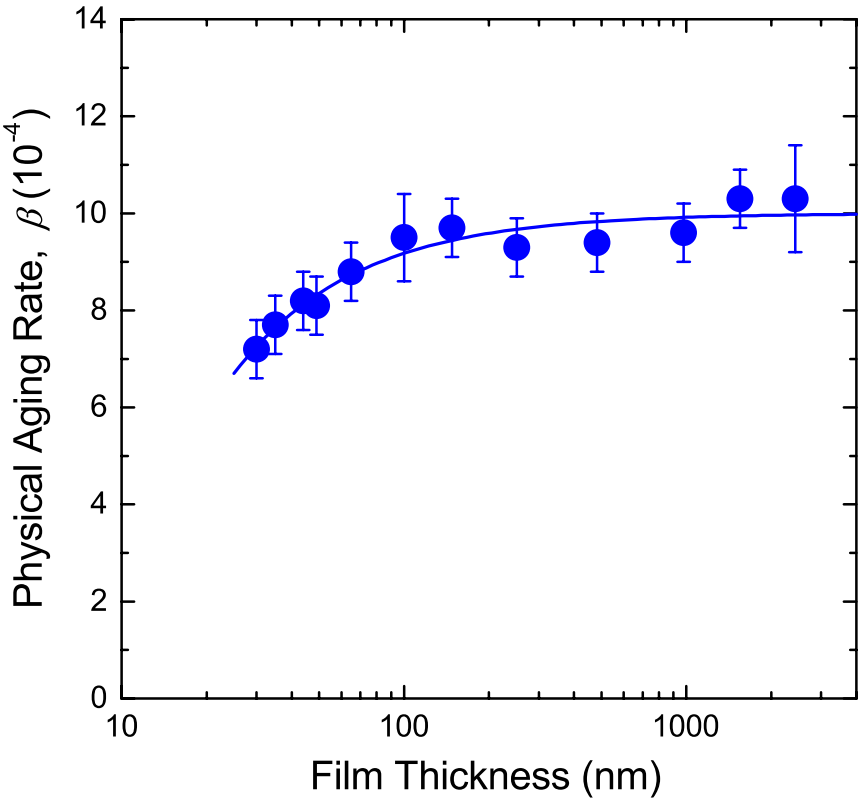

Figure 3.2: Physical aging rate β plotted as a function of film thickness for PS films supported on silicon for data collected at an aging temperature of 338 K over a period of 360 min. Each data point corresponds to an average of 2–6 samples. The curve is a best fit to Eq. 3.2 with $\beta_{bulk} = 10 \times 10^{-4}$ and $A = 8 \pm 1$ nm for this aging temperature.

The data shown in Figure 3.2 indicate that for PS film thicknesses ≥100 nm, the measured aging rate is independent of film thickness, while for films <100 nm in

thickness we see a progressive decrease in the physical aging rate. Because of the well-known reductions in T_g with decreasing film thickness that have been abundantly characterized for PS films supported on silicon for thicknesses less than ~100 nm,[69,92] our initial interpretation of the data shown in Figure 3.2 was that a shift in the temperature dependence of the aging rate to lower temperatures had occurred corresponding to the shift in T_g. In other words, the decrease in the aging rate for films with thicknesses <100 nm was associated with the peak in the aging rate no longer corresponding to 338 K. This would be consistent with recent observations in the research literature which used DSC to measure stacked PS films for aging temperatures down to T_g-15K,[99] and with those studies that have measured no physical aging for ultrathin PS films at aging temperatures below bulk T_g but above the reduced T_g of the film.[97,98]

To test this assumption, we measured the temperature dependence of the physical aging rate for 29 ± 1 nm thick PS films supported on silicon. Figure 3.3 compares the temperature dependence of the physical aging rate for 2430 ± 120 nm and 29 ± 1 nm thick PS films, both collected over an aging period of 360 min with β evaluated using Eq. 2.1. It is clear from the data that the physical aging rate for the thinner films is generally reduced at all temperatures, and has not simply shifted to lower temperatures as anticipated by the reduced average T_g of these films. The reduced physical aging rates imply that the percentage decrease in film thickness during the 360 min aging process is less for the thinner films.

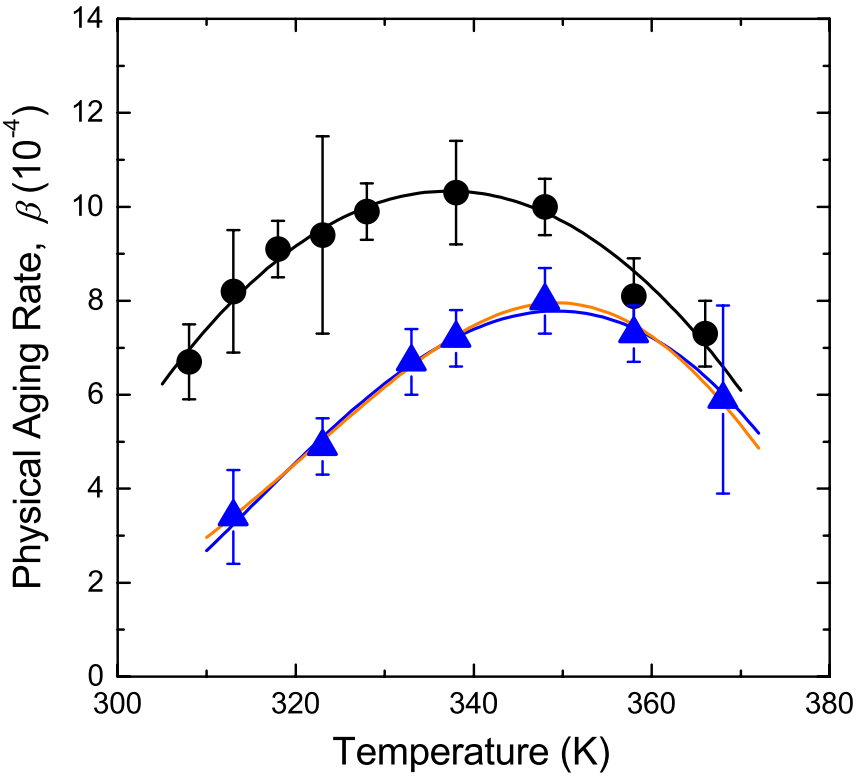

Figure 3.3: Temperature dependence of the physical aging rate β plotted for 2430 ± 120 nm thick PS films (filled circles) and for 29 ± 1 nm thick PS films (open triangles). Each data point corresponds to an average of 2-6 samples measured over an aging period of 360 min evaluated using Eq. 2.1. The curve through the ~2500 nm thick PS films is simply a second-order polynomial fit to parameterize the temperature dependence of the data, $\beta_{bulk}(T)$. The blue curve through the ~29 nm thick PS films is for Eq. 3.2 with $A(T)$ given by the best fit of Eq. 3.3 to the $A(T)$ data shown in Figure 3.4, while the orange curve is for Eq. 3.5 with $\lambda(T)$ given by the best fit of Eq. 3.3 to the $\lambda(T)$ data shown in Figure 3.4.

On first consideration, it may appear that the results presented in Figure 3.2 and Figure 3.3 are not consistent with the fluorescence measurements by Priestley *et al.* which found no change in the physical aging rate between 500 nm and 20 nm thick PS films supported on silica measured over an aging period of 80 min at 305 K.[98] However, the pyrene fluorescence studies by Ellison and Torkelson,[48] which demonstrated the T_g gradient in PS films as a function of depth from the free surface, also found that films thinner than 25 nm can no longer support a gradient in the T_g dynamics. Thus, significant differences in the film dynamics may exist between 20 and 30 nm thick films.

Unfortunately, we are unable to reliably measure films less than ~30 nm with ellipsometry.

Numerous studies presented in the research literature have demonstrated that the *average* T_g of 30 nm thick PS films are reduced from the bulk value by 5–10 K.[69,92] It is clear that the results of Figure 3.3 are *not* consistent with the thinner films having simply a single T_g value reduced from the bulk, since that would be observed as a simple shift in the temperature dependence of the bulk aging rate in Figure 3.3 to lower temperatures by 5–10 K. What is most peculiar is that we observe physical aging of 29 ± 1 nm thick PS films at an aging temperature of 368 K, only a few degrees below bulk T_g. This indicates that some portion of the ~30 nm thick films must be in the glassy state, which would be consistent with these films having a gradient in T_g dynamics across the thickness of the film, as has been measured experimentally using fluorescence.[48] The large error bar associated with this data point arises from the small variation in film thickness between the measured films. At an aging temperature of 368 K, very close to bulk T_g, the measured aging rate is very sensitive to film thickness. The five films measured at 368 K that gave an average aging rate of $(5.9 \pm 2.0) \times 10^{-4}$ are: 30.0 nm with $\beta = 8.2 \times 10^{-4}$; 29.0 nm with $\beta = 5.9 \times 10^{-4}$; 28.3 nm with $\beta = 7.2 \times 10^{-4}$; 28.2 nm with $\beta = 5.2 \times 10^{-4}$; and 27.3 nm with $\beta = 2.9 \times 10^{-4}$.

We now demonstrate that the results of Figure 3.2 and Figure 3.3 are consistent with a gradient in T_g dynamics across the thickness of the film. One can envision modeling a gradient in T_g dynamics by dividing a 30 nm thick film into six layers of 5 nm each, with each layer exhibiting its own T_g and aging rate β. The bottom-most layer next to the substrate interface would exhibit nearly bulk-like properties,[48] while the top-most

layer next to the free surface would exhibit nearly liquid-like properties.[48,71] It is reasonable to assume that the region of the film immediately next to the free surface does not undergo any physical aging because its local T_g, much reduced from the average film T_g, would be lower than the aging temperature. However, ellipsometry is only able to measure a single average β value across the entire thickness of the film. Thus, with a single measured parameter, the most sophisticated layer-type model we are able to interpret is a simple two-layer model with a liquid-like layer at the free surface that does not undergo any physical aging at the aging temperature and a bulk-like aging layer underneath. Such a two-layer model gives rise to a simple parameterization for the data:

$$\beta(h,T) = \beta_{\text{bulk}}(T)\frac{1-A(T)}{h} \tag{3.2}$$

where our single measured parameter can be used to comment on the liquid-like layer thickness $A(T)$ that characterizes the depth from the free surface that the enhanced mobility persists. Numerous other studies with similar limitations have interpreted their data in this manner, obtaining a liquid-like layer thickness of 5–10 nm at the free surface of PS.[30,35,36,97] However, all these studies have also remarked that although the analysis is performed with a simple two-layer model, it is far more likely that the change in dynamics across the thickness of the film occurs uniformly as a gradient in dynamics as a function of depth.[48,51,71] This point should not be forgotten.

A fit of Eq. 3.2 to the $\beta(h)$ data presented in Figure 3.2 at an aging temperature of 338 K, gives best fit values of $\beta_{\text{bulk}} = 10 \times 10^{-4}$ and a liquid-like layer thickness of $A = 8 \pm 1$ nm, which is independent of the overall film thickness. The data in Figure 3.2 are well fit by the simple two-layer model, and provide a liquid-like layer thickness consistent with previous work.[30,35,36,97] To determine if this analysis is consistent with the physical

aging rates measured over the range of temperatures shown in Figure 3.3, we parameterize the $\beta_{bulk}(T)$ data in Figure 3.3 by fitting the 2430 ± 120 nm thick films to a second-order polynomial and use it to extract $A(T)$ values from the $\beta(T)$ data for the 29 ± 1 nm thick films shown via Eq. 3.2. This surface layer thickness $A(T)$ is plotted in Figure 3.4.

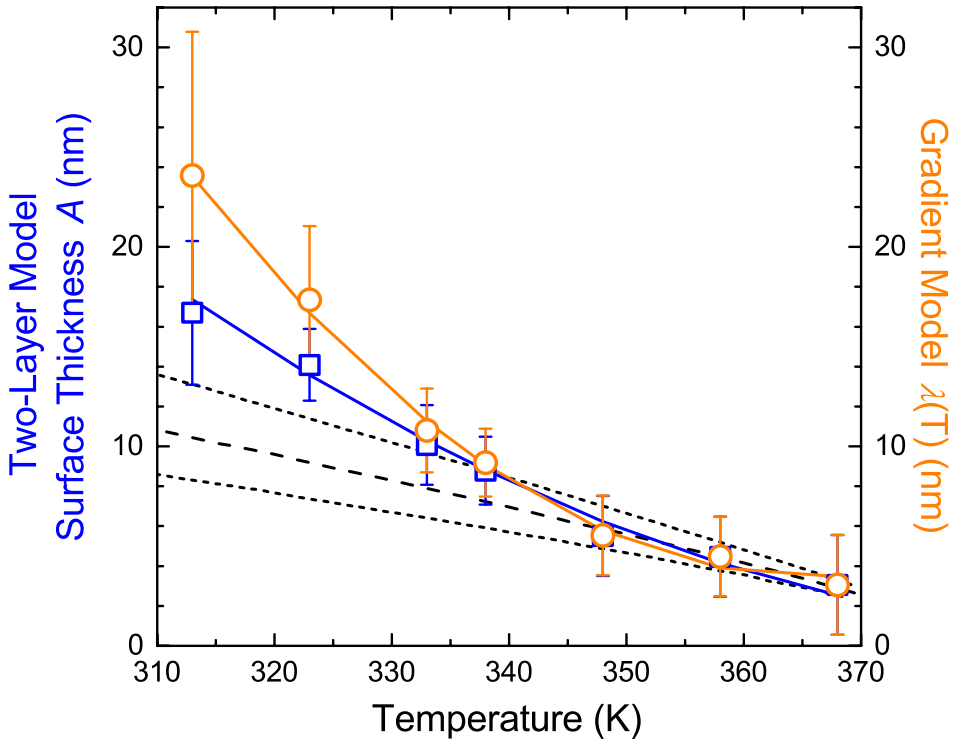

Figure 3.4: Squares correspond to the temperature dependence of the surface layer thickness $A(T)$ for the two-layer model, determined using Eq. 3.2 from the $\beta(T)$ data for the 29 ± 1 nm thick PS films, while the solid curve is a best fit of Eq. 3.3 to the data. The dashed and dotted curves represent the range of surface layer thickness $A(T)$ values obtained by Forrest and Mattsson[35,36] using a similar two-layer model analysis from T_g measurements on low MW free-standing PS films. Circles correspond to the temperature dependence of the characteristic length $\lambda(T)$ for the gradient model, determined using Eq. 3.5 from the $\beta(T)$ data for the 29 ± 1 nm thick PS films, while the solid curve is a best fit of Eq. 3.3 to the data. See text for details of the best fit parameter values.

From the $A(T)$ data plotted in Figure 3.4, it is immediately apparent that the effective surface layer thickness increases with decreasing temperature starting from ~3 nm just below bulk T_g. This may initially appear counter intuitive, but has been

previously observed by Forrest and Mattsson[35,36] who performed a similar layer-model analysis of their $T_g(h)$ data for free-standing low molecular-weight PS films. We note that the *low* MW free-standing film data exhibit the same functional form for $T_g(h)$ as supported films with no MW dependence; the only difference being that for free-standing films, the T_g reduction for a given film thickness h is equivalent to that of a supported film of thickness $h/2$ because of the presence of two free surfaces.[35,36,68,69] This is in contrast to the $T_g(h)$ data for *high* MW free-standing films which exhibit a qualitatively different behavior with a strong MW dependence.[68,69] For comparison, we include dashed- and dotted-lines in Figure 3.4 (from Ref. 36) depicting the range of their calculated values for the surface-layer thickness. Given that their values were obtained from T_g measurements on free-standing PS films using Brillouin light scattering[36] and ours were obtained from physical aging measurements on supported PS films using ellipsometry, the agreement is quite remarkable. The similarity also strongly suggests that our reduced physical aging rates observed for PS films <100 nm thick are related to the T_g reductions observed in these films.

How should this growing surface-layer thickness $A(T)$ with decreasing temperature be interpreted? $A(T)$ represents, in some (unfortunately) ill-defined manner, the depth to which the enhanced free-surface mobility propagates into the film. Recent computer simulations by Baschnagel and coworkers[51,120] have observed that the length scale over which the enhanced dynamics at the free surface transition continuously into bulk-like dynamics increases with decreasing temperature, consistent with this observation. Forrest and Mattsson[35,36] related the temperature dependence of the surface-layer thickness to the temperature dependence of the cooperativity length $\xi(T)$ suggesting

that the propagation of enhanced mobility from the free surface may be correlated with cooperative motion. Although this is an appealing idea, it is not clear that T_g-nanoconfinement effects correlate directly with the cooperativity length scale.[33,121,122]

Following Forrest and Mattsson,[35] we fit the temperature dependence of our surface-layer thickness $A(T)$ to a functional form for $\xi(T)$ proposed by Donth and coworkers:[127–129]

$$A(T) = \xi(T) = r_0 + \alpha(T_{ons} - T)^{\gamma} \quad (3.3)$$

The characteristic length $\xi(T)$ grows with decreasing temperature starting from an onset temperature for cooperative motion T_{ons} (in the vicinity of the $\alpha\beta$ splitting region), with a minimum $\xi(T_{ons})$ size of r_0 assumed to be one monomer diameter[129] (for PS, Forrest and Mattsson[35] took r_0 = 0.6 nm). For bulk PS, T_{ons} is estimated[35,36,127,128] to be 463 ± 15 K, ~90 K above T_g. The power-law dependence of $\xi(T)$ is characterized by two fitting parameters α and γ. A possible estimate γ is 2/3, based on data by Kahle *et al.*[128] of the number of particles for N_α per cooperatively rearranging region estimated from modulated DSC measurements of poly(n-butyl methacrylate-stat-styrene) copolymers. However, the plot suggesting $N_\alpha \sim (T_{ons} - T)^2 \sim V_\alpha \sim \xi^3$ is over a limited temperature range of only 25 K. Our data cannot be adequately fit with a value of γ near 2/3. Forrest and Mattsson[35] obtained best fit values of γ = 2.0 ± 0.1, α = (2.95 ± 0.30) x 10^{-3}, and T_{ons} = 485 ± 6 K, holding r_0 fixed at 0.6 nm. Using the temperature dependence of Eq. 3.3 for their free surface layer, Forrest and Mattsson also obtained an effective T_g for their surface layer by fitting their average film $T_g(h)$ data for low MW free-standing films to a three-layer model comprised of two outer layers of thickness $\xi(T)$ with T_g^{surf} and an inner layer of thickness $h - 2\xi(T)$ with T_g^{bulk} (see Figure 6 of Ref. 36) giving a value of T_g^{surf} =

300 ± 7 K.[35] We have fit Eq. 3.3 to our $A(T)$ data presented in Figure 3.4 with r_0 and γ fixed at the values obtained by Forrest and Mattsson,[35] r_0 = 0.6 nm and γ = 2, obtaining best fit values of $\alpha = (2.4 \pm 1.0) \times 10^{-3}$ and $T_{ons} = 396 \pm 13$ K. Allowing γ or r_0 to vary did not substantially improve the fit or alter the parameters. If we assume that T_g occurs approximately 90 K below the onset of cooperative motion T_{ons}, then this would suggest a T_g for our surface layer of $T_g^{surf} \approx 306$ K, in the same temperature range previously estimated by Forrest and coworkers.[35,36] Although this agreement with previous estimates of a surface T_g is intriguing, we hesitate to attach undue weight to this particular form of Eq. 3.3, as the $A(T)$ data could be equally well described by other functional forms. Several functional forms for the temperature dependence of the cooperative length scale $\xi(T)$ have been proposed, as described in Refs. 130 and 131. We should note that Forrest and coworkers[39] have also recently applied this similar type of analysis to nanoparticle embedding measurements and obtained reasonable agreement with the results presented in Figure 3.4.

To demonstrate that this temperature dependence of $A(T)$ describes the observed $\beta(T)$ values for the ~29 nm thick PS films, we include in Figure 3.3 the curve corresponding to $\beta(T)$ from Eq. 3.2 with $A(T)$ given by Eq. 3.3. This analysis demonstrates that the temperature dependence of the physical aging rate for the $h \approx 29$ nm thick PS films shown in Figure 3.3 is consistent with the presence of a gradient in dynamics as a function of depth from the free surface. In addition, this analysis indicates that the depth to which the enhanced dynamics penetrate into the film from the free surface increases with decreasing temperature suggesting that the mechanism for the propagation of enhanced dynamics from the interface is related to cooperative motion.

Alternatively, we can fit our data to a more realistic gradient-type model that more accurately represents the continuous change in dynamics with depth. A reasonable (simplest) approach would be to assume a single exponential decay of the aging rate from zero at the free surface to its bulk value, $\beta_{bulk}(T)$, at a depth z sufficiently far from the free surface:

$$\beta(z,T) = \beta(T)\left[1 - e^{-z/\lambda(T)}\right] \tag{3.4}$$

This would define a characteristic length scale $\lambda(T)$ that would describe the depth to which the enhanced dynamics at the free surface propagate into the film. We believe that such a definition of $\lambda(T)$ has a more well-defined meaning than the $A(T)$ parameter describing a "liquid-like" layer size of the somewhat artificial two-layer model. The general functional form of Eq. 3.4 is supported by the fluorescence multilayer measurements of Priestley *et al.*,[71] and by a more recent observation indicating that no physical aging occurs at a free surface.[132] We note that there is a much more solid basis in the literature for a gradient in T_g with depth. While we have already shown that a simple shift of the temperature dependence of the *average* physical aging rate $\beta(h,T)$ to lower temperatures corresponding to the *average* reduced $T_g(h)$ for thin films does not occur, a similar shift may occur for the *local* aging rate $\beta(z,T)$ at a given depth z due to the reduced *local* T_g at that depth $T_g(z)$.

From Eq. 3.4, we define the average, experimentally measured, film thickness dependent aging rate as the arithmetic mean:

$$\beta(h,T) = \frac{1}{h}\int_0^h \beta(z,T)dz = \beta_{bulk}(T)\left\{1 - \frac{\lambda(T)}{h}\left[1 - e^{-h/\lambda(T)}\right]\right\} \tag{3.5}$$

Lipson and Milner[78] have recently discussed whether or not such a "democratic" average, versus perhaps a weighted average, is the most appropriate. Baschnagel and coworkers[51]

have also remarked that even though the average $T_g(h)$ of the film may be a simple arithmetic mean, this does not imply that other quantities, such as the average relaxation time of the film, are also a simple average of the local depth dependent values. However, without a specific reason to try something more complicated, we proceed here with the simplest definition. Nevertheless, it is worth keeping in mind that different experimental techniques may average across the distribution in dynamics in a different manner.[70]

The $\lambda(T)$ data shown in Figure 3.4 were obtained from the $\beta(T)$ data for the 29 ± 1 nm thick films via Eq. 3.5 in a manner similar to how the $A(T)$ data were obtained from Eq. 3.2. In Figure 3.4, the $\lambda(T)$ data are fit to $\lambda(T) = \xi(T)$ given by Eq. 3.3, and the dashed curve in Figure 3.3 corresponds to $\beta(h$=29nm,$T)$ for the $\lambda(T)$ data. The best fit parameters of $\lambda(T) = \xi(T)$ to Eq. 3.3 were $\alpha = (7.1 \pm 4.4) \times 10^{-3}$, $T_{ons} = 366 \pm 13$ K, and $r_0 = 3.4 \pm 2.0$ nm with $\gamma = 2$ fixed. We note that the errors for the $\lambda(T)$ data and the corresponding fit parameters are larger than for the $A(T)$ data and, therefore, do not assign any significant weight to their specific values other than to parameterize the data. It is also worth noting that Eq. 3.5, the $\beta(h,T)$ for the gradient model, reduces to Eq. 3.2, the $\beta(h,T)$ for the two-layer model, when the film thickness is large (i.e., $h \gg \lambda$). This explains why the $\lambda(T)$ and $A(T)$ values overlap for the higher aging temperatures (see Figure 3.4) when $\lambda(T) <$ ~10 nm, sufficiently less than the $h \approx 29$ nm film thickness. Both $\lambda(T)$ and $A(T)$ are of order 10 nm and increase with decreasing temperature. These two parameters are not significantly different, but simply illustrate two different methods of characterizing the depth to which the enhanced dynamics at the free surface propagate into the film.

Here we have demonstrated for the first time that the temperature dependent length scale characterizing the depth to which enhanced dynamics are propagated from

the free surface of PS is the same for both reductions in the physical aging rate and reductions in T_g, strongly suggesting that both effects are caused by the same mechanism. This mechanism appears to be responsible for both the MW independent $T_g(h)$ reductions observed in supported PS films[30,32,33,48,69] and the MW independent $T_g(h)$ reductions of *low* MW free-standing PS films,[35,36,68] which are both qualitatively similar, following the Keddie, Jones and Cory[30] functional form. (This is in contrast to *high* MW free-standing films which exhibit a qualitatively different $T_g(h)$ behavior with a strong MW dependence as discussed in Chapter 2.[68,69]) This mechanism manifests as a gradient in enhanced dynamics near a free surface that propagates into the film for some distance before bulk-like dynamics are recovered. We have observed that the length scale characterizing this gradient in dynamics grows with decreasing temperature bringing renewed support to the idea that the mechanism that propagates the enhanced dynamics from the free surface is related to cooperative motion of the segmental units.

The fact that the length scale of the effect grows with decreasing temperature may explain some discrepancies in the research literature pertaining to the size of the near surface region that exhibits enhanced dynamics. For instance, studies of surface mobilities at elevated temperatures near bulk T_g or when more liquid-like properties are probed tend to observe enhanced dynamics to a depth of only a few nanometers.[39,43] In contrast, fluorescence multilayer measurements by Torkelson and coworkers have indicated that bulk-like dynamics are not recovered till depths of 30-40 nm from the free surface of PS.[48] Both of these results are consistent with our observations. As shown in Figure 3.4, the characteristic length describing the depth to which the enhanced dynamics propagate from the free surface is only a few nanometers near bulk T_g, but grows to

approximately 15-20 nm for temperatures 50-60 ^{o}C below bulk T_g. At the temperatures at which the Torkelson fluorescence measurements observe a reduced T_g of the PS surface,[48] T_g^{bulk} - 32 K ≈ 67 K, our characteristic length $\lambda(T)$ for the exponential decay of the enhanced dynamics near the free surface is ~8 nm. For a single exponential decay that forms the basis of Eqs. 3.4 and 3.5, four to five characteristic length λ's, i.e. 32-40 nm, would be necessary before the dynamics would appear bulk-like (to within experimental error). However, we note that these results do not agree with the extremely large length scale effects observed by the gas permeation community[106–111] that find differences in physical aging rates for film thicknesses of several microns. Because no corresponding T_g changes are observed at micron length scales, this suggests that other, unrelated effects may be the cause of those results. A stress related explanation is tested and confirmed for free-standing PS films in Chapter 4. Another open question is whether or not confined systems age to the same equilibrium state as that of bulk. It is clear that the rate at which structural relaxation occurs in confined geometries is frequently different and does not necessarily correlate with T_g changes,[133,134] but there is also evidence[96] that when equilibrium can be reached, it is not the same equilibrium state as that of bulk.

3.4 Conclusions

Using ellipsometry, we have measured the temperature dependence of the physical aging rate for thick (2430 nm) and ultrathin (29 nm) PS films supported on silicon. We find that the thinner films have reduced physical aging rates at nearly all temperatures, a result that does not correspond simply to the shift in the average T_g of these films. The reduced physical aging rates of these films are consistent with a depth

dependent gradient in dynamics that is approximated by a two-layer model with a nearly liquid-like surface layer of order 10 nm. The thickness of the surface layer, which characterizes the depth to which the enhanced mobility at the free surface penetrates into the film, grows with decreasing temperature suggesting that the mechanism for the propagation of enhanced dynamics from the interface is related to cooperative motion. Our physical aging measurements using ellipsometry on ultrathin supported PS films can be explained with an analysis similar to that used by Forrest and Mattsson[35,36] for T_g measurements using Brillouin light scattering of low MW free-standing PS films, strongly suggesting that the reduced physical aging rates observed in PS films <100 nm thick are related to the T_g reductions observed in these films. We also present an analysis in terms of a gradient model that more realistically characterizes the continuous distribution in dynamics believed to exist at the free surface of these films.

3.5 Addendum

Since these results were published as a paper in *Macromolecules* in 2010,[24] the main result of reduced physical aging rates in ultrathin films has been replicated by Peter Green's group at the University of Michigan.[135] They used the same streamlined ellipsometric method developed earlier in our lab,[23] and used in this chapter, to collect physical aging data of linear and star shaped PS. They found reduced physical aging rates for thinner films of both linear and 8-arm star PS (with both 10 kg/mol and 25 kg/mol arm lengths) and measured the same temperature dependence of β for their linear PS.

Our method of defining an increasing length scale to which the enhanced mobility at the free surface penetrates into the film has been an important finding in linking

confinement to cooperativity length scales and dynamic heterogeneity.[136,137] In contrast with this view, several subsequent measurements have shown the enhanced dynamics from the free surface in polymer films to increase in length scale when the temperature is *increased*. Measurements that show an increasing length scale with *increasing* temperature include particle embedding,[39] surface flow on a molecular glass,[138] modulus measurements,[139] and segmental relaxation detected *via* dye reorientation.[46] The difference in temperature dependence is striking, but not that unexpected when one considers the properties actually being probed. In Refs. 39,46,135,138, the measurements are determining at what length scale the material is fully liquid like, or alternatively, at what depth the material no longer relaxes *at a given rate or time*. Simulations,[51,120] some T_g measurements,[35,36] and the present physical aging measurements[24] instead determine the depth to which the dynamics *deviate from bulk*. The first length scale will, *by definition*, diverge as you increase the temperature, regardless of what the temperature dependence of the surface dynamics is, because at some temperature the whole sample must be liquid like. There are two very recent attempts at quantifying this difference in definition for the length scale associated with enhanced free surface dynamics.[28,136]

Chapter 4

Physical Aging of Thin Free-Standing Polystyrene Films: Stress Effects

A version of this chapter was published as Pye, J. E.; Roth, C. B. *Macromolecules* **2013**, *46*, 9455–9463.
http://pubs.acs.org/articlesonrequest/AOR-pzVUZ8SFnzxG7CRdFx5d

4.1 Introduction

The non-equilibrium nature of glasses results in materials whose mechanical, electrical, and optical properties evolve with time as the system slowly relaxes towards equilibrium, a process referred to as structural relaxation or physical aging. Understanding how physical aging of polymer glasses is affected by thermal and processing histories in thin films is crucial for applications ranging from gas separation membranes to barrier and dielectric layers.[20,140] During the past 18 years, a number of studies have reported "accelerated" or faster physical aging of free-standing polymer films with decreasing thickness.[106–110,113,125,141] These deviations from bulk properties have been observed at surprisingly large length scales when films are still hundreds to thousands of nanometers in thickness. This is in contrast to changes in physical aging observed in films less than ~100 nm in thickness[24,71,97–99,102,104,135] that have been linked to changes in the glass transition temperature (T_g).[66,69] Previous studies have interpreted the cause of the accelerated aging at the longer length scales as some inherent film thickness dependence associated with glassy dynamics by fitting the data to a free volume diffusion model with lattice contraction.[100,108,111,125,142,143] More recently, Gray et al. proposed an alternative explanation suggesting that the accelerated aging may result

from increased stress imparted to the films by their mechanical support.[113] Here, we present results that demonstrate there is no inherent film thickness dependence (above 220 nm) to the aging rate of free-standing polystyrene (PS) films when held by rigid frames that impart a thickness-independent stress on cooling.

Accelerated physical aging of thin polymer films was first characterized by gas permeation measurements.[106–109,141] As a function of aging time, the gas permeability of the films, which is extremely sensitive to free volume in the membranes, was found to decrease more rapidly for thinner films. Although it is not straightforward to determine a physical aging rate from permeability data,[111] McCaig and Paul[108,142] interpreted their results in terms of a free volume diffusion and lattice contraction model originally developed by Curro et al.[144] This model proposes a microscopic interpretation for volume recovery that treats vacancy propagation as an effective diffusion of local free volume. The only adjustable parameter is a somewhat arbitrary diffusion length scale that defines the characteristic relaxation time.[144] To avoid a dependence of T_g and physical aging rate on the macroscopic size of the sample, Curro et al. suggested that some "internal length scale" might exist over which free volume can be created or annihilated. To date, the existence of such "internal interfaces" has not yet been definitively determined.[125] Following an idea originally proposed by Alfrey et al.[145] where free volume 'holes' that diffuse to the surface of a sample would disappear, McCaig and Paul[108,142] related the diffusion length scale to the macroscopic thickness of their free-standing films. Such a model was found to fit the data remarkably well and has since been adapted by others to explain accelerated aging behavior observed in thin films by positron annihilation lifetime spectroscopy (PALS),[100,105,143] differential scanning

calorimetry,[125] dielectric spectroscopy,[100] ellipsometry and gas permeation.[111,143,146] Similar ideas have also been applied to accelerated aging observed in polymer nanocomposites where possible voids at the nanofiller interface are assumed to contribute to the internal interfaces at which free volume can be annihilated.[147,148] In many of these studies, this internal length scale is treated as a fitting parameter with values typically being several microns in size.[100,125,143,147,148] Recently, Rowe et al.[105] have used variable energy PALS to measure the local free volume as a function of depth near the free surface. Although the size of the free volume "holes" were found to be reduced near the free surface, the size and number of holes maintained a constant depth profile with aging time in contrast to what would be anticipated based on the free volume diffusion model.[142] Overall, these studies argue the key to accelerated aging is the presence of free surface or internal interface at which free volume can be annihilated or created, implying an inherent film thickness dependence to physical aging.

More recently an alternative explanation has been proposed to account for the accelerated physical aging behavior observed in micron thick films. Gray et al.[113] observed that the thickness-dependent accelerated aging was only present for films that were quenched free-standing on thin wire frames mimicking the sample preparation of the gas permeation studies.[141] It was proposed that these wire frames (made of 0.009 in. diam. spring steel) flexed, acting as small springs imparting a stress, $\sigma = Force/Area$, to the samples that depended on the cross-sectional area of the films (film thickness × width), such that the stress increased with decreasing film thickness.[113] This is in contrast to free-standing films supported by inflexible rigid frames which impart a thickness-*independent* stress to the films on cooling that depends on the thermal expansion

mismatch between the polymer films and rigid frame (as calculated below). Such stresses on free-standing films supported by rigid frames caused by thermal expansion mismatch are equivalent to the well-documented and experimentally measured[149–151] stresses experienced by supported polymer films on rigid substrates (e.g., silicon). For PS on silicon the difference in thermal expansion coefficients is roughly two orders of magnitude resulting in stress values of ~15 MPa when cooled to room temperature, consistent with experimental measurements.[149,150] The idea of stress during the thermal quench affecting the subsequent aging of the glass is supported by work on ortho-terphenyl confined to nanoporous glasses,[96] polymer nanospheres,[152] and from observations that the aging rate is independent of film thickness for supported films above ~100 nm in thickness.[24,113]

In this chapter, we present results strongly suggesting that unintended stresses during thermal cooling from differences in thermal expansion between film and support can strongly affect the subsequent physical aging behavior of micron thick free-standing glassy films. To accomplish this, we have developed a method of measuring the volumetric physical aging rate of polymer films that have been quenched and remain free-standing during the aging process. To our knowledge, this is the first report of in-situ physical aging measurements by ellipsometry on films that remain in their free-standing state during the aging process. Free-standing films held by rigid frames are used to impart a well-defined and film-thickness-independent stress to the films during the thermal quench. The time dependent decrease in thickness and increase in index of refraction resulting from the densification of the films as a function of aging time was measured by transmission ellipsometry. For films between 220 and 1800 nm in thickness,

we observe no change in physical aging rate as a function of film thickness for films held by stainless steel (SS) frames with a circular opening. This is consistent with the thickness-independent in-plane stress of $\sigma \approx 4.5$ MPa imparted to the films during the thermal quench to an aging temperature of 65 °C, caused by thermal expansion mismatch between PS and the SS frame. We establish that this stress affects the physical aging rate and verify its source by demonstrating that the aging rate of PS correlates with the stress caused by thermal-expansion mismatch between film and rigid support for a series of different frame materials: polycarbonate (PC), polysulfone (PSF), aluminum (Al), stainless steel (SS) and silicon (Si).

4.2 Experimental

Films were made by spin-coating PS (M_w = 3,240 kg/mol, M_w/M_n = 1.05, Polymer Laboratories) dissolved in toluene onto silicon or freshly cleaved mica. Film thickness was controlled by adjusting the spin speed and solution concentration. Films were typically spun at speeds between 600 and 1000 rpm; no effect of spin speed on aging was observed even for films spun at 4000 rpm. All films were annealed for at least 12 hours at 130 °C under vacuum to remove residual solvent and relax stresses induced during spin-coating, and then cooled slowly on mica at < 0.5 ^{o}C/min through T_g. Free-standing films were produced by floating onto polycarbonate (PC) (RowTec), polysulfone (PSF) (Tecason S), 6061 aluminum (Al), 304 stainless steel (SS), or Si (<100> orientation) frames with a 5 mm diameter circular opening. To initiate the aging measurements, PS films were rejuvenated for 20 min at 120 °C before quenching to room temperature at 90 °C/min in the free-standing state using an Instec hot stage with liquid nitrogen cooling. The Instec hot stage has a small interior chamber (50 mm in length × 38 mm in width × 2

mm in height) giving only 3.8 cm^3 volume of air surrounding the free-standing film that needs to be heated or cooled. As discussed in Gray et al.[113] heat transfer to thin free-standing films from the surrounding air is very efficient. The free-standing film is oriented horizontally in the chamber with the cover containing a window such that the film can be viewed during the annealing step. Shortly after heating above T_g surface tension acts to smooth out wrinkles after which the film remains flat. Rapid cooling of the film is achieved by pumping liquid nitrogen through the heater base. Using an external thermocouple mounted to the sample, we have measured this to be 90 ^oC/min. Immediately after quenching, films were transferred to another heater that had been equilibrated at the aging temperature for at least 30 min. The time from the beginning of the quench to the start of the aging measurement was kept as short as possible (~4 min). Measurements were performed with a J.A. Woollam M-2000 ellipsometer in transmission and reflection geometry for free-standing and supported films, respectively. Free-standing films were held at an angle of 45° with respect to the beam and modeled by a single Cauchy layer with $n(\lambda) = A + B/\lambda^2 + C/\lambda^4$ for λ from 400 to 1000 nm.[66] Supported films were measured at 65° angle of incidence and modeled as a Cauchy layer on top of a silicon substrate (with temperature dependent optical properties) and a 2 nm native oxide layer.[24]

4.3 Results and Discussion

4.3.1 Physical Aging of Films Quenched and Measured Free-standing via Ellipsometry

Previous efforts in our lab to test the impact of stress imparted to films during the thermal quench caused by differences in thermal expansion mismatch were hampered by

excessive wrinkling and buckling of the free-standing films limiting reproducability.[113] For the present study, we have made three key improvements to our experimental procedure that prevent wrinkling of the films: smaller samples sizes (5 mm diam. instead of 19 mm), a more controlled quench environment that minimizes air currents and has a controlled quench rate of 90 °C/min, and measurement of the aging rate in the free-standing state via transmission ellipsometry such that the films do not need to be transferred to silicon substrates for the subsequent aging. These changes enable the measurement of reproducible physical aging rates for free-standing films quenched on rigid frames where the stress imparted by thermal expansion mismatch between the film and frame can be explicitly calculated.

Figure 4.1 plots the normalized film thickness (h/h_0) as a function of logarithmic aging time for several 515 ± 10 nm thick free-standing PS films draped across SS frames with a circular opening aged at different temperatures. We quantify the physical aging rate by calculating the slope of the data plotted in this manner: $\beta = -\partial(h/h_0)/\partial(\log t)$, where h_0 is the film thickness at an aging time of 10 minutes and t is the aging time.[23,24,113] Defined in this way, β is equivalent to a volumetric aging rate,[23] as originally established by Struik.[22] Figure 4.1 shows data collected at three different aging temperatures with several aging measurements shown for each temperature demonstrating reproducibility: $\beta = (4.3 \pm 0.4) \times 10^{-4}$ at 35 °C, $(8.7 \pm 0.4) \times 10^{-4}$ at 65 °C, and $(6.6 \pm 0.3) \times 10^{-4}$ at 95 °C. The errors are calculated based on the standard deviation of 2-3 measurements at each aging temperature on nominally identical samples. We note the data shown in Figure 4.1 are for aging times up to 6 h, but measurements were also done for aging times up to 24 h with no deviation observed in the linear decrease in film

thickness with logarithmic aging time, giving identical aging rates for longer runs when the aging temperature was 65 °C and above, while at 35 °C the aging rates of the shorter runs only deviated by 6% relative to the longer runs. For experimental efficiency, aging runs were typically limited to 6 h.

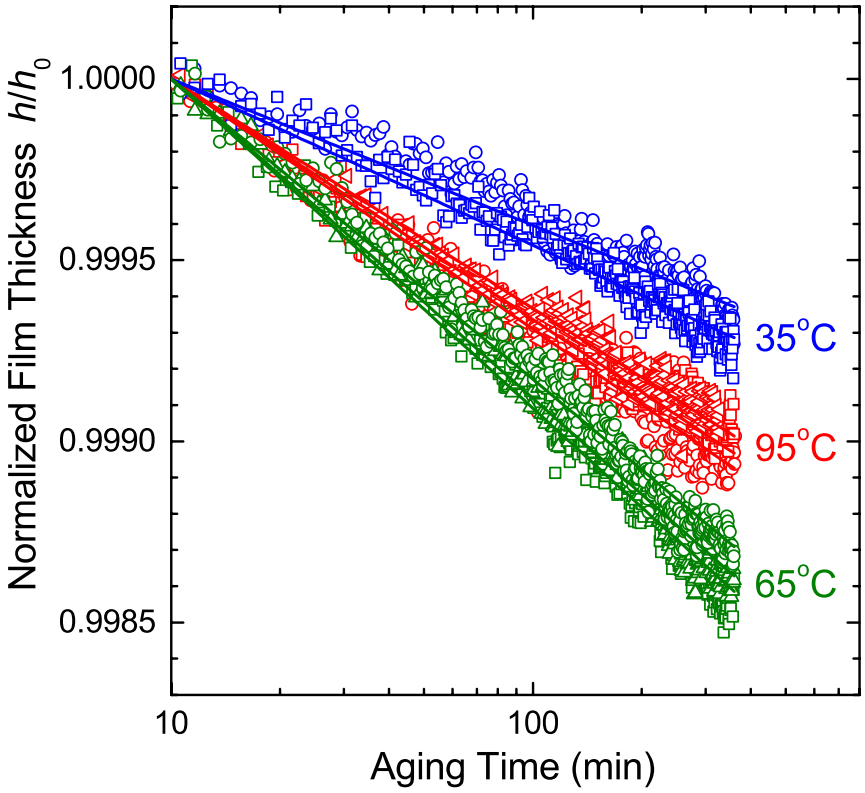

Figure 4.1: Normalized film thickness h/h_0 *vs*. logarithmic aging time for 515 ± 10 nm thick free standing films on stainless steel (SS) frames aged at 35, 65, and 95 °C. Several aging measurements and fit lines are shown for each aging temperature demonstrating the excellent reproducibility of the measurement.

The temperature dependence of the physical aging rate for 515 ± 10 nm thick free-standing PS films on SS frames is plotted in Figure 4.2. For comparison, the temperature dependence of supported PS films of equivalent thickness (490 ± 10 nm) on silicon are also graphed. The supported data is consistent with our previous measurements on supported PS films,[23,24] but has been retaken to match the quench rate of the free-standing films in this study (90 °C/min), as differences in cooling rate can

affect the measured aging rate.[113] The physical aging rates of both free-standing and supported films exhibit a qualitatively similar temperature dependence with a peak near 65 °C. The small quantitative difference in aging rates can be explained by the small difference in stress applied to the films, as described below. The peak in aging rate occurs because as the temperature is decreased below T_g, the driving force for structural relaxation increases with decreasing temperature until, at sufficiently low temperatures, the reduced thermal energy available limits any significant motion of the local structural units.

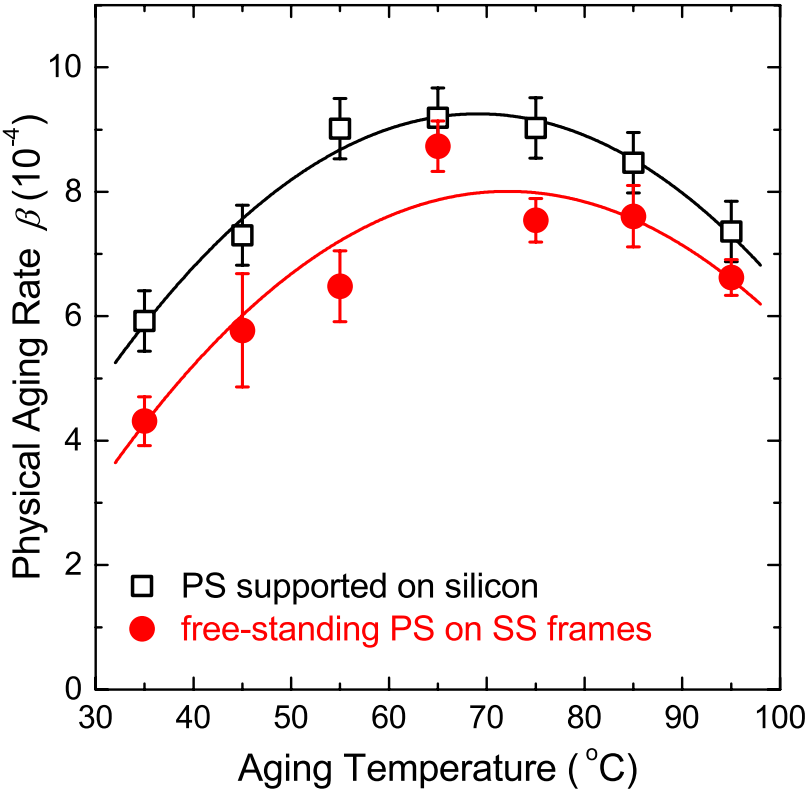

Figure 4.2: Temperature dependence of physical aging rate β for ~500 nm thick PS films held free-standing on stainless steel frames (solid red circles) and supported on silicon (open black squares). Error bars for free-standing films are the stardard deviations of several measurements. For the supported films, several measurements were taken at 65 °C to determine a representative error bar for all temperatures.

Focusing on the peak in aging rate at 65 °C, measurements as a function of film thickness were carried out on free-standing films held by the SS frames. Figure 4.3 shows that for free-standing films with thicknesses between 220 and 1800 nm, the measured physical aging rates are all within experimental error of each other: $\beta_{220nm} = (8.0 \pm 0.4) \times 10^{-4}$, $\beta_{500nm} = (8.7 \pm 0.4) \times 10^{-4}$, $\beta_{1330nm} = (8.3 \pm 0.4) \times 10^{-4}$, and $\beta_{1800nm} = (8.2 \pm 0.6) \times 10^{-4}$. These results are in contradiction with predictions by the free volume diffusion model previously used to explain faster aging rates with decreasing thickness observed in free-standing films.[100,108,111,125,142,143] However, as discussed in the following section, these results are in agreement with a constant, film-thickness-independent stress occurring from the thermal expansion mismatch between film and support.

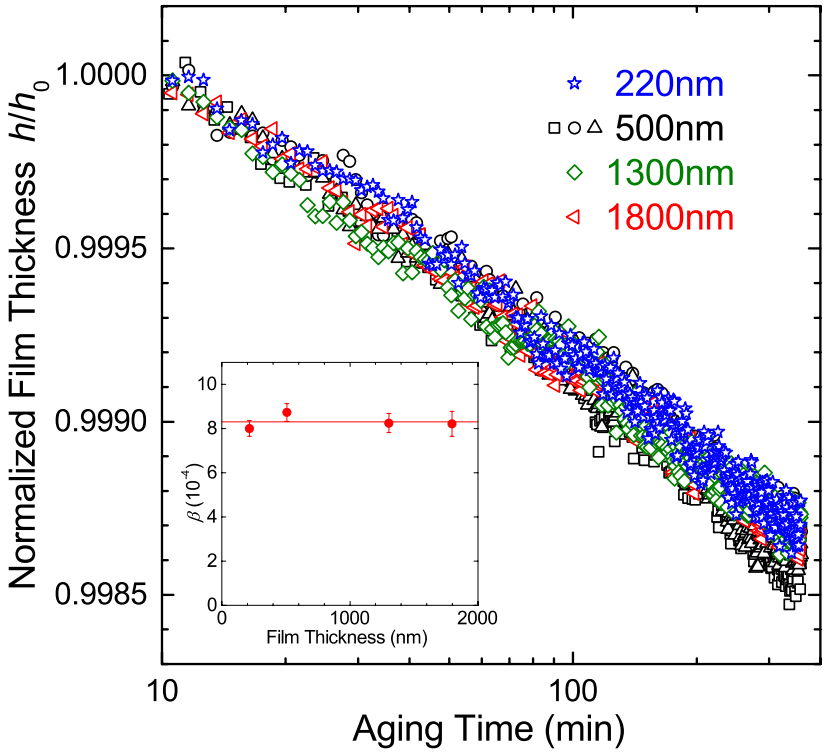

Figure 4.3: Normalized film thickness h/h_0 *vs*. logarithmic aging time for free-standing PS films held by SS frames and aged at 65 °C. Data for varying thicknesses from 220 to 1800 nm are plotted, with several measurements of 500 nm thick films shown for comparison indicating sample-to-sample variability. Inset: Average physical aging rate β as a function of film thickness.

4.3.2 Thermal Stresses Imparted to Free-standing Films by Rigid Frames on Cooling

For a thin polymer film cooled on a rigid support, the in-plane strain of the polymer film is constrained to match that of the rigid support. For the case of PS supported on silicon, the difference in thermal expansion between film and substrate is roughly two orders of magnitude. Thus, during a thermal cool, the PS film will try to thermally contract more than the underlying silicon. Forcing the PS strain to match that of the silicon substrate imparts an equibiaxial in-plane stress onto the PS film. The magnitude of this stress can be readily determined from standard stress-strain considerations.

Starting from the general elastic stress-strain relationships for a triaxial stress with thermal strain,[153] for an equibiaxial strain ($\varepsilon_x = \varepsilon_y$) under plane-stress conditions we set $\sigma_x = \sigma_y = \sigma$ and $\sigma_z = 0$ because there is no stress normal to the film plane as the film is unconstrained in this direction. The in-plane (ε_x) and out-of-plane (ε_z) strains are written as

$$\varepsilon_x = \frac{\sigma}{E_{PS}}(1 - \upsilon_{PS}) + \alpha_{PS}\Delta T \tag{4.1}$$

$$\varepsilon_z = -\frac{2\,\upsilon_{PS}}{E_{PS}}\sigma + \alpha_{PS}\Delta T \tag{4.2}$$

where we define E_{PS}, υ_{PS}, and α_{PS} as the modulus, Poisson's ratio, and linear thermal expansion coefficient of PS. The PS strain is forced to match the thermal expansion of the underlying support (e.g., silicon), in the *x* and *y* directions:

$$\varepsilon_x = \varepsilon_y = \alpha_{sup}\,\Delta T \tag{4.3}$$

such that Eqs. 4.1 and 4.3 can be used to solve for the equibiaxial in-plane stress imparted to the PS:

$$\sigma = \frac{-E_{PS}}{1-\nu_{PS}}\left[\alpha_{PS} - \alpha_{sup}\right]\Delta T \tag{4.4}$$

The negative sign out front in Eq. 4.4 means that on cooling (negative ΔT) a positive stress is generated implying tension in the film, as the thermal expansion coefficient of PS is larger than that of the rigid support for all frame materials studied here. (Note that in other works, this negative sign may be omitted[149,150] or ΔT defined differently.[113] In Eq. 4.9 below, the limits of integration have been swapped to accommodate the negative sign.)

The PS strain in the z direction will be affected by this equibiaxial stress, which by substituting Eq. 4.4 into Eq. 4.2, is

$$\varepsilon_z = \alpha_{PS}\Delta T + \frac{2\,\upsilon_{PS}}{1-\upsilon_{PS}}\left[\alpha_{PS} - \alpha_{sup}\right]\Delta T \tag{4.5}$$

such that on cooling, negative ΔT, both terms lead to a decrease in ε_z, i.e., film contraction. Eq. 4.5 is useful because the measured thermal expansion coefficient determined from the film thickness h by ellipsometry is

$$\alpha_{\text{measured}} = \frac{1}{h}\left(\frac{dh}{dT}\right) = \frac{\epsilon_z}{\Delta T} \tag{4.6}$$

such that from Eq. 4.5, we get

$$\alpha_{\text{measured}} = \alpha_{PS} + \frac{2\,\upsilon_{PS}}{1-\upsilon_{PS}}\left[\alpha_{PS} - \alpha_{sup}\right] \tag{4.7}$$

Thus, Eq. 4.7 demonstrates that the experimentally measured thermal expansion coefficient, α_{measured}, typically determined from the temperature dependence of the film thickness $h(T)$, is not the same as the stress free, "true" linear thermal expansion coefficient of PS, α_{PS}, but is altered by the thermal expansion coefficient of the underlying support, α_{sup}, and the Poisson's ratio of PS, ν_{PS}. However, Eq. 4.7 also

enables us to determine the "true" (or corrected) linear thermal expansion coefficient of PS from standard film thickness measurements:

$$\alpha_{PS} = \left(\frac{1-\upsilon_{PS}}{1+\upsilon_{PS}}\right)\alpha_{\text{measured}} + \left(\frac{2\,\upsilon_{PS}}{1+\upsilon_{PS}}\right)\alpha_{sup} \tag{4.8}$$

If we consider typical values for α_{measured} above and below T_g, we get good agreement with literature values for the "true" (corrected) linear thermal expansion coefficient for PS quoted in polymer handbooks.[154] In the glassy region below T_g, $\upsilon_{PS} \approx 1/3$, such that $\alpha_{PS} \approx \frac{1}{2}\alpha_{\text{measured}} + \frac{1}{2}\alpha_{sup}$, while in the melt region above T_g, $\upsilon_{PS} \approx 1/2$, such that $\alpha_{PS} \approx \frac{1}{3}\alpha_{\text{measured}} + \frac{2}{3}\alpha_{sup}$. For PS on silicon ($\alpha_{sup} \approx 3 \times 10^{-6}$ K^{-1}), ellipsometry measurements typically give $\alpha_{\text{measured}} \approx 1.6 \times 10^{-4}$ K^{-1} below T_g and $\alpha_{\text{measured}} \approx 6 \times 10^{-4}$ K^{-1} above T_g,[17,70,155,156] which correspond to "true", corrected linear thermal expansion coefficients for PS of $\alpha_{PS} \approx 0.8 \times 10^{-4}$ K^{-1} in the glassy region below T_g and $\alpha_{PS} \approx 2 \times 10^{-4}$ K^{-1} in the melt region above T_g, in agreement with values found in polymer handbooks[154] and bulk dilatometry[157] (with $\alpha_{\text{volume}} = 3\ \alpha_{\text{linear}}$ in the stress free state typically experienced in dilatometry).

Returning now to the calculation of the equibiaxial in-plane stress imparted to the PS film, because E_{PS}, υ_{PS}, and α_{PS} are all strong functions of temperature, changing dramatically through T_g, Eq. 4.4 needs to be solved in integral form:

$$\sigma\left(T_g, T_{\text{aging}}\right) = \int_{T_{\text{aging}}}^{T_g} \frac{E_{PS}(T)}{1-\upsilon_{PS}(T)}\left[\alpha_{PS}(T) - \alpha_{sup}(T)\right]dT \tag{4.9}$$

with the stress depending on the temperature range over which the film is cooled. Eq. 4.9, representing the initial stress imparted to the films after cooling, has been found to agree well with experimental measures of the stress formed on cooling for PS films supported on substrates.[149,150] Thus, even though Eq. 4.9 treats the polymer film as a purely elastic

material, this turns out to be a remarkably good approximation, suggesting that a formal viscoelastic treatment would only result in a small correction. As discussed and verified previously by Gray et al.,[113] stress does not begin to build up in the PS film as long as it remains an equilibrium liquid above T_g, as experimentally found by Zhao et al.[149] from direct measurements of the stress. Consequently, regardless of the initial annealing temperature above T_g, the relevant temperature range for Eq. 4.9 is from T_g down to the aging temperature T_{aging}. Note that the stress builds up slowly upon cooling below T_g, such that even for the case of PS on silicon (the largest stress values in the present study), the stress from thermal expansion mismatch is still well below the yield stress of the material.

Both supported films and free-standing films held by a rigid frame across a circular opening experience the same in-plane equibiaxial stress, given by Eq. 4.9, imparted during the thermal quench due to the mismatch in thermal expansion between the film and support. From Eq. 4.9, it is clear that the stress imparted to the films on cooling depends directly on the difference in thermal expansion coefficient between the PS film and rigid support over the temperature range cooled. Thus, to determine the stress imparted to the films on cooling, we first need temperature-dependent values for the linear thermal expansion coefficient of the materials of interest.

The "true", corrected linear thermal expansion coefficients of the polymers studied here (PS, PSF, and PC) were determined via Eq. 4.8 from ellipsometry measurements of the temperature-dependent film thickness $h(T)$ for bulk (~500 nm thick) films on silicon measured at 1 °C/min on cooling, where $\alpha_{measured}$ was calculated using Eq. 4.6. Tabulated values for the temperature-dependent linear thermal expansion

coefficients of silicon[158] and Poisson's ratio of PS[159] were used, while the Poisson's ratios of PSF and PC were taken to be $\nu_{PSF} = 0.37$ and $\nu_{PC} = 0.38$ based on manufacturers' specifications across the temperature range of T_g^{PS} to T_{aging} where PSF and PC remain in their glassy state. Figure 4.4a plots the temperature dependence of the measured thermal expansion coefficient $\alpha_{measured}$ for a 500 nm thick PS film on silicon, determined via Eq. 4.6, and the corrected ("true") linear thermal expansion coefficient of PS, α_{PS}, determined using Eq. 4.8. From the graph, we can see that that the largest difference between the measured and "true" thermal expansion coefficients occur above T_g in the melt state where a larger fraction of the underlying silicon's thermal expansion contributes because the Poisson's ratio for PS is larger in the melt state, as a nearly incompressible liquid. To compare the various materials used in the present study, Figure 4.4b plots the temperature dependence of the true (corrected) linear thermal expansion coefficient of PS, PSF, PC, (6061) aluminum,[160] (304) stainless steel,[161] and silicon[158] where tabulated literature values have been used for the various inorganic materials.

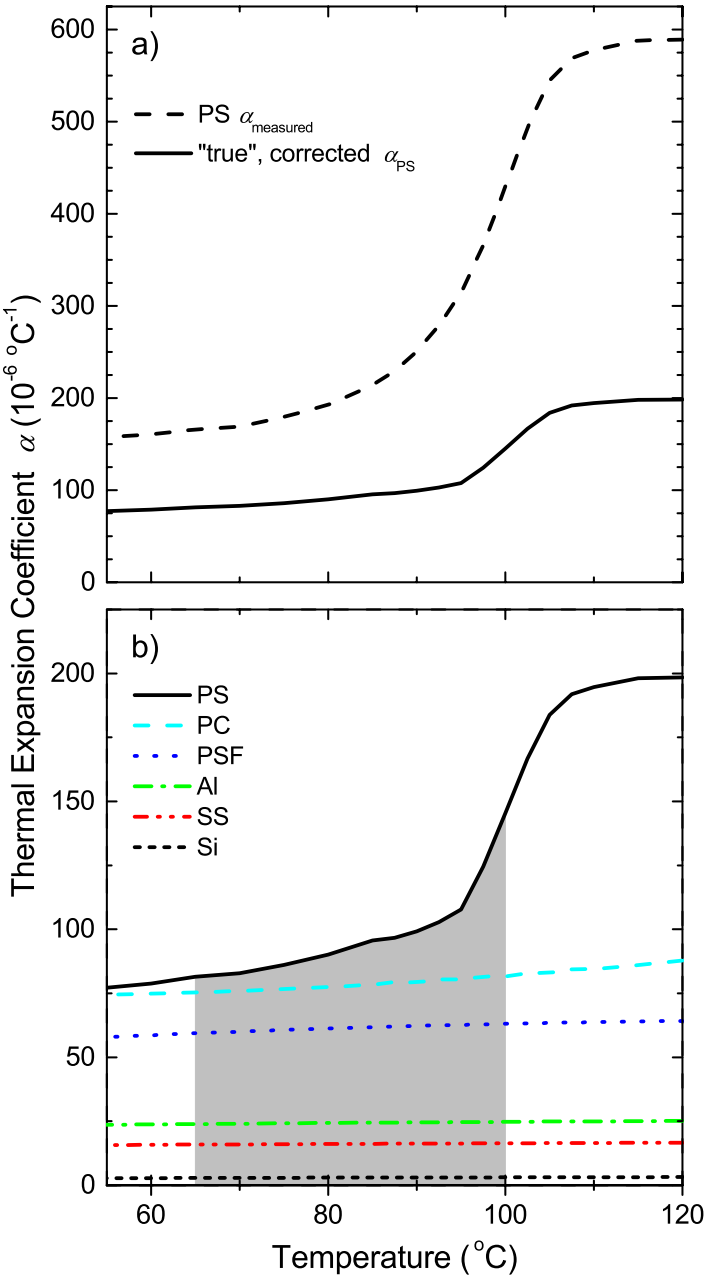

Figure 4.4: Temperature dependent thermal expansion coefficients, $\alpha(T)$: (a) PS $\alpha_{measured}$ based on film thickness $h(T)$ data using Eq. 4.6, measured on cooling at 1 °C/min for a 500 nm thick PS film supported on Si using ellipsometry (dashed line). The "true" α_{PS}, corrected using Eq. 4.8 to remove the vertical strain component induced by the underlying silicon, is plotted as a solid curve. (b) "True" α for all of the materials used in this study where the relevant temperature range for stress buildup on cooling (T_g^{PS} = 100 °C to T_{aging} = 65 °C) has been highlighted. "True" α for the polymers [PS (solid black curve), PSF (dashed cyan curve), PC (dotted blue curve)] are corrected using Eq. 4.8 from measurements on cooling at 1 °C/min for bulk (~500 nm) films supported on Si. Tabulated data are used for Al (dash-dot green curve),[160] SS (dash-dot-dot red curve),[161] and Si (short dashed black curve).[158]

The temperature dependent linear thermal expansion coefficients presented in Figure 4.4b enable direct comparison of the thermal expansion mismatch between PS and the various materials for the supporting frames. The magnitude of the relative stress differences between the various materials will depend directly on the integrated thermal expansion mismatch over the temperature range that stress builds up in the PS films: T_g^{PS} = 100 °C to T_{aging} = 65 °C. For easy comparison, we list in Table 4.1 the thermal expansion coefficient (average value over the temperature range of 65-100 °C, although the values vary by less than 8% over this range) and the integrated thermal expansion mismatch with PS for the various supporting frame materials used in the present study. This thermal expansion mismatch $\Delta\alpha$ was calculated numerically, from T_g^{PS} = 100 °C to T_{aging} = 65 °C, as

$$\Delta\alpha = \int_{T_{aging}}^{T_g} \left[\alpha_{PS}(T) - \alpha_{sup}(T)\right] dT \tag{4.10}$$

using the data presented in Figure 4.4b. Formally, this is equivalent to the total strain built up in the glassy PS film as it is cooled below its T_g. These $\Delta\alpha$ values are a robust measure of the relative magnitude of the stress differences imparted by the various frame materials, and is perhaps more reliable than the explicit values of stress calculated from Eq. 4.9 because they do not depend on the Young's modulus of PS, $E_{PS}(T)$. Although the temperature-dependent Poisson's ratio for PS changes only from 0.5 to 0.35 in going from the melt to the glassy state, Young's modulus $E_{PS}(T)$ varies by more than three orders of magnitude.

Table 4.1: Thermal expansion coefficient α, integrated thermal expansion mismatch $\Delta\alpha$ relative to PS from Eq. 4.10, stress σ imparted to the PS films on cooling to T_{aging} = 65 °C based on Eq. 4.9 for the various materials used in the present study, and physical aging rate β_{PS} (average of 3-5 measurements) for ~500 nm thick free-standing PS films held by frames of the materials listed (or supported on silicon) at 65 °C.

Frame material	α (10^{-6} °C^{-1})	$\Delta\alpha$ with PS	σ (MPa)	β_{PS} (10^{-4})
PC	78.1	0.00064	0.7	4.8 ± 0.2
PSF	61.4	0.00123	1.7	6.5 ± 0.6
Al	23.8	0.00254	4.0	6.6 ± 0.5
SS	16.1	0.00281	4.5	8.7 ± 0.4
Si	2.97	0.00327	5.3	8.9 ± 0.4
Supported on Si	2.97	0.00327	5.3	9.2 ± 0.5

To explicitly calculate the stress imparted to the films via Eq. 4.9, values for the temperature-dependent Young's modulus of PS, $E_{PS}(T)$, are also needed. The precise values of the stress imparted to the films depend significantly on the values of $E_{PS}(T)$ because $E_{PS}(T)$ changes by more than three orders of magnitude over the temperature range that the stress builds up on cooling. Obtaining reliable values for the temperature-dependent Young's modulus of PS from the literature proved to be harder than expected, such that future measurements of $E_{PS}(T)$ on even bulk PS films would be warranted. For the present calculation, we decided to use the $E_{PS}(T)$ data given in Beaucage et al.[159] because they are matched with reasonable $\nu_{PS}(T)$ data, a rare occurrence,[162] and the stress values calculated from Eq. 4.9 using these data for PS films supported on silicon cooled to room temperature ($\sigma \approx 15$ MPa) were found to be consistent with independent experimental measures of the stress (15-16 MPa) for such samples.[149,150] Values of the

equibiaxial in-plane stress imparted to PS films, upon cooling to an aging temperature of 65 °C, when supported by rigid frames of the various materials studied are included in Table 4.1 based on numerical integration of Eq. 4.9. We note that even though the $E_{PS}(T)$ data may not be the most ideal, we are confident in the values of thermal expansion coefficients that define the thermal expansion mismatch between the different materials. Because $E_{PS}(T)$ only shows up as a numerical prefactor in Eq. 4.9 and the $\alpha(T)$ data for the frame materials all have similarly weak temperature dependences, we are confident in the *relative* differences between the different stress values calculated, which is what is found to correlate with the relative differences in physical aging rate.

4.3.3 Correlating Physical Aging Rate with Thermal Expansion Mismatch and Applied Stress

The expression for the equibiaxial in-plane stress σ, given by Eq. 4.9, imparted during the thermal quench (i.e., glass formation) due to the thermal expansion mismatch between film and support explicitly shows that there is no film thickness dependence to the stress for free-standing films supported on rigid (nonflexible) frames or for supported films on rigid substrates. Thus, the results presented in Figure 4.3 showing no change in physical aging rate with film thickness for free-standing PS films (220-1800 nm thick) held by SS frames are in agreement with films of all thicknesses being formed with the same stress value. In addition, the results represented in Figure 4.2 are consistent with the idea that the physical aging rate is affected by stress imparted during the thermal quench with larger stresses leading to larger aging rates because the stress for PS films supported on silicon ($\sigma \approx 5.3$ MPa) is slightly larger than that for free-standing PS films held by rigid SS frames ($\sigma \approx 4.5$ MPa), as shown in Table 4.1.

To further test the idea that stress resulting from thermal expansion mismatch between film and support correlates with the observed physical aging rates, we have made rigid frames containing a circular opening from materials with different thermal expansion coefficients. For example, PSF and PC have thermal expansion coefficients significantly different from SS and Si, and much closer to PS (see Table 4.1). Figure 4.5 compares the observed physical aging at 65 °C for ~500 nm thick free-standing PS films held by PC, PSF, SS and Si, as well as a 482 nm thick PS film supported on Si. We find that the observed physical aging rates correlate with the stress imparted to the films due to the thermal expansion mismatch between film and support, as given by Eq. 4.9. The average physical aging rates (based on 3-5 measurements) for ~500 nm thick PS films are listed in Table 4.1. The lowest physical aging rate, $\beta = (4.8 \pm 0.2) \times 10^{-4}$, is observed for free-standing films held by PC frames that impart the lowest stress, $\sigma \approx 0.7$ MPa, while the highest aging rates are $\beta = (8.9 \pm 0.4) \times 10^{-4}$ for free-standing films on silicon frames and $\beta = (9.2 \pm 0.5) \times 10^{-4}$ for supported films on silicon, both with $\sigma \approx 5.3$ MPa, the highest stress. The data are consistent with Eq. 4.9 predicting that both free-standing and supported films have the same stress ($\sigma \approx 5.3$ MPa) for the same supporting material.

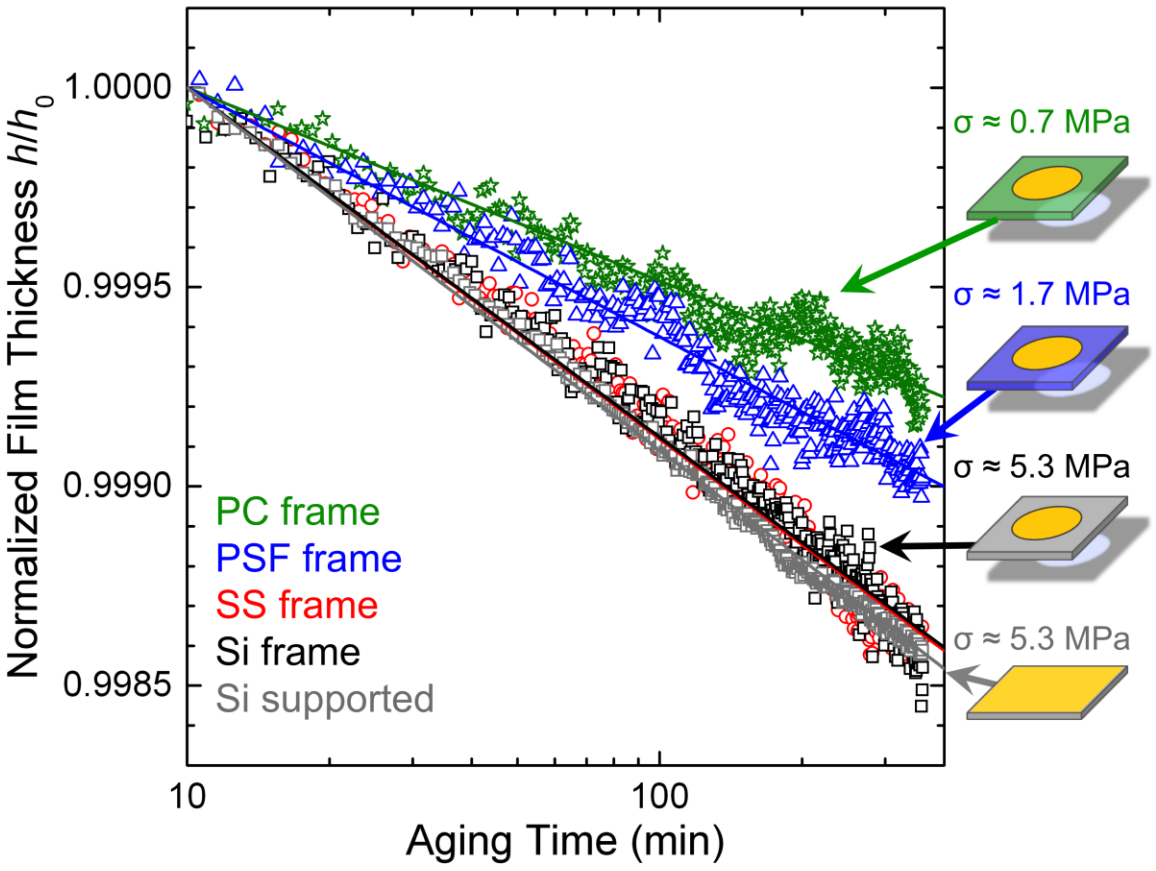

Figure 4.5: Normalized film thickness h/h_0 *vs*. logarithmic aging time for ~500 nm thick PS films held free-standing on a PC frame (green stars), PSF frame (blue triangles), SS frame (red circles) and silicon frame (black squares), as well as for a supported PS film on silicon (gray squares). Physical aging rates (average of 3-5 samples) correlate with the stress imparted on cooling from thermal expansion mismatch between film and support as listed in Table 4.1.

Figure 4.6 demonstrates the correlation between the observed physical aging rate at 65 °C for ~500 nm thick PS films with the thermal expansion mismatch $\Delta\alpha$ and applied stress σ. Data shown are based on measurements collected on 3-5 nominally identical samples of free-standing PS films for each of the different frame materials: Si, SS, Al, PSF, and PC (open red circles). A data point (solid back square) is also included for PS films supported on silicon wafers. The same physical aging rate is observed for free-standing and supported films when held by frames (or substrates) of the same material, consistent with the stress prediction from Eq. 4.9 where the equibiaxial in-plane stress

depends only on the thermal expansion mismatch between film and support. We plot the physical aging rate both as a function of thermal expansion mismatch $\Delta\alpha$ and stress σ because $\Delta\alpha$ is the more well-defined quantity. As discussed above, the *absolute* value of stress strongly depends on the $E(T)$ literature data used for PS, as it varies by more than three orders of magnitude over the temperature range integrated in Eq. 4.9. However, note that the *relative* differences in the stress between the various frame materials are reliable because they depend only on the relative difference in thermal expansion cofficients. It is clear from the data that a larger thermal expansion mismatch $\Delta\alpha$, and hence stress σ build up on cooling, results in a larger physical aging rate, where the increased stress from $\sigma_{PC} \approx 0.7$ MPa to $\sigma_{Si} \approx 5.3$ MPa leads to a near doubling of the physical aging rate of ~500 nm thick free-standing PS films aged at 65 °C. There is no reason to believe that the trend in $\beta(\sigma)$ should be linear, and future work will focus on measuring $\beta(\sigma)$ by directly controlling stress on cooling.

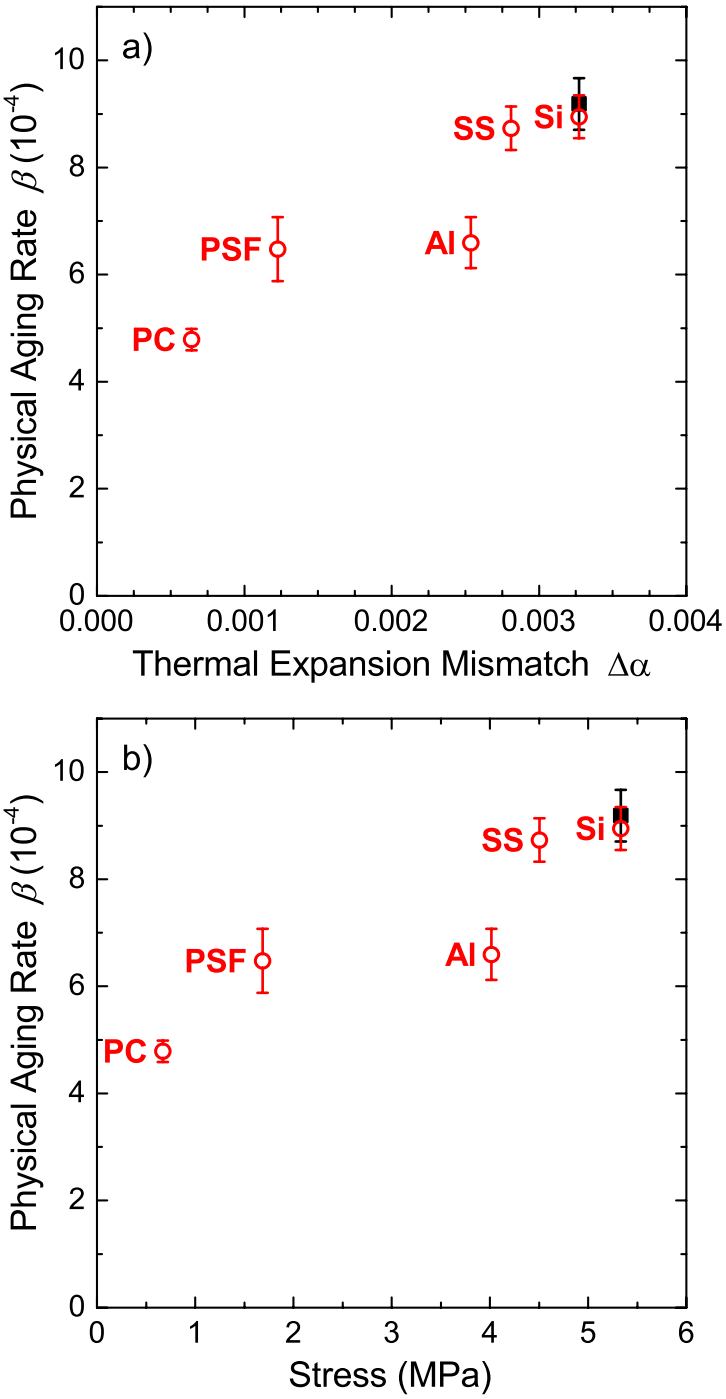

Figure 4.6: Physical aging rate β for ~500 nm thick PS films aged at 65 °C as a function of: (a) thermal expansion mismatch $\Delta\alpha$ between PS and the supporting frame material, as defined in Eq. 4.10; (b) stress imparted to PS on cooling to 65 °C as determined by Eq. 4.9 for the different supporting frame materials: polycarbonate (PC), polysulfone (PSF), aluminum (Al), stainless steel (SS), and silicon (Si). Data plotted are based on an average of 3-5 samples with free-standing PS films held by rigid frames containing circular openings shown as open red circles, while that for supported PS films on Si is given as a solid black square.

Given this correlation between stress and physical aging, we reconsider in this context previous reports in the literature that made efforts to correlate physical aging with sample-size dependence. Often cited as the first such test, Braun and Kovacs compared the physical aging behavior of powdered PS samples (containing fibrous sheets 100-1000 nm in thickness) with bulk (same powdered PS molded into 1 mm thick samples).[163] They found that the physical aging rate of PS did not depend on the sample geometry or "state of division of the sample". This study would be in agreement with the present work as the powdered and molded samples suspended in a mercury filled dilatometer would be unconstrained and free to thermally expand and contract as necessary.

Recently Gray et al.[113] found that thickness *dependent* faster physical aging for micron thick PS films only occurred when samples were supported on a wire frame during the thermal quench. In this study, the free-standing PS films were supported by 0.009 in. diam. stainless spring steel wire frames with the PS film spanning across two sides of the rectangular wire frame during the annealing step and thermal quench from above T_g down to room temperature before being transferred onto silicon wafers for the aging measurements. The aging rate at 65 ^oC for PS free-standing films held by these wire frames during the thermal quench were $\beta = (6.1 \pm 0.6) \times 10^{-4}$ for 1380 ± 100 nm thick films and $\beta = (8.1 \pm 0.6) \times 10^{-4}$ for 570 ± 50 nm thick films. In contrast, when these same thickness films were quenched supported on silicon (σ = 5.3 MPa according to Table 4.1) the aging rates were $\beta = (9.5 \pm 0.6)$ and $\beta = (9.3 \pm 0.6)$.[113] Because Gray et al. observed that film-thickness-*dependent* physical aging only occurred when samples were supported on these wire frames during the thermal quench, they hypothesized that the wire frames acted as small springs imparting a force F leading to a film-thickness-

dependent stress $\sigma = F/(hw)$ applied to the films during the quench, where (hw) represents the cross-sectional area (height × width) of the films.[113] Efforts to directly quantify this stress were not possible. Although Gray et al. proposed and attempted physical aging measurements of free-standing films quenched on rigid frames that would impart thickness-*independent* stresses, such measurements were not successful until the improvements made here in the present study. From the β vs. stress data presented in Figure 4.6b, we can extrapolate that the physical aging rate for PS films quenched stress free should be $\sim 4 \times 10^{-4}$. Thus, it would appear from the aging rates measured for the PS films held by the wire frames that the stresses imparted to these films are quite substantial. A direct comparison cannot be made because the sample geometry in the present study imparts a biaxial stress, compared with the uniaxial stress imparted by the rectangular wire frames. However, separate measurements in our lab applying uniaxial stresses find a similar β vs. stress behavior and the same aging rate of $\sim 4 \times 10^{-4}$ in the limit of zero stress. As PS has been shown to not be a good model system[164] for gas separation membranes, these conclusions of how stress imparted during the thermal quench can affect the subsequent physical aging rate would need to be tested on the higher T_g, stiff backbone polymers that are used as gas separation membranes (e.g., PSF, polyimide, etc.), in particular at the operating temperatures used for gas separation (typically 35 ^{o}C), before any broad applicability could be made.

Simon et al. have also correlated changes in physical aging upon confinement with increased stress (hydrostatic tension) resulting from thermal expansion mismatch between the glass former (ortho-terphenyl) and surrounding support (nanoporous matrix).[96] However, in this study it is the time to reach equilibrium that was accelerated,

with insufficient data presented to comment on the aging rate itself. Unfortunately, a number of studies have involved sample geometries for which it is not possible to estimate what unintended stresses might be imparted during thermal cooling.[100,101,125,147,148,165,166] In several such studies, it is not the aging rate that is faster, but the time to reach equilibrium that is "accelerated."[125,147,148,165,166] Work by Priestley et al. on silica capped PS nanospheres may enable further confirmation of how stress development from thermal expansion mismatch during thermal cooling affects physical aging by being able to more finely control internal stresses.[152,167]

For this discussion we omit the numerous studies that have observed changes in physical aging rate at length scales ~100 nm or less,[24,71,97–99,102,104,135] some of which have been directly correlated with T_g changes.[24,71,97–99,135] Such 'nanoconfinement' effects *do* correlate with the surface-to-volume ratio of samples such that free volume diffusion type models[168,169] may be effective in explaining glassy dynamics at these smaller length scales.

The nature of how deformation (stress or strain) imparts mobility to glasses is a long standing problem that unifies concepts in polymer glasses, colloids, and granular materials.[170] In theoretical models, stress or strain are treated as facilitating energy barrier hopping[171,172] or equivalently tilting of the potential energy landscape,[173,174] an idea that was originally proposed by Eyring.[175] Such an interpretation of stress induced mobility in polymer glasses is supported by work that shows glassy dynamics not correlating with free volume,[176–178] but depending on a glass' position within the energy landscape.[174,179] The vast majority of studies in this field on how mobility is increased by the application of mechanical stress or strain investigate glasses that have been formed

stress free. The present work is different in that the stress is applied during glass formation (vitrification), and that even the presence of small stresses are found to have a noticeable effect on the subsequent physical aging and stability of the material. Future studies of how physical aging in polymer glasses can be altered by stress during glass formation by directly controlling the stress on cooling are underway.

4.4 Conclusions

The results presented here demonstrate that there is no thickness dependence to the physical aging rate for free-standing PS films, for thicknesses between 220 and 1800 nm, when held by rigid frames that impart a thickness-*independent* stress on cooling. This is consistent with data for supported films on silicon, which also have a constant, thickness-*independent* stress imparted to them on cooling, that show the physical aging rate is independent of film thickness above ~100 nm[24,113] (i.e., where T_g is equivalent to bulk). These combined results for free-standing and supported films held by rigid supports observe no inherent film thickness dependence to physical aging (for films > 200 nm in thickness). Our conclusion is that the physical aging rate of free-standing PS films correlates with the stress imparted to the films during cooling (i.e., glass formation) due to thermal expansion mismatch between film and support.

Chapter 5

Above, Below, and In-Between the Two Glass Transitions of Ultrathin Free-Standing Polystyrene Films: Thermal Expansion Coefficient and Physical Aging

5.1 Introduction

There has been a long history of work on confinement effects in polymers and other glass formers.[30,35,48,53,55,65,69,159,163] This work has been motivated not just by its inherently interesting qualities, but also by the importance of understanding current glass transition theories,[10,180,181] and for applications in the fields of gas separation,[109] photolithography, nanocomposites,[182] membranes, and fibers. Given our incomplete understanding of confinement effects, significant developments are still being made including work on fragility effects,[60,183–186] cooling rate effects,[187,188] and modulus.[87,139,189,190] However, there have also been some interesting new questions brought up regarding polymer-polymer interfaces,[67,94,183,191] preparation stress effects,[112,113] and a possible dichotomy of segmental dynamics and measured glass transition temperature (T_g).[38,134,137,192] Additionally, renewed interest has been shown in understanding the full details of free-standing polymer films as they *should* be the

simplest system, containing only two symmetric air-polymer interfaces and no substrate interactions.[58–60,63,64,66,85,87,88,125,189]

We recently showed that high molecular-weight (MW) free-standing polystyrene (PS) films have two reduced T_gs by performing measurements over an expanded temperature range,[66] where the film thickness, MW, and temperature range were carefully chosen such that both transitions were visible. Figure 5.1 shows the temperature dependent film thickness of two ~55 nm thick films with (a) M_w = 934 kg/mol and (b) M_w = 2257 kg/mol, in which two transitions are visible for each film. The lower T_g matches that previously measured for films of these molecular weights[54,55,59,63] (and predicted by the Dalnoki-Veress et al. $T_g(h, M_w)$ scaling[55]), showing a very strong M_w dependence. The upper transition is independent of MW and had not previously been seen in free-standing films for these high MWs, but matches the thickness dependence seen for low MW free-standing PS films.[36] These results, as well as the large body of work on thin polymer films,[30,35,48,53,55,65,69] molecular glasses,[138,193] and confined colloidal glasses[73,194] led us to propose that the mechanism of the $T_g(h)$ reduction for the upper transition may be universal to all glass formers. The lower T_g has only been seen (so far) in high MW free-standing polymer films, which suggests that chain connectivity may be important for this mechanism. These recent results lead us to ask if the film is truly glassy between the two transitions, and if so, how much of the film is glassy?

Here we examine the thermal coefficient of expansion (TCE) of these ultrathin high MW free-standing films, as well as present physical aging measurements below and in-between the two observed transitions. The TCE data show that the upper transition accounts for solidification of ~90% of the film, while only ~10% of the film remains

mobile until passing through the lower transition, which we interpret as meaning some small portion of the film or dynamics remains accelerated to much lower temperatures. By performing physical aging measurements on these films, we see that between the two transitions, physical aging does indeed occur. This indicates that the upper transition is an actual glass transition below which physical aging occurs and accounts for solidification of most of the film, in agreement with the TCE measurements. Additionally, the physical aging rates we measure for films held between and below the two transitions are significantly faster than would be expected based on our previous measurements on the thickness dependence of the aging rate in supported PS films.[24]

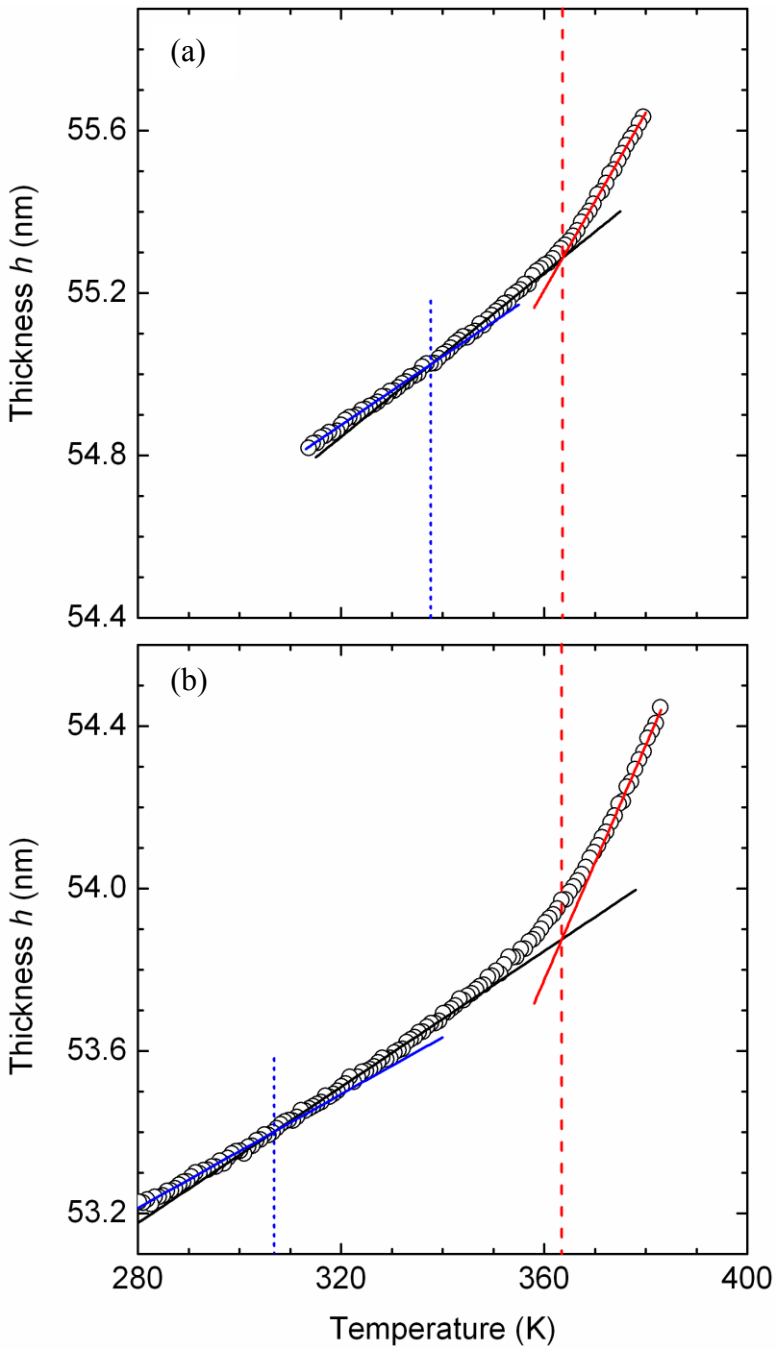

Figure 5.1: Film thickness vs. temperature for (a) 54.7 nm thick, M_w = 934 kg/mol, film and (b) 53.2 nm thick, M_w = 2257 kg/mol, film. The vertical red dashed and blue dotted lines indicate the upper and lower T_g as fit by Eq. 5.1. The upper T_g is the same within experimental error for the two MWs: 364 ± 2 K for the 934 kg/mol film and 363 ± 2 K for the 2257 kg/mol film. For the lower T_g, we measure 338 ± 3 K for the 934 kg/mol film and 307 ± 3 K for the 2257 kg/mol film. The solid lines are guides to the eye. The data were smoothed by a nine point Savitzky-Golay algorithm and only every third data point is displayed for clarity

5.2 Experimental

Films were made by spin-coating PS (M_w = 934 kg/mol with M_w/M_n = 1.14, M_w = 2257 kg/mol with M_w/M_n = 1.17, or M_w = 10100 kg/mol with M_w/M_n = 1.09) dissolved in toluene onto freshly cleaved mica. Samples were vacuum annealed for at least 16 hours followed by a slow cool to room temperature (< 0.5 K/min). Films were then draped across stainless steel frames with 5 mm openings *via* water transfer to produce free-standing films, while pieces from the same mica sample were transferred to silicon for additional thickness measurements. Free-standing films were allowed to dry under ambient conditions before being measured. Transmission ellipsometry (J.A. Woollam M-2000) with a custom built heater for free-standing films, held at 45° angle of incidence, was used for thickness measurements as a function of temperature for TCE data or time for physical aging measurements.[66,112] All free-standing films were modeled as a single Cauchy layer with $n(\lambda) = A + B/\lambda^2 + C/\lambda^4$ for λ from 400 to 1000 nm.[66,112]

The TCE data are for the films measured in Ref. 66 and shown in Chapter 2. Briefly, films were initially heated to slightly above T_g, 383 K for thin films and 391 K for bulk films, to remove wrinkles and then ramped several times at 0.5 K/min while measuring thickness and index of refraction on cooling and heating. To reduce the likelihood of hole formation, a limited number of ramps through the upper T_g were performed while several additional ramps through the lower T_g were collected. The TCEs for the region between and below both transitions were determined by fitting the lower transition to the integrated tanh function used previously by Dalnoki-Veress et al.:[55]

$$h(T) = w\left(\frac{M-G}{2}\right)\ln\left[\cosh\left(\frac{T-T_g}{w}\right)\right] + \left(T - T_g\right)\left(\frac{M+G}{2}\right) + c \quad (5.1)$$

where w is the width of the transition (held to 2 K for the lower transition), M and G are the slopes of the melt and glassy regions respectively, and c is the thickness of the film at T_g. The TCE values are calculated according to $\alpha = \frac{1}{h}\frac{dh}{dT}$. Above and below the lower transition, the fit values for the slopes M and G in Eq. 5.1 give dh/dT, with the reference thickness for the 1/h normalization chosen to be h(298 K) below the lower T_g and h(338 K) above the lower T_g. To determine the TCE in the melt region above the upper T_g, the melt data are fit to a straight line and the TCE is calculated from this slope with the reference thickness at h(378 K). A simple linear fit works better to determine the TCE above the upper T_g for several reasons. The breadth[17,70] and asymmetry[70] of the transition combined with the limited data at high temperatures to minimize hole formation, causes Eq. 5.1 to be less reliable in determining the TCE above the upper transition compared to a linear fit. All the TCE values were calculated from data collected on cooling ramps from the liquid state above both transitions.

Physical aging measurements were performed using a similar protocol to our recent work on physical aging of bulk (220-1800 nm thick) free-standing PS films.[112] After drying, free-standing films were placed in an enclosed Instec hot stage at 363 K. Films were then ramped up to 379 K at 1 K/min, held at 379 K for 1 min, and then quenched to 313 K using liquid nitrogen cooling at 90 K/min. Immediately after the quench is completed, films were placed in the custom heater that was pre-equilibrated at the aging temperature for at least 30 min, and ellipsometry data were collected as a function of aging time. This annealing protocol was designed to mimic the same

temperature profile commonly used to get reliable T_g measurements[66] and ensure that the thermal history was reset, while minimizing hole formation by limiting time at higher temperatures.[55,66]

Films were viewed under an optical microscope at up to 1000× magnification to check for imperfections before and after physical aging measurements. Holes can be distinguished from dust in the film by using transmission bright field illumination. Under reflection illumination, tiny holes and pieces of dust are nearly indistinguishable, both appearing as dark spots on the film. However, under bright field transmission illumination, holes appear lighter than the surrounding film while dust remains darker. In reflection illumination, differential interference contrast was used to check the uniformity of the film and identify any out of plane deformations while dark field illumination causes any imperfection in the film to stand out against the smooth, dark background of the flat film. These microscopy techniques were used to pick films that were only of the best quality for the physical aging measurements and to confirm that they did not exhibit any hole nucleation or growth during the annealing or physical aging measurement.

5.3 Results and Discussion

5.3.1 Thermal expansion above, below, and between the two transitions

The thermal coefficient of expansion (TCE) data, calculated in this chapter from our previous T_g measurements on ultrathin, high-MW, free-standing polystyrene films,[66] are presented in Figure 5.2. The red down triangles, black circles, and blue up triangles indicate the TCE calculated in the liquid state above both transitions, the intermediate state between the two transitions, and the fully glassy state below both transitions,

respectively. Both the data for films with M_w = 934 kg/mol (solid symbols) and 2257 kg/mol (open symbols) show the same qualitative TCE results. Upon close inspection, there is a slight decrease in all three TCEs as the film thickness is reduced, however this decrease is similar in magnitude to the scatter in the data. The uncertainties and scatter in the TCE data are fairly large due both to the scatter in the $h(T)$ data affecting the TCE calculation, and significant variations from both film to film and cooling ramp to cooling ramp. This sample to sample variation of TCE has been discussed in earlier measurements of free-standing films with both ellipsometry[55] and Brillouin light scattering (BLS).[36]

It should be noted that in any experiment that determines TCE of a supported or free-standing film from the temperature dependence of the film thickness, such as the ellipsometry measurements reported here, the measured TCE is not the same as the stress-free, "true" linear thermal expansion of the film material.[112] As discussed in Chapter 4 (Ref. 112), the measured TCE is altered by Poisson's ratio (ν_{PS}) effects caused by the lateral constraint of the support on the film:

$$\alpha_{\text{measured}} = \frac{1}{h}\left(\frac{dh}{dT}\right) = \alpha_{PS} + \frac{2\,\upsilon_{PS}}{1-\upsilon_{PS}}\left[\alpha_{PS} - \alpha_{sup}\right] \tag{5.2}$$

α_{sup} is the TCE of the support holding the film, in either a supported or free-standing state. To compare TCE values measured on substrates or frames of different TCE or with bulk dilatometry measurements, Eq. 5.2 must be used to correct the TCE values. Below T_g, where $\nu_{PS} \approx 1/3$, $\alpha_{measured} \approx 2\alpha_{PS} - \alpha_{sup}$ and above T_g, where $\nu_{PS} \approx 1/2$, $\alpha_{measured} \approx 3\alpha_{PS} - 2\alpha_{sup}$. This lateral constraint effect on the measured TCE has been recognized by some,[34,47,115,195] but not all authors who report TCE values from film thickness

measurements. In this chapter, we will simply use $\alpha_{measured}$ for simplicity and to not make any assumptions about the values of ν_{PS} in ultrathin films.

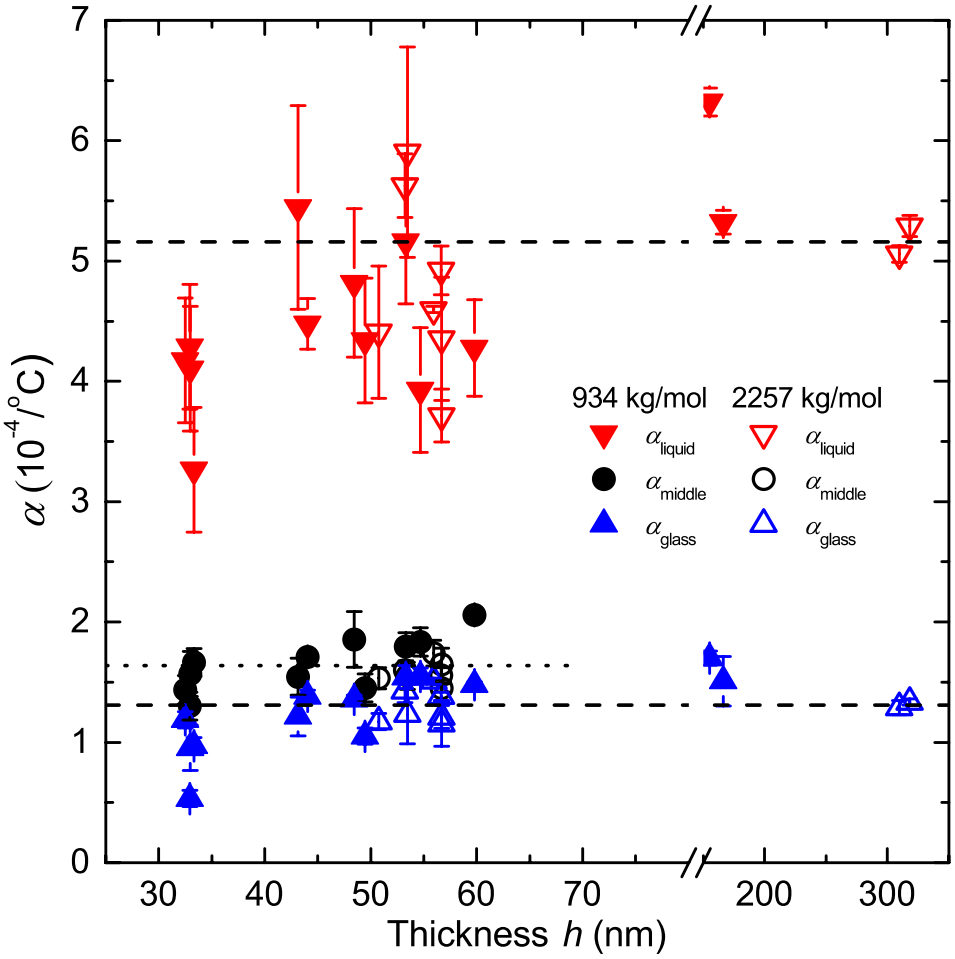

Figure 5.2: Thermal expansion α as a function of film thickness for free-standing PS films. Data for films with M_w = 934 kg/mol are shown as solid symbols while data for M_w = 2257 kg/mol are shown as open symbols. Different symbol shapes and colors represent α above (red downward pointing triangles), between (black circles), and below (blue upward pointing triangles) both transitions. The dashed lines represent the liquid and glassy thermal expansions for bulk films and the dotted line is the average thermal expansion between the two transitions. Error bars are the standard deviation when multiple cooling ramps were collected, or the uncertainty in the fit used to determine α when only one cooling ramp was available.

TCE data were not reported in Ref. 55 but calculating them from the single provided thickness *vs*. temperature data set (Figure 1b in Ref. 55) for a 71 nm thick film

with M_w = 2240 kg/mol gives $\alpha_{<Tg}$ = 1.6 × 10^{-4} K^{-1} below the observed transition and $\alpha_{>Tg}$ = 4.3 × 10^{-4} K^{-1} above the transition. This (single) observed transition in Ref. 55 agrees quantitatively with our lower transition while our upper transition is outside of their measured temperature range. Thus, for the purpose of comparison one would expect their TCE values to agree with our measure of α_{glass} and α_{middle}. Although their $\alpha_{<Tg}$ is in agreement with our α_{glass}, their $\alpha_{>Tg}$ is within the range of our α_{liquid}, as opposed to our α_{middle} as anticipated. However, this comparison may not be warranted since they commented that the TCEs above and below the transition were not reproducible. Ref. 55 used both stainless steel and nylon for the free-standing frames and it is not stated which frame material was used in Figure 1b in Ref. 55, but we assume here that it was stainless steel.

Subsequent work by one of the same authors (but in a different lab) provided an excellent test of the effect of free surfaces wherein they measured the T_g of high MW films in a free-standing state, transferred them to silicon wafers, and subsequently measured T_g again on the same films without any further annealing.[58] They found that the reduced T_g of the free-standing film (only one T_g is reported) returns to the bulk value when it is transferred to silicon (T_g reductions for supported films of the tested thicknesses are small) and that the contrast between the TCEs above and below the T_g is increased. They do not report the actual TCEs of the films, but from the single 57 nm film for which thickness *vs.* temperature data is shown, $\alpha_{<Tg}$ = 1.5 × 10^{-4} K^{-1} and $\alpha_{>Tg}$ = 2.3 × 10^{-4} K^{-1} in the free-standing state (Figure 1 in Ref. 58) in good agreement with our α_{glass} and α_{middle} results in Figure 5.2 and changes to $\alpha_{<Tg}$ = 3.1 × 10^{-4} K^{-1} and $\alpha_{>Tg}$ = 6.6 × 10^{-4} K^{-1} after transferring to silicon (Figure 2 in Ref. 58) in reasonable agreement with

our previous α_{glass} and α_{liquid} measurements on supported films in Chapter 4 (Ref. 112). In Ref. 58, only stainless steel wafers were used.

The only other TCE data on free-standing PS films that we know of is from X-ray reflectivity studies in Ref. 62. They include TCE *vs*. thickness for both the low (M_w = 303 kg/mol) and high (M_w = 2890 kg/mol) MW films above and below the T_g they measure. There is significant scatter in the data, but both MW show strongly reduced $\alpha_{<Tg}$ and $\alpha_{>Tg}$ for thinner films, with a slightly higher onset thickness for the higher MW. $\alpha_{<Tg}$ varies from $1 - 2 \times 10^{-4}$ K^{-1} for thick films to essentially zero (within error) as the thickness is reduced below ~55 nm. While we do not see as strong of a reduction in α_{glass} with film thickness, the average value is in good agreement with our results. While they used aluminum frames, the difference in TCE between our stainless steel frames, $\alpha_{SS} \approx 1.6 \times 10^{-5}$ K^{-1} and aluminum frames, $\alpha_{Al} \approx 2.4 \times 10^{-5}$ K^{-1} would lead to a less than 5% difference in measured α_{PS} at all temperatures, far smaller than either their or our measurement uncertainties. The $\alpha_{>Tg}$ data are more intriguing because they find $\alpha_{>Tg} \approx 5.5 \times 10^{-4}$ K^{-1} for h $\gtrsim$ 55nm and $\alpha_{>Tg} \approx 1 \times 10^{-4}$ K^{-1} for $h \lesssim 55$ nm. The thicker film value of $\alpha_{>Tg}$ is in agreement with the α_{liquid} we measure above both transitions while their value of $\alpha_{>Tg}$ for thinner films is close to the α_{middle} we measure in between the two transitions. We were not able to reliably measure both transitions for films much thicker than 60 nm as they are no longer clearly separated and begin to blend in to one another. As such, it is not unreasonable to assume that for $h \gtrsim 55$ nm in Ref. 62 a blending of the transitions occurred leading to the higher reported $\alpha_{>Tg}$. This scenario seems even more likely due to the measurements being performed on heating with at least 10 minute holds[156] every 3 K to collect the X-ray reflectivity data, presumably until holes formed at higher

temperatures. There is no thickness *vs*. temperature data shown for any high MW films to test this hypothesis. It should be noted that the $T_g(h)$ data presented appear to deviate from previous literature results for films $\lesssim$ 55 nm, likely due to the difficulties in determining T_g when the contrast of the transition is weak. In short, their temperature-dependent thickness data, with data only every 3 K, is probably insufficient to comment on the TCE in the thin films in great detail.

Thermal expansion has been measured and discussed in interpreting T_g reductions in thin supported polymer films since the very first measurements.[30,159] Unfortunately, both the magnitude and direction of the change in TCE both above and below T_g with decreasing film thickness for polystyrene films is not in agreement across the various studies.[17,30,34,36,47,55,62,70,155,156,196–198] Table 5.1 lists the change TCE as film thickness is reduced among the relevant studies available in the literature. We list the results in this section by technique not to imply that there is a definitive relation between the experimental technique and result, but to make the summary more useful for the reader and the references easier to follow. One particularly interesting study on supported PS films was that by Inoue *et al*. who used neutron reflectivity to measure the T_g and TCE of 20 nm thick layers as a function of distance from both the silicon substrate and the free surface by building alternating deuterated and hydrogenated multilayer PS films.[198] They found that the substrate layer had a zero TCE and exhibited no T_g between 298 and 403 K, while the center of the film exhibited bulk T_g and TCE values, and the surface layer showed a T_g reduced by ~20 K with bulk TCE both above and below T_g.

Table 5.1: Literature summary of the change in thermal expansion with decreasing film thickness. ↑, -, and ↓ indicate an increase, no change, or decrease, respectively, in TCE as film thickness is reduced. A "dead layer" refers to a near substrate layer exhibiting zero or glassy TCE at all measurement temperatures. A "liquid(-like) layer" refers to a near free-surface layer exhibiting TCE at all measurement temperatures. A √ in these columns indicates that the Reference's results require that layer to exist in a layer model picture. Some results can also be explained by a three-layer model and are indicated in the "both" column. Experimental techniques are listed for completeness, not to imply that the results are technique dependent.

Supported PS						
Technique	α_{glass}	α_{liquid}	dead layer	liquid layer	or both	Ref.
X-ray reflectivity	↓	-	√			197
X-ray reflectivity	↓	-	√			156
neutron reflectivity	↓	↓	√		√	198
positron annihilation lifetime spectroscopy	-	↓	√		√	34
X-ray reflectivity	-	↓	√		√	47
ellipsometry	-	-				155
ellipsometry	-/↑	-		√	√	70
capacitive dilatometry	↑	↓			√	196
ellipsometry	↑	-		√		30
ellipsometry	↑	-		√		17
Free-standing PS						
Technique	α_{glass}	α_{liquid}				Ref.
ellipsometry	-	↓				55
BLS	-	↓				36
X-ray reflectivity	↓	↓				62

As previously discussed for free-standing films, there is already a limited number of T_g studies and even fewer of those are with a technique able to measure the thermal expansion as shown in Table 5.1.[36,55,62] Additionally, the reproducibility of the TCEs was

reported to be poor with BLS[36] and ellipsometry[55] such that only $\alpha_{liquid}/\alpha_{glass}$ ratio data were shown in the BLS study (and only for low MW) while only qualitative descriptions were given in the ellipsometry study. Both the BLS[36] and ellipsometry[55] study reported a relatively constant $\alpha_{<Tg}$ while $\alpha_{>Tg}$ was reported to qualitatively decrease with decreasing film thickness. The X-ray reflectivity study saw a decrease in both $\alpha_{<Tg}$ and $\alpha_{>Tg}$ for both low and high MW PS films,[62] as previously discussed in this section.

To make sense of all of the literature reports on the thickness dependence of TCE in thin PS films, we can attempt to evaluate the results with the popular layer model of depth dependent dynamics in thin polymer films. For simplicity, and in the interest of brevity, we will use a layer model in which the layer thickness is constant as a function of temperature. This temperature-independent layer model has successfully been employed in the past,[30] but it should be noted that several results require a temperature-dependent layer thickness for successful modeling,[24,36,135] including our own physical aging measurements on thin supported PS films.[24] Evidence also points to a gradient in dynamics as opposed to discrete layers.[48,120] The commonly employed layers are a so-called "dead layer" near the substrate that exhibits a zero or glassy TCE, and a liquid-like surface layer with a liquid TCE at all temperatures. We can calculate a film's measured TCE by averaging the TCEs as a function of depth or layer.

If a polymer film has a dead layer that is bound to the substrate such that it shows no thermal expansion, then both the measured α_{liquid} and α_{glass} will be reduced from the bulk values in agreement with Ref. 198. If the substrate layer simply maintains α_{glass}^{bulk} at all temperatures, with no T_g in the measured temperature range, then α_{liquid} will be reduced and α_{glass} will show no change in agreement with Refs. 34,47,156,197. A liquid-

like free surface layer that exhibits α_{liquid}^{bulk} at all temperatures, with no T_g in the measured temperature range, would cause α_{liquid} to show no change with film thickness and α_{glass} to be increased in agreement with Refs. 17,30,70. Finally, if a film has both a dead substrate layer and a liquid surface layer then α_{liquid} will be reduced and α_{glass} will be increased, unaffected, or decreased depending on the relative size of the altered layers, in agreement with Refs. 34,47,70,196,198. This layer model analysis of the results is summarized in Table 5.1. Examining the layer model analysis results in Table 5.1, it appears that measurements performed with X-ray reflectivity, neutron reflectivity, and positron annihilation lifetime spectroscopy can be interpreted with at least a dead substrate layer while measurements performed with ellipsometry, for the most part, can be interpreted with a liquid surface layer. We will not speculate on the reason for this grouping.

Puzzlingly, the reported TCEs for free-standing films[36,55,62] do not match with the (constant thickness) liquid-like surface layer model as expected. A constant thickness liquid-like surface layer on each free surface would lead to no change in α_{liquid} and an increase in α_{glass}, but measurements on free-standing films have only reported a decrease in α_{liquid} and either no change or a decrease in α_{glass}, both inconsistent with a liquid-like surface layer. However, we showed previously[66] and earlier in this chapter that there are two transitions and thus three TCEs in high MW free-standing PS films: α_{glass}, α_{middle}, and α_{liquid}. This makes the application of the layer model more ambiguous. In the BLS study[36] and the M_w = 303 kg/mol data in the X-ray reflectivity study,[62] the reported behavior of $\alpha_{<Tg}$ and $\alpha_{>Tg}$ are for low MW free-standing films. This means that the mechanism of high MW T_g reduction may not be active, leading to only one transition

that corresponds to our upper transition such that $\alpha_{<Tg}$ and $\alpha_{>Tg}$ are the same as α_{glass} and α_{liquid}. The conflict with the liquid-like layer model prediction of TCEs still stands (even with a temperature dependent liquid-like layer thickness). In the ellipsometry study[55] and M_w = 2890 kg/mol data in the X-ray reflectivity study,[62] the reported behavior of $\alpha_{<Tg}$ and $\alpha_{>Tg}$ are spanning transitions likely corresponding to our lower transition such that $\alpha_{<Tg}$ corresponds with our α_{glass} and $\alpha_{>Tg}$ corresponds with our α_{middle}. Since the liquid-like layer model analysis has previously been successfully applied to supported (with constant layer thickness) and low MW free-standing films (with temperature dependent layer thickness), it seems likely that the liquid-like layer would be contained entirely in the upper transition and may not contribute at all to the lower transition. Further work on TCE behavior in ultrathin polymer films would be recommended, but what is needed most is a way to reconcile these results with some insight into the response of the various techniques or experimental variables that lead to the disparity. Of note, some recent progress has been made towards a better understanding of the length scales associated with the liquid-like layer of enhanced mobility, specifically that a liquid-like layer may not be a useful definition of the depth from the free surface to which dynamics are enhanced.[28,38,136]

In the present results on ultrathin free-standing PS films, we have not just a liquid and glass TCE, but also an intermediate TCE between the two transitions we observe. By comparing the TCEs above, in-between, and below the transitions, we can determine the relative strength of the two transitions. To do so, we calculate the fraction of the total change in TCE that occurs on passing through the lower transition $(\alpha_{middle} - \alpha_{glass}) / (\alpha_{liquid} - \alpha_{glass})$. We consider this a measure of the fraction of the film that is still mobile

between the two transitions. This calculation assumes that both of the transitions are true glass transitions such that the film is not completely liquidy or glassy between the two transitions. This assumption will be tested in the next section *via* physical aging measurements. For the ultrathin films for which two transitions are visible ($h \leq 60$ nm), the mobile fraction was found to be 11 ± 5 %. We interpret this result as indicating that ~90% of the film solidifies on cooling through the upper transition and ~10% of the film remains mobile to much lower temperatures (up to 60 K below the upper T_g), finally solidifying at the lower transition. Given the spread in our TCE data, we cannot make any statements about the thickness dependence of the mobile fraction beyond the fact that if one exists, it is fairly weak.

The ~10% mobile fraction that exists between the two transitions is likely not due to the center of the film solidifying at the upper transition with the free surface solidifying at the lower transition. The complete argument and literature discussion of this point is contained in Chapter 2 (Ref. 66). Strong support for this argument is in the quantitative match between the thickness and (lack of) M_w dependence of the upper transition we measure with the $T_g(h)$ observed in low MW free-standing films, which were modeled as the average of a reduced T_g at the free surfaces and a bulk T_g at the center of the film.[36] The free surface and associated gradient in dynamics, often observed as a broadening of the glass transition as the film thickness is reduced in supported films,[17,70,199] is contained entirely within the upper transition.[24,36,48]

The fact that we are able to perform these T_g measurements at all is confirmation that the majority of the film is glassy between the two transitions. If the lower transition was the true and only glass transition, then one would expect the films to rapidly

disintegrate through hole formation and growth as they are brought tens of degrees above T_g.[36,55,83,84] We propose that the majority of the film, including the near free surface region, solidifies at the relatively broad upper transition, providing a rigid matrix in which some small portion of the film remains mobile to much lower temperatures. A full discussion of this interpretation of the films and literature is in Section 2.3 (Ref. 66). We next test whether the two transitions are both actual glass transitions, and the interpretation of a ~10% mobile fraction between the two transitions, by performing physical aging measurements below and in-between the two transitions in ultrathin, high-MW free-standing PS films.

5.3.2 Physical aging below and between the two transitions

The first and potentially most important question to ask about these two reduced T_gs we have observed in ultrathin, high MW, free-standing PS films is whether they are both actual glass transitions, and if not, then which one is actually the film's glass transition? Since one of the most important and fundamental properties of the glass transition is the non-equilibrium state of the material below T_g, physical aging measurements of films held between and below the two transitions is a critical test of the film's glassy state. To illustrate the parameters of the physical aging measurements required to perform this test, we diagram the relevant information in Figure 5.3. For a particular film thickness (below ~70 nm), a sample will exhibit two transitions. The thickness dependence of the upper transition is given by the dashed blue and cyan curve in Figure 5.3. The thickness dependence of the lower transition depends on the molecular

weight and is shown for the two MW used in this study, M_w = 2,257 kg/mol (solid blue line) and M_w = 11,000 kg/mol (solid cyan line).

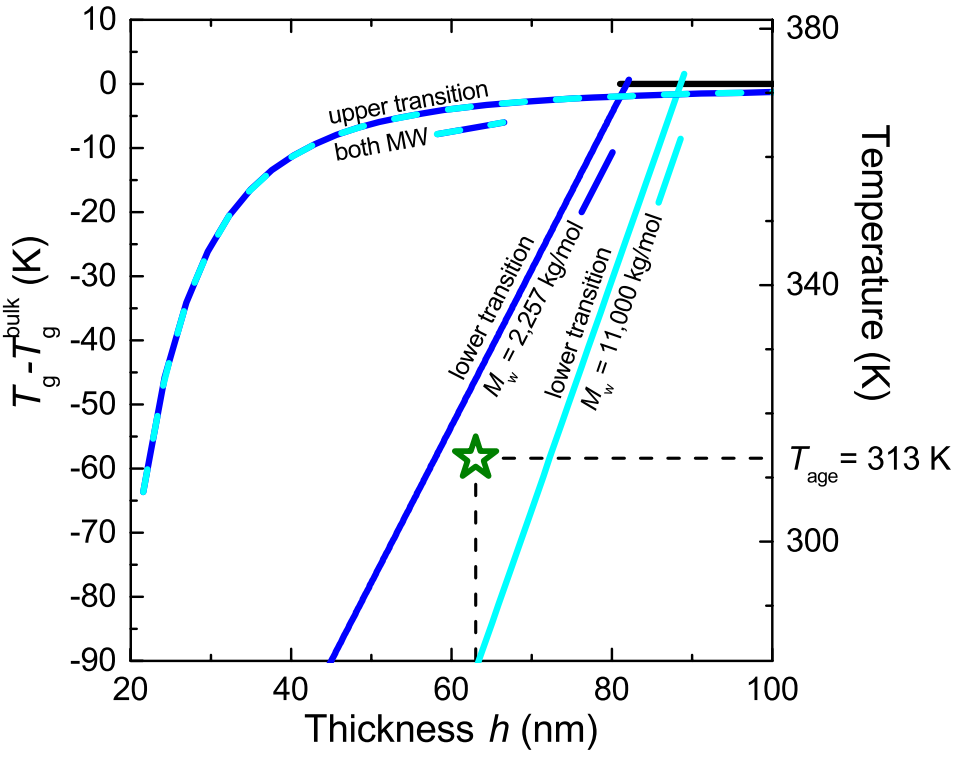

Figure 5.3: Illustration of the T_gs for high MW free-standing PS films and the relative location of the aging experiment performed in this work. Physical aging measurements were performed with parameters given by the green star: $T_{age} = T_g^{bulk} - 58.4$ K = 313 K and $h \approx 63$ nm. The dashed blue/cyan curve represents the low MW free-standing PS $T_g(h)$ film data from Mattsson *et al.*[36] which matches the upper transition we previously observed in high MW free-standing PS films.[66] The two solid lines represent the $T_g(h, M_w)$ from the scaling provided by Dalnoki-Veress *et al.* in Ref. 55 of the MW used for our physical aging measurements, M_w = 2,257 kg/mol (blue) and M_w = 11,000 kg/mol (cyan). For the M_w = 2,257 kg/mol film physical aging (green star) is performed below both transitions while for the M_w = 11,000 kg/mol film, the physical aging measurement (green star) takes place between the two transitions.

On first glance, one may propose to vary the film thickness with a constant aging temperature or vary the aging temperature with a constant film thickness such that the physical aging data span across the thickness/temperature region in which the lower transition occurs for a given MW. However, this type of data would require a large

number of measurements to be collected and either multiple levels of analysis or significant assumptions. This is due to the temperature dependence of the aging rate that exists even in the bulk[19,23,163] and the thickness dependence of the aging rate in supported films that we previously showed was due to the $T_g(h)$ reduction that occurs in ultrathin supported films.[24] Distinguishing the unknown effect of the lower transition on physical aging behavior in ultrathin, high-MW, free-standing PS films from the dependence of aging on thickness due to just the upper transition and/or temperature in general would likely be quite difficult, if not impossible given the experimental uncertainty of the aging rate we can measure for these ultrathin free-standing films.

To form a simpler and more elegant test, we have chosen to perform physical aging measurements at one aging temperature on films with identical film thickness but of different molecular weights. Note that physical aging is inherently independent of molecular weight as it represents only very local motion of chain segments. As such, by varying only the molecular weight we can alter the corresponding location of the lower transition for the two sets of films. This allows a more straightforward determination of the effect of the lower transition on the physical aging behavior on ultrathin high-MW free-standing PS films. All physical aging measurements were performed with the aging temperature T_{age} = 313 K and film thickness h = (63 ± 1) nm represented by the green star in Figure 5.3. For a film with M_w = 2,257 kg/mol, the two transitions are given by the dashed blue/cyan line and the solid blue line such that the aging temperature is below both transitions for a film with h = 63 nm. For a film with M_w = 11,000 kg/mol, the two transitions are given by the dashed blue/cyan line and the solid cyan line such that the aging temperature is between the two transitions for a film with h = 63 nm. The solid

lines representing the lower transition for the M_w = 2,257 kg/mol (blue) or M_w = 11,000 kg/mol (cyan) films is calculated using the scaling from Dalnoki-Veress et al. for $T_g(h, M_w)$ of high MW free-standing films.[55] We have previously measured T_g for M_w = 2,257 kg/mol films[66] and found that the lower transition we measure is in agreement with, though slightly higher than, the predicted values from the Dalnoki-Veress *et al*. scaling.[55] We are in the process of performing T_g measurements to confirm that at the aging temperature used here, T_{age} = 313 K, the ~63 nm, M_w = 11,000 kg/mol films are between the two transitions.

Figure 5.4 shows the normalized film thickness h/h_0 as a function of logarithmic aging time for (63 ± 1) nm thick free-standing PS films of M_w = 2,257 kg/mol (open blue symbols) and M_w = 11,000 kg/mol (closed cyan symbols) aged at 313 K. When plotted in this manner, the physical aging rate $\beta = -\partial(h/h_0)/\partial(\log t)$ is the slope of the data,[23,24,113,135,200] where h_0 is the film thickness at an aging time of 10 minutes and t is the aging time. For comparison, the black line in Figure 5.4 represents the physical aging rate expected for bulk, 500 nm thick films aged at the same aging temperature of 313 K, $\beta_{bulk} = (5.2 \pm 0.3) \times 10^{-4}$.[112] The average physical aging rates measured are $\beta_{below}^{2M} = (5.4 \pm 0.2) \times 10^{-4}$ for the M_w = 2,257 kg/mol films aged below both transitions and $\beta_{between}^{11M} = (3.4 \pm 0.3) \times 10^{-4}$ for the M_w = 11,000 kg/mol films aged between the two transitions. These data are limited due to the extreme difficulty in preparing the ultrathin free-standing samples and performing the physical aging measurements. However, one of the 11,000 kg/mol films was successfully run a second time and showed the same aging behavior, indicating that we were observing physical aging and not some other, non-reversible process.

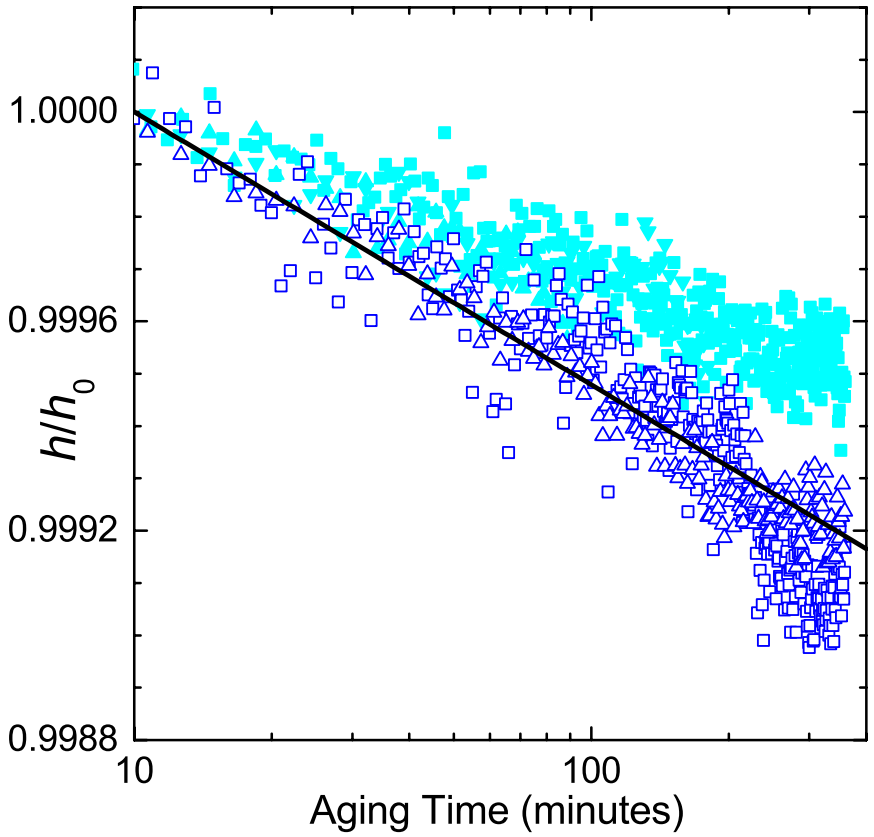

Figure 5.4: Normalized film thickness h/h_0 *vs*. logarithmic aging time for (63 ± 1) nm thick free-standing PS films of M_w = 2,257 kg/mol (open blue symbols) and M_w = 11,000 kg/mol (closed cyan symbols) aged at 313 K. Multiple measurements for each MW are shown as different symbol shapes to demonstrate reproducibility. The solid black line is what would be expected for a bulk film aged at the same temperature (based on our previous temperature dependent aging measurements of ~500 nm free-standing films).[112]

It should be noted that the annealing protocol to remove thermal history used here for physical aging measurements on ultrathin free-standing films is significantly reduced from that for the bulk data used for comparison in the previous paragraph and Figure 5.4. In previous physical aging measurements on supported films of all thicknesses and bulk free-standing films, samples were annealed at T_g + 20 K = 383 for at least 20 minutes to completely remove any previous thermal history.[23,24,112,113,200] This annealing protocol unfortunately leads to hole growth almost immediately in the ~63 nm thick free-standing films studied here. To allow for erasure of thermal history while eliminating hole

nucleation and growth, we adopted an annealing protocol similar to the temperature profile we previously used in T_g measurements on ultrathin free-standing films in Chapter 2 (Ref. 66). The reduced annealing protocol consists of heating from 363 – 383 K at 0.5 K/min and holding for 1 min followed by a quench at 90 K/min. This annealing resulted in aging rates for bulk films equivalent to previous aging measurements. Unfortunately, this reduced annealing protocol still produced tiny holes in the ~63 nm thick films. On reducing the maximum temperature of the protocol to 379 K holes were no longer formed. This further reduced annealing protocol has not yet been confirmed to produce the same aging rates in bulk films as the more aggressive annealing does, therefore comparison of aging rates with bulk films should be done with caution.

Since we observe physical aging in high MW free-standing PS films even when held at a temperature below the upper transition but *above the lower transition*, we conclude that the upper transition is an actual glass transition. This agrees with several previous results in the literature and our TCE findings that ~90% of the film solidifies at the upper transition. The ability to hold these ultrathin films tens of degrees above the lower transition for near perpetuity without hole formation indicates that a large part of the film or mode of relaxation is frozen to flow. Previous hole growth measurements on ultrathin high MW free-standing PS films would be consistent with the upper transition controlling the properties of flow.[83,84] Paeng *et al*. have done a series of studies using a photobleaching dye reorientation to measure the dynamics in thin free-standing films of various polymers.[46,88] They found a relaxation that corresponds to the bulk α-relaxation as well as a faster population that they attributed to the free surface.[46] However, both of these relaxations were MW independent, are the same for both low (M_w = 170 kg/mol)

and high (M_w = 955 and 6,041 kg/mol) MW, and are the same in supported and free-standing films. In addition, all of the measurements were performed at temperatures well above where the lower T_g would be expected for the film thicknesses and high MWs they studied. Thus, the fast dynamical population they observed, and associated with the free surface, occurs within the temperature range of our upper transition. Lastly, O'Connell and McKenna have determined T_g from the creep of high MW (M_w = 994 kg/mol) free-standing PS nanobubbles.[65,189] The $T_g(h)$ values they find are closer to the upper transition than the $T_g(h)$ expected for their high MW.

Ngai and coworkers have recently used the Coupling Model to propose an explanation for our finding of two T_gs in high MW free-standing films, although only qualitative discussion of the effect of film thickness on the different coupling parameters for α-relaxation and sub-Rouse mode relaxations was included.[201] They propose that the lower transition is the "true" α-relaxation, while the upper transition corresponds to motion of sub-Rouse modes inherent in the Coupling Model. Sub-Rouse modes are relaxations that occur between the segmental relaxation and the shortest Rouse mode relaxation.[202] Such a theoretical explanation seems to be in contradiction to our findings here of physical aging occurring above the lower transition because the freezing out of α-relaxations leading to non-equilibrium structural relaxation has long been associated with the glass transition.[10,203]

The mechanism by which Ngai and coworkers propose the α-relaxation exhibits an increase in mobility, and concomitant decrease in the lower T_g, is due to chain orientation as the film thickness becomes smaller than the radius of gyration R_g of the polymer.[201] However, chain orientation effects would be the same in supported and free-

standing films, yet no lower transition has been reported in supported films to date. An unintentionally direct test of the chain orientation basis of the lower T_g was performed by fluorescence measurements of multi-layer high-MW free-standing PS films by Kim and Torkelson.[64] They found that free-standing films of $h < 60$ nm report the same average and individual layer T_g when made out of one, two, or three layers. The amount of chain orientation in such a multi-layer sample should increase with increasing number of layers as the chains are restricted to relatively smaller portions of the film, yet no effect on T_g is observed. In addition, the exceedingly high quality $T_g(h, M_w)$ data by Dalnoki-Veress *et al*.[55] allowed them to perform a detailed analysis[55,68] of the MW dependence of what we observe as the lower transition. They found that the data do *not* scale as $M_w^{1/2}$ but that the slope of $T_g(h)$ is a logarithmic function of M_w, indicating that the T_g reduction is not directly related to the chain size ($R_g \sim M_w^{1/2}$).

The only other theoretical proposal specifically designed to explain the high MW free-standing T_g reductions is based on the "sliding model" idea by de Gennes.[80,81] As the film thickness approaches the size of the polymer (roughly $2R_g$) significant numbers of chains have large "loops" that meet the same free surface at two points and "bridges" that span the thickness of the film from one free surface to another. In the sliding model, the enhanced mobility at the free surface is able to propagate into the depth of the film along the backbone of the chain through these loops and bridges such that enhanced mobility reaches much further into the film than the immediate free surface, with the distance and magnitude of enhancement increasing with MW. Later, Lipson and Milner worked out a quantitative test of de Gennes' sliding mode picture in what they called a delayed glassification model.[37,90] The results of this effort showed a $T_g(h, M_w)$ reduction

that was linear in film thickness as experiments observe. However, the $T_g(h, M_w)$ prediction for different molecular weights intersected at a single point of small film thickness such that the difference in T_g between different MWs became smaller as thickness was reduced.[37] This is in direct contrast with experiments in which the $T_g(h, M_w)$ data intersect at larger film thickness and different MWs show increasingly different T_g as film thickness is reduced.[55]

Returning to the results of our physical aging measurements, we find that the physical aging rate we measure for a M_w = 11,000 kg/mol film held between its two transitions, $\beta_{between}^{11M}$ = (3.4 ± 0.3) × 10^{-4}, is significantly less than that for a M_w = 2,257 kg/mol film held below both of its transitions, β_{below}^{2M} = (5.4 ± 0.2) × 10^{-4}, which itself is nearly identical to that predicted for 500 nm thick free-standing PS films based on our previous $\beta(T)$ measurements in Chapter 4 (Ref. 112), β_{bulk} = (5.2 ± 0.3) × 10^{-4}. While small differences in annealing protocol between the ultrathin and bulk free-standing films still need to be verified, we discuss here the importance of these results. In Chapter 3 (Ref. 24) we found the aging rates of (29 ± 1) nm thick supported PS films to be reduced at all aging temperatures compared to bulk films because a portion of the film near the free surface, whose length scale increases with decreasing temperature, does not participate in aging due to a gradient in local T_g. For supported films aged at 313 K there is a large reduction in the physical aging rate from $\beta_{Sup.bulk}$ = (8.2 ± 1.3) × 10^{-4} for bulk films to $\beta_{Sup.29nm}$ = (3.4 ± 1.0) × 10^{-4} for (29 ± 1) nm thick films. This is a nearly 60% reduction in aging rate for the thinner films due to the presence of the free surface. For the 63 nm thick, M_w = 11,000 kg/mol free-standing films aged between its two transitions we will suppose, for the purpose of a simple comparison, that the ~90% fraction of the

film solidified at the upper transition would age with a rate similar to a supported film of half the film thickness (two free surfaces *vs*. one free surface), and the ~10% mobile fraction with much lower T_g does not age. Conveniently, the thickness of the thin supported films we previously measured (29 nm) is about half the thickness of the thin free-standing films measured in this chapter (63 nm), facilitating a simple comparison. Based on this reasoning we might expect an aging rate of *glass fraction* × ($\beta_{thinSup.}$/ $\beta_{thickSup.}$ × β_{bulkFS}) ≈ 90% × (40% × 5.2 × 10^{-4}) = 1.9 × 10^{-4}. However, our measured rate of $\beta_{between}^{11M}$ = (3.4 ± 0.3) × 10^{-4} is significantly faster than this simple comparison would predict.

It is unclear what the temperature dependence would be of the aging behavior for the portion of the film solidifying at the lower transition but we will assume for now that at 313 K this ~10% mobile fraction of the film exhibits an aging rate of no more than the maximum we measured for bulk free-standing films, ~8 × 10^{-4}. If the 10% mobile fraction of the film ages at this maximum rate in the M_w = 2,257 kg/mol film aged below both transitions, then we can combine this with the type of analysis done in the previous paragraph. Starting from the supported film measurements we would expect an aging rate of *glass fraction* × ($\beta_{thinSup.}$/ $\beta_{thickSup.}$ × β_{bulkFS}) + *mobile fraction* × $\beta_{10\%}$ ≈ 90% × (40% × 5.2 × 10^{-4}) + 10% × 8 × 10^{-4} = 2.7 × 10^{-4}. Again, this is much lower than the measured rate of β_{below}^{2M} = (5.4 ± 0.2) × 10^{-4}. Alternatively, we could start with the aging rate we measure for the M_w = 11,000 kg/mol films aged between the two transitions. In such a case, assuming that only 90% of the 11,000 kg/mol film ages between its two transitions, we could back out the aging rate of that portion of the film $\beta_{90\%} = \beta_{between}^{11M}/glass\ fraction$ = 3.4 × 10^{-4}/90% = 3.8 × 10^{-4}. Applying this to a similar aging rate prediction would give

$\beta_{between}^{11M}$ + *mobile fraction* × $\beta_{\max}$ = 3.4 × 10^{-4} + 10% × 8 × 10^{-4} = 4.2 × 10^{-4}, still lower than our measured aging rate of β_{below}^{2M} = (5.4 ± 0.2) × 10^{-4}. So it appears that this basic analysis is not sufficient to explain the physical aging rates of our ultrathin high MW free-standing films. Further measurements may be more successful with a more thorough analysis. However, at present we still conclude that the aging rate for ultrathin high MW free-standing films held both between and below the two transitions appears to be anomalously high given our previous analysis of film thickness dependent aging rates in supported PS films. Additionally, the difference between the aging rate of a film held between the two transitions and a film held below both transitions is much larger than one would expect given that the TCE results indicate that only ~10% of the film solidifies at the lower transition.

5.4 Conclusions

The results presented here further support our previous finding that ultrathin high MW free-standing films exhibit two glass transitions.[66] The lower, MW dependent transition we measure matches that previously seen in high MW free-standing films while the upper, MW independent transition we measure matches the $T_g(h)$ reduction observed in low MW free-standing films. In this chapter we further measured the thermal coefficient of expansion (TCE) above, between, and below the two transitions. We find that ~90% of the film solidifies on passing through the upper transition, while only ~10% of the film remains mobile until freezing out at the second transition, and that there is only a minor decrease in all of the TCE values as the film thickness is reduced.

We have also performed physical aging measurements on films held between and below the two transitions. Since we observe physical aging of a film held between the two transitions, we conclude that the upper transition is an actual glass transition and thus associated with the α-relaxation, in contradiction with the recent Coupling Model prediction of our two observed T_gs.[201] The aging rate we measure for a film held between the two transitions is significantly slower than that held below both transitions, indicating a stronger effect than would be expected given the ~10% mobile fraction finding from the TCE measurements. Both of the aging rates are also faster than one would expect based on a simple analysis following our previous physical aging measurements on ultrathin supported PS films. The combined conclusion from our measurements of T_g, TCE, and physical aging rate of ultrathin high MW free-standing PS films is that the upper MW independent transition is an actual glass transition that accounts for solidification of most of the film (below which physical aging occurs), the lower MW dependent transition is due to some smaller fraction of the film solidifying at a much lower temperature, and that the lower transition contributes to the physical aging rate in a potentially stronger than expected way.

Chapter 6
Summary

6.1 Introduction

There has been a long history of work on confinement effects in polymers and I hope to have contributed to the advancement in understanding the glass transition and physical aging behaviors of thin and ultrathin supported and free-standing polystyrene (PS) films. While I, of course, believe each of the chapters in this dissertation are important and have provided a significant contribution to the field, the real test is through the reception by others in the field. The results of Chapters 2 and 3 were published in 2011[66] and 2010[24], and have since gathered significant numbers of citations. However, the results of Chapter 4 have only recently been published,[112] while Chapters 5 and the Appendix are currently unpublished. This Summary Chapter describes the main impacts of this work on the field, as judged by the literature, and highlights outstanding questions related to these important findings.

The first significant impact is measurement and discussion of what is the length scale associated with the free surface dynamics of PS as determined by physical aging measurements on ultrathin PS films.[24] We find that because the physical aging rate is reduced in thin PS films, with a larger reduction at lower temperatures, the depth to which the physical aging rate is perturbed by the free surface must increase with

decreasing temperature. This is in agreement with confinement being related to the idea of cooperative motion, known to occur in glassy systems.[9,28]

A second main impact of this dissertation work is the discovery of two simultaneous mechanisms of T_g reduction in ultrathin high molecular weight (MW) free-standing PS films leading to two reduced T_gs.[66] The lower transition is MW dependent and has previously been observed in these high MW free-standing films,[55] while the upper transition is MW independent, has not been seen before in these films, and matches the T_g reduction previously measured in low MW free-standing films.[36] We anticipate that our measurement of physical aging between the two reduced T_gs described in Chapter 5 will further strengthen the finding of two T_gs in ultrathin high MW free-standing PS films.

The final significant impact we cover in this summary chapter is the finding that when a free-standing PS film is stressed as it is cooled into a glass, the resulting physical aging rate is increased by nearly a factor of two compared to a film cooled into the glassy state nearly stress free. This significant change in physical aging rate is brought about by a stress that is simply due to the thermal expansion mismatch between the polymer film and the frame on which it is held. Finally, the Appendix will hopefully provide the background and methods necessary for future students and researchers to perform the full thermoviscoelastic calculation of this thermal expansion mismatch based stress in polymer films, should they so desire.

6.2 Free Surface Length Scale

In 2010, the thin film physical aging results of Chapter 3 were published,[24] reporting that the depth to which the enhanced free surface mobility propagates into the film decreases with increasing temperature. This finding is in agreement with the magnitude and temperature dependence of previous estimates of a length scale of enhanced dynamics determined by T_g measurements on low MW free-standing films[36] and nanoparticle embedding experiments.[39] Since then, there have been several other reports on the temperature dependence of a free surface length scale in polymer films.[40,46,135,204,205] However, all of this recent work has determined a free surface length scale that increases with increasing temperature.

Anisotropic photobleaching based dye reorientation measurements on ultrathin free-standing[46] and supported[204] PS films by Paeng *et al*. found two populations of relaxations, one with bulk-like dynamics and one with much faster dynamics. Assuming the fast population is located near the free surface, they calculated the thickness of a "mobile surface layer" and found that it grew with increasing temperature, reaching 7 nm at T_g. This "mobile surface layer" thickness did not depend on MW or film thickness for free-standing films and showed the same behavior in supported films less than 28 nm thick. Nanoparticle embedding experiments performed slightly below T_g similarly show two relaxations with a two step embedding process corresponding to relaxation of bulk and the free surface.[39,40] The embedding due to the free surface relaxation stops at a depth that increases with increasing temperature, reaching 5 nm at T_g. Another mechanical measurement that probes the elastic modulus behavior, compared to the viscous behavior from nano-embedding experiments, are the surface wrinkling measurements developed at

NIST.[150,206] By varying T_g *via* MW[205] or side group[139], Torres *et al*. were able to characterize the reduction in modulus as a function of distance from T_g. By fitting their data to a bilayer model with a reduced modulus surface layer, Torres *et al*. also found that the size of such a "soft surface layer" increased as the experimental temperature approached the material's bulk T_g.

Particularly illuminating in comparison with our work is the reported increase in a "mobile free surface layer" thickness in PS films with increasing aging temperature as measured by methods nearly identical to those previously developed in our lab[23] and used in the ultrathin supported PS film physical aging study of Chapter 3 (Ref. 24). Frieberg *et al*.[135] measured the physical aging rate for thin films of linear or star shaped PS molecules as a function of temperature and film thickness. They modeled their data by assuming that material at a depth z into the film will age with a rate given by the distance from the aging temperature to the local $T_g(z)$: $\beta(z) = \beta[T_{age} - T_g(z)]$ using a $T_g(z)$ that is described by a slightly less commonly used 1/h type function from Kim *et al*.[118] In this analysis, their "mobile free surface layer" thickness is defined as the depth into the film at which the local aging rate is explicitly zero. This is quite different from our definition[24] where a two layer model was used to determine what layer thickness $A(T)$ near the free surface does not exhibit a bulk aging rate. Although not appreciated at the time, our enhanced dynamics layer thickness $A(T)$ is equivalent to the fraction of the film that does not exhibit bulk-like aging dynamics, assuming a monotonic increase in aging rate from a reduced (or zero) aging rate at the free surface to a bulk, temperature-dependent aging rate deep in the film.

Given these different temperature dependences of a length scale describing free surface effects in PS films as reported by several authors, including from near identical measurements by different groups, it is imperative to be explicit about how these length scales are being defined. Some recent efforts have been made in this direction, [28,38,136] and their terminology and descriptions are adapted here to describe the problem. There are essentially two main ways to define a free surface length scale: the depth to which the film has *liquid-like dynamics* λ_τ and the depth to which the film has *enhanced dynamics* λ_A. A more precise way to define a *liquid-like layer size* λ_τ is the depth at which the *local relaxation time is equal to a chosen time scale* τ^*, typically the experimental time scale. Similarly, a depth of *enhanced dynamics* λ_A can be defined as the depth where the *local relaxation time is a specified amount faster than the bulk value* (e.g. $\tau_{local} = 80\% \tau_{bulk}$) as described in Ref. 28.

The significant difference between these two definitions becomes apparent when one considers the very strong temperature dependence of relaxation times near T_g. As temperature is increased, the constant time liquid-like length $\lambda_\tau(T)$ must, *by definition*, diverge at the temperature where the bulk relaxation time is equal to the chosen time scale (*i.e.* when $\tau_{bulk} = \tau^*$). This increase and divergence occurs regardless of whether or not the fundamental length scale of surface effects has any temperature dependence at all.[136] Therefore, measurements of $\lambda_\tau(T)$ based on a fixed relaxation time τ^*, such as the dye reorientation, nanoparticle embedding, or modulus experiments discussed above, which see an increasing $\lambda_\tau(T)$ with increasing temperature do not provide a reliable measure of the depth to which dynamics are perturbed by the free surface. Nevertheless, Ref. 28 argues that if $\lambda_\tau(T)$ is determined at many different time scales τ^*, then $\lambda_A(T)$ can

be extracted from these depth dependent relaxation times. Since nearly all length scales associated with the glass transition in the bulk decrease with increasing temperature,[9] it is reasonable to expect that the depth to which enhanced free surface dynamics propagate into a polymer, $\lambda_A(T)$, will also decrease with increasing temperature. We thus conclude that the mobile surface length scale we calculate in Chapter 3 (Ref. 24) from our physical aging measurements, representing the fraction of the film not exhibiting bulk-like dynamics, is a reliable measure of $\lambda_A(T)$.

As is discussed in Ref. 28, it may be possible to collect data that measures the *liquid-like layer size* $\lambda_\tau(T)$ (based on a fixed relaxation time) in a way to calculate the more relevant *enhanced dynamics layer size* $\lambda_A(T)$. Such a type of analysis was done in Ref. 39 to convert a *liquid-like layer size* $\lambda_\tau(T)$ from nanoparticle embedding depths to a measure of an *enhanced dynamics layer size* $\lambda_A(T)$. This discussion of the significant difference between possible surface length scales suggests that any new measurements of such surface length scales and their interpretation must clearly define the relevant length scale. Additionally, physical aging measurements performed to equilibrium could in principle be able to provide not only another measure of the free surface length scale, but would also provide information about the nature of the equilibrium state in thin films. However, measurements to equilibrium are unfortunately limited to typically a few degrees below T_g with equilibration at lower temperatures not possible in accessible timescales.[21]

6.3 Two T_gs in Ultrathin High MW Polystyrene Films

In 2011, we published the results of Chapter 2,[66] showing the first direct experimental evidence that two separate mechanisms act *simultaneously* in high MW free-standing PS films leading to two reduced T_gs. While this is likely the most significant new finding of this dissertation,[10,58,137,169,207–211] it has yet to be directly confirmed by another group. However, several groups have noted indirect agreement with our results. The result most immediately comparable is from ellipsometric measurements contrasting high MW free-standing and supported PS films by Bäumchen *et al*.[58] who commented that *"The low contrast in the reduced transitions in freestanding films could signify that this transition is not the only (or even main) structural relaxation of the polymer films, an observation that is consistent with those made by Pye and Roth* [Ref. 66]*."*

As outlined in Chapter 2 (Ref. 66) and Chapter 5, we have previously found support for our upper transition from the dye reorientation measurements on ultrathin free-standing films by Paeng *et al*.,[46] which found a fast population in their films that is independent of MW, similar in both free-standing[46] and supported[204] films, and exists in the thickness and temperature range of the upper transition. In a recent review, Ediger and Forrest[137] describe a very similar argument to the one we have previously articulated. *"Some ideas for how to reconcile these results are suggested by recent ellipsometry experiments on free-standing polystyrene films*[Ref. 66]*; these measurements utilized an extended temperature range in comparison to earlier measurements"* concluding that *"If we focus attention on the stronger transition, there is reasonable qualitative*

agreement between the new ellipsometry results and the results in Figures 1 [Ref. 46, dye reorientation measurements] *and 2* [Ref. 40, nanoparticle embedding measurements].*"*

Continued support is also found from the nano-scale creep measurements by McKenna and coworkers.[65,190,212] An effective measure of reduced $T_g(h)$ values for ultrathin high MW free-standing PS was obtained from their nanobubble inflation measurements by identifying T_g from the transition from glassy to rubbery compliance behavior of the film.[65] Such $T_g(h)$ values determined for high MW (M_w = 994 kg/mol) free-standing films were in closer agreement with those $T_g(h)$ values previously measured in low MW free-standing films, consistent with our upper transition. If ~90% of a high MW free-standing PS film solidifies at the upper transition as we observed in Chapter 5, it seems reasonable for compliance from McKenna's creep measurements, a measure of the film's entire mechanical properties, to be in closer agreement with our upper transition.

Additionally, a recent set of physical aging measurements by Cangialosi *et al*. [211] on bulk PS found a two-step enthalpy recovery, interpreted by the authors as due to two equilibrium time scales. In their paper,[211] Cangialosi *et al*. make an analogy with our two T_gs observed in high MW free-standing films proposing that our data suggest *"... the presence of two equilibration time scales, since two jumps in second order thermodynamic properties were detected…"*. More recently, in a topical review on polymer glasses,[210] Cangialosi elaborates that *"This suggests that two equilibration time scales exist in thin PS films, which is a result analogous to that found in bulk by monitoring the enthalpy recovery of several polymer glasses in the physical ageing regime. Here, the only difference is that the more efficient equilibration of thin films*

allows us to probe the presence of two mechanisms of equilibration over significantly shorter time scales (seconds [Ref. 66] *as compared to years* [Ref. 211]*).”* It should be noted that Koh and Simon[21] have not observed the first aging plateau reported by Cangialosi and coworkers,[213] expressing concern with their analysis protocol. Thus, it may be premature to relate the two equilibration times observed by Cangialosi *et al*.[211] with our two T_gs in free-standing films.

The only proposal specifically designed to address the MW dependent mechanism of high MW free-standing films is the sliding model (described in Chapter 5) by de Gennes.[80,81] However, Lipson and Milner found that when the model was fully borne out, it did not give qualitative or quantitative agreement with experimental results.[37,90] The sliding model was also recently shown to be invalid by fluorescence measurements of multilayer high MW free-standing films, which still observed a T_g reduction for layers that do not have the free surface loops and bridges required by the sliding model.[64]

Prevosto, Capaccioli, and Ngai[201] have also very recently applied the Coupling Model to our two measured T_gs of Chapter 2 (Ref. 66). They propose that only the lower transition is associated with the true α-relaxation and that the upper transition corresponds instead to sub-Rouse modes. However, only a qualitative description of the effect of film thickness on the two relaxations is provided with no form for T_g or τ_α as a function of MW or film thickness. From the agreement of our upper transition with the dye reorientation[46] and nanobubble inflation measurements[65] discussed above, the physical aging we observe between the two T_gs in Chapter 5, and other reasons described in Chapter 5, we do not agree with Ngai and coworkers’ assignment of our lower transition to the α-relaxation and our upper transition to their sub-Rouse modes.

Efforts to determine additional parameters associated with the mechanism responsible for the MW dependent lower transition we observe in ultrathin high MW free-standing films are warranted, though it is uncertain what the clearest path towards this goal entails. The first step would be independent confirmation of our results, by another group, observing two mechanisms that result in two reduced transitions from a direct measurement on high MW free-standing films. A commonly suggested direction is to study different polymers, but in the case of free-standing films, choice of polymer should be made carefully. High enough MW must be used for the lower T_g to show a significant reduction and there must be enough of a separation between the two transitions that they are distinguishable from one another. Since we do not believe that the second mechanisms is simply due to the freezing out of the surface modes of relaxation (Chapter 2 and Chapter 5), efforts should be made to identify the location of the mobile fraction in the film by using novel sample geometries, molecular architecture, or techniques able to isolate mobile population fractions. Due to the very strong MW and thickness dependence of the lower transition (T_g changes by several degrees from a change in film thickness of only 1 nm),[55] the choice of M_w, film thickness, and temperature range of an experiment is very important.

6.4 Quench Stress Effects on Physical Aging

Our work on the physical aging of free-standing PS films in Chapter 4 (Ref. 112) found that the thermal expansion mismatch between the free-standing polymer film and the rigid frame strongly affects the physical aging rate. This thermal expansion mismatch generates a stress in the film that builds up as the film is passes through the glass

transition and is cooled further into the glassy state. The effect of the stress applied to a polymer film *as it is quenched into the glassy state* on the resulting physical aging rate of the film, and a possible interpretation in terms of the potential energy landscape picture, is being further pursued in our lab by Laura Gray. She has found that even after the stress has been removed, a glass that has been formed under a state of stress can exhibit a faster physical aging rate.[200] The most intriguing aspect of her results is that there is a minimum threshold stress below which there is no change in the aging rate with increasing stress.[200] The significant and potentially long-term modification of aging behavior in a film that is stressed as it is formed into a glass provides another interesting avenue to explore in terms of deformation effects on glassy behavior. These combined results showing that the physical aging rate can increase by nearly a factor of two just by changing the stress applied to the film, both when the stress is maintained during and removed before the aging process, indicate that future work may need to consider the stresses being applied to the film as a possible compounding factor with the parameters being studied.

Chapter 7: Appendix

Thermoviscoelastic Stress Calculation

7.1 Introduction

This appendix is an overview on the background, theory, and data needed to perform a *thermoviscoelastic* calculation of the stress developed in thin polymer films during a quench from a high temperature equilibrium state through T_g to a glassy state due to the thermal expansion mismatch between the film and the frame, either free-standing or supported. The goal is to provide the information necessary for others to perform similar calculations or to evaluate the veracity of work encountered in the literature. Viscoelasticity is one of the most significant aspects of polymer behavior and should be considered any time there is a rapid change in size or shape of a polymer melt. Often times the effects are not significant but it is important to know when they must be taken into account. It turns out that the elastic calculation of the stress built up in a PS film supported on a substrate agrees fairly well with experimental measurements in which the system was cooled through T_g to the measurement temperature.[149,150] One of the intentions of this appendix was to explore the limits of the elastic solution.

Stress σ is a measure of the forces within a material due to either externally applied forces or internally due to residual stresses. For a purely elastic material in the linear regime, the stress is proportional to the strain ε with a proportionality factor given by the modulus (E, G, K, etc.) of the material and geometry of deformation, e.g. $\sigma = E\,\varepsilon$. In elastic theory as described by Tschoegl and Riande[3,214] (others may have different

notation conventions) the full strain tensor $\varepsilon_{ij} = \partial u_i/\partial x_j$ is broken into an antisymmetric component $\omega_{ij} = ½ (\partial u_i/\partial x_j - \partial u_j/\partial x_i)$ that represents rigid body rotation and a symmetric component $\gamma_{ij} = ½ (\partial u_i/\partial x_j + \partial u_j/\partial x_i)$ that represents the deformation free of rigid body rotation. The normal components of the full strain and symmetric component are equal $\varepsilon_{ii} = \gamma_{ii} = \partial u_i/\partial x_i$, but the shear components are different by a factor of two, e.g. for simple shear in one direction $\varepsilon_{12} = 2\gamma_{12} = \partial u_1/\partial x_2$. Since the deformation geometry used in this chapter does not include any shear, we will simply refer to ε as strain to match experimental convention for the rest of the Appendix that follows after the next paragraph.

In a fully three dimensional representation, the stress σ_{ij} and strains γ_{ij} and ε_{ij} are second order tensors (3x3) and the modulus is a fourth order tensor C_{ijkl} (3x3x3x3) with 81 terms of which 21 are independent such that[214]

$$\sigma_{ij} = C_{ijkl}\gamma_{kl} \tag{7.1}$$

For the form of the equations in this paragraph, the symmetric strain component γ_{ij} is used following Tschoegl and Riande.[3,214] In isotropic materials, the tensor equation can be simplified greatly with only two independent constants left in the modulus tensor for the shear and bulk responses. The other terms in C_{ijkl} are important for materials with various forms of anisotropy. The generalized stress-strain Hooke's law for linear isotropic solids is

$$\begin{pmatrix}\sigma_1\\ \sigma_2\\ \sigma_3\\ \sigma_4\\ \sigma_5\\ \sigma_6\end{pmatrix} = \begin{pmatrix}\lambda+2G & \lambda & \lambda & 0 & 0 & 0\\ & \lambda+2G & \lambda & 0 & 0 & 0\\ & & \lambda+2G & 0 & 0 & 0\\ & & & 2G & 0 & 0\\ & & & & 2G & 0\\ & & & & & 2G\end{pmatrix}\begin{pmatrix}\gamma_1\\ \gamma_2\\ \gamma_3\\ \gamma_4\\ \gamma_5\\ \gamma_6\end{pmatrix} \tag{7.2}$$

(Eq. 4.47 from Riande)[3] or more compactly written as (Eq. 4.75 from Riande and Eq. 1.4-55 from Tschoegle)[3,214]

$$\sigma_{ij} = \lambda \Delta \delta_{ij} + 2G\gamma_{ij} \tag{7.3}$$

where G is the shear modulus, λ is Lamé's first parameter, $\Delta = trace\, \gamma_{ij} = \gamma_{11} + \gamma_{22} + \gamma_{33} = \varepsilon_{11} + \varepsilon_{22} + \varepsilon_{33} \approx \Delta V/V_0$ (where V is the volume), and δ_{ij} is the Kronecker delta (1 when $i = j$ and 0 otherwise).

Moduli have been defined for several specific geometries of deformation. In uniaxial tension there is only stress in one direction, σ_{11}, the strain in the two other directions are equal, $\varepsilon_{22} = \varepsilon_{33}$, and the Young's (tensile) modulus is defined by $E = \sigma_{11}/\varepsilon_{11}$. By plugging these definitions for uniaxial tension into Eq. 7.3, E can be written in terms of G and λ. The same procedure can be done for any deformation geometry and it should now be clear that any elastic parameter can be written in terms of any two other elastic parameters. The four most common elastic parameters are Young's modulus E for uniaxial tension, the shear modulus $G = \sigma_{12}/\varepsilon_{12}$ for parallel plate shear, the bulk modulus $K = -\sigma_{ii}/p$ for isotropic pressure p changes, and Poisson's ratio ν. Poisson's ratio is the ratio of the contraction in the transverse direction to the elongation in the direction of applied stress in a uniaxial tension experiment: $\nu = -\varepsilon_{11}/\varepsilon_{22}$. More simply, it is how much a material shrinks in one direction when you pull it in another direction. The last defined parameter is the P-wave modulus (or longitudinal bulk modulus) M, useful for acoustic pressure waves. These elastic parameters and conversion relations are defined and valid in the same limits in which Eqs. 7.1-7.3 are valid, i.e. for solid materials that are homogeneous, isotropic, and under the linear range of deformation.

Table 7.1: Conversion between elastic parameters for homogeneous isotropic linear elastic solids. Formulae available from any textbook covering elastic theory.[214]

	(K, E)	(K, λ)	(K, G)	(K, ν)	(E, G)	(E, ν)	(λ, G)	(λ, ν)	(G, ν)	(G, M)
$K =$	K	K	K	K	$\frac{EG}{3(3G-E)}$	$\frac{E}{3(1-2\nu)}$	$\lambda + \frac{2G}{3}$	$\frac{\lambda(1+\nu)}{3\nu}$	$\frac{2G(1+\nu)}{3(1-2\nu)}$	$M - \frac{4G}{3}$
$E =$	E	$\frac{9K(K-\lambda)}{3K-\lambda}$	$\frac{9KG}{3K+G}$	$3K(1-2\nu)$	E	E	$\frac{G(3\lambda+2G)}{\lambda+G}$	$\frac{\lambda(1+\nu)(1-2\nu)}{\nu}$	$2G(1+\nu)$	$\frac{G(3M-4G)}{M-G}$
$\lambda =$	$\frac{3K(3K-E)}{9K-E}$	λ	$K - \frac{2G}{3}$	$\frac{3K\nu}{1+\nu}$	$\frac{G(E-2G)}{3G-E}$	$\frac{E\nu}{(1+\nu)(1-2\nu)}$	λ	λ	$\frac{2G\nu}{1-2\nu}$	$M - 2G$
$G =$	$\frac{3KE}{9K-E}$	$\frac{3(K-\lambda)}{2}$	G	$\frac{3K(1-2\nu)}{2(1+\nu)}$	G	$\frac{E}{2(1+\nu)}$	G	$\frac{\lambda(1-2\nu)}{2\nu}$	G	G
$\nu =$	$\frac{3K-E}{6K}$	$\frac{\lambda}{3K-\lambda}$	$\frac{3K-2G}{2(3K+G)}$	ν	$\frac{E}{2G} - 1$	ν	$\frac{\lambda}{2(\lambda+G)}$	ν	ν	$\frac{M-2G}{2M-2G}$
$M =$	$\frac{3K(3K+E)}{9K-E}$	$3K - 2\lambda$	$K + \frac{4G}{3}$	$\frac{3K(1-\nu)}{1+\nu}$	$\frac{G(4G-E)}{3G-E}$	$\frac{E(1-\nu)}{(1+\nu)(1-2\nu)}$	$\lambda + 2G$	$\frac{\lambda(1-\nu)}{\nu}$	$\frac{2G(1-\nu)}{1-2\nu}$	M

The geometry we are interested in consists of a thin polymer film held as a free-standing membrane over a circular hole in a rigid frame or supported on a rigid substrate. We will use support to refer to both the free-standing frame and supported substrate from now on. When the system is cooled, both the film and the support shrink according to their respective thermal expansion coefficients. However, the thermal expansion of the polymer film is larger than that of the support and thus the support prevents the film from contracting as much as it would like to in the plane of the film. Thus, there is a strain, and therefore stress, applied to the film as the system is cooled. If the film is flat and does not have any non-uniform flow during the experiment, the free-standing and supported geometries are equivalent as equibiaxial plane stress systems. This means that there is no stress in the direction perpendicular to the plane of the film and that the stress is equal in all directions in the plane of the film:[153]

$$\sigma_{\perp} = 0, \ \sigma_{\parallel} = \frac{E}{1-\nu}\varepsilon_{\parallel} \tag{7.4}$$

We will now only be referring to the stress in the plane and will drop the parallel subscript.

7.2 Elastic Stress Calculation

The most basic and common calculations of stress are those using the linear elastic approximation. In this approximation the material is deemed elastic, i.e. the moduli do not depend on time with no viscous flow, and linear, i.e. the moduli do not depend on the amount of strain (no yield, strain hardening, strain softening, etc.). However, in most materials the moduli change as a function of temperature and for polymers in particular, they cannot be approximated as constants as a function of temperature, especially near T_g. This means that the stress must be calculated as an integral over the relevant temperatures. The derivation and calculation for the elastic case of a film held in either a free-standing state or supported on a substrate was already covered in Section 4.3.2 and published.[112] To summarize, since the film is bound to the support, the strain is defined by the mismatch in thermal expansion coefficients, such that Eq. 7.4 becomes

$$\sigma\left(T_g, T_{aging}\right) = \int_{T_{aging}}^{T_g} \frac{E_{PS}(T)}{1-\nu_{PS}(T)}\left[\alpha_{PS}(T) - \alpha_{sup}(T)\right]dT \qquad (4.9)\ \&\ (7.5)$$

when integrated from T_g, where stress starts to build up in the elastic approximation, to T_{aging} where the quench is stopped. α_{PS} and α_{sup} are the thermal expansion coefficients of the polystyrene film and support (either the free-standing frame or substrate), respectively. This elastic calculation of the stress built up in a PS film supported on a substrate has been found to agree fairly well with experimental measurements in which the system was slowly cooled through T_g to the measurement temperature.[149,150]

A side result of this stress calculation is that the thermal expansion coefficient measured by ellipsometry is different from what would be measured in a stress free state, such as in a dilatometer. The Poisson's ratio effect causes the strain in the out-of-plane *z*

direction to be affected by the equibiaxial in-plane stress giving a measured thermal expansion coefficient of

$$\alpha_{\text{measured}} = \alpha_{PS} + \frac{2\,\upsilon_{PS}}{1-\upsilon_{PS}}\left[\alpha_{PS} - \alpha_{sup}\right] \qquad (4.7)\ \&\ (7.6)$$

The "true" (or corrected) linear thermal expansion coefficient of the PS can be obtained from ellipsometric measurements by simply inverting Eq. 7.6

$$\alpha_{PS} = \left(\frac{1-\upsilon_{PS}}{1+\upsilon_{PS}}\right)\alpha_{\text{measured}} + \left(\frac{2\,\upsilon_{PS}}{1+\upsilon_{PS}}\right)\alpha_{sup} \qquad (4.8)\ \&\ (7.7)$$

Most polymers have a Poisson's ratio approaching 1/2 above T_g and a Poisson's ratio approaching 1/3 far below T_g, allowing us to use Eq. 7.7 to calculate the approximate corrections for the thermal expansion above and below T_g:

$$\text{far above } T_g\text{: } \nu_{PS} \approx \frac{1}{2} \rightarrow \alpha_{PS} \approx \frac{1}{3}\alpha_{\text{measured}} + \frac{2}{3}\alpha_{sup} \qquad (7.8)$$

$$\text{far below } T_g\text{: } \nu_{PS} \approx \frac{1}{3} \rightarrow \alpha_{PS} \approx \frac{1}{2}\alpha_{\text{measured}} + \frac{1}{2}\,\alpha_{sup} \qquad (7.9)$$

7.3 Viscoelastic Effects

7.3.1 Basics of Viscoelasticity

The two ideal material types from a mechanical perspective are an elastic solid and a viscous liquid. As described above, in a purely elastic solid the stress is directly proportional to the strain with the proportionality constant being the elastic modulus, as in a bed of springs. In a purely viscous liquid the stress is directly proportional to the rate of strain $\sigma = \eta\, d\varepsilon/dt$ where the proportionality constant η is the viscosity of the liquid, as in the proverbial dashpot. When a stress or strain is imposed on a viscoelastic material such as a polymer melt, the components of the material respond and in real materials these responses require a finite time. If these times are far shorter than the experimental time scale, the material responds in a viscous manner and all the deformation energy is

dissipated as heat. If the response times are far larger than the experimental time (or infinite), the material exhibits an elastic response and all the energy of the deformation is stored within the material, recoverable when the forces used to deform it are removed. In principle, all real materials are viscoelastic and exhibit both viscous and elastic responses due to finite relaxation times, but in many cases the pure elastic or viscous treatment is more than adequate. This can be expressed with the Deborah number $N_D = \tau_{mat}/\tau_{exp}$ where a purely viscous material has $N_D = 0$ and a purely elastic material has $N_D = \infty$. The closer N_D is to one, the more viscoelastic a material is.[214]

The main consequence of viscoelasticity is that the previously described stress and strain relations cannot be made using material constants. The behavior of viscoelastic materials is described by material functions and the stress (strain) depends on the entire strain (stress) history. This is commonly expressed with time dependent moduli [$E(t)$, $G(t)$, etc.]. At short times in viscoelastic liquids, you have an elastic response that decays to a viscous response at longer times. This leads to stress relaxation as beautifully exemplified by Silly Putty. There have been many models to describe various viscoelastic systems, typically made up of purely viscous (dashpot) and purely elastic (spring) components. The most basic models are the Maxwell element with a spring and dashpot in series to represent a viscoelastic liquid and the Voigt element with a spring and dashpot in parallel to represent a viscoelastic solid. The standard viscoelastic solid and liquid are represented by three and four elements respectively but only accurately represent special materials or limited situations.

Polymers have many relaxation times associated with the numerous Rouse modes of the chains as well as the additional long times associated with entanglement and

reptation. The large difference in relaxation times between the longest Rouse mode and reptation leads to an often long period of time where a polymer melt shows solid-like behavior known as the rubbery plateau. The distribution(s) of relaxation times can often be approximated by a stretched exponential (or double stretched exponential)[215]

$$G(t) = G_\infty + (G_0 - G_\infty)\sum_{i=1}^{2} w_i \exp\left[-\left(\frac{t}{\tau_i}\right)^{\beta_i}\right], w_1 + w_2 = 1 \qquad (7.10)$$

where $G(t)$ is the modulus of interest, G_∞ is the relaxed modulus, G_0 is the unrelaxed or glassy modulus, and w_i are the relative strengths of the distributions with average relaxation times τ_i and stretching exponents β_i.

7.3.2 Time-Temperature Superposition

As most real materials do, polymers exhibit temperature dependent moduli. However, the time dependent moduli of most polymers exhibit a special temperature dependence that follows what is called time-temperature superposition. "If all molecular motions contributing to the response have the same temperature dependence, temperature alters only the timescale of the response and the material is thermorheologically simple; that is, the behavior conforms to the time-temperature superposition principle"[216] This is also based on the idea that if all motions underlying a specific property of a material are governed by the same friction coefficient, the changes in temperature are equivalent to a change in timescale. Practically, if two modulus (or compliance) curves are collected at slightly different temperatures, one curve can be shifted along the (log) time axis such that it will overlap the other curve for some range of times. This can be done over a range of temperatures to give what is called a master curve with the modulus (compliance) of the material at a specific temperature over a much larger range of times than can be collected at that temperature by any single technique, often reaching 15

orders of magnitude in time or frequency. The amount that each curve is shifted horizontally along the time axis is called the shift factor $a_T(T)$ and can be used to generate master curves at any of the measured temperatures.

As a caveat, this method is only valid for what are called thermorheologically simple materials in which the shift factors are the same for all relaxation times. Polystyrene and most ordinary polymers, are typically considered a thermorheologically simple material although there is some evidence that the viscosity and segmental relaxation may have different temperature dependences.[5] This is not likely a big concern for our calculations since we are staying well below the viscous flow regime. Another approach to test time-temperature superposition is by comparing the temperature dependence of a material's response to different kinds of deformation. Although not much work has been done on the subject, it has been shown recently that for linear entangled polystyrene, the bulk and shear responses have the same molecular mechanisms at short times.[217,218] The bulk response is narrower and disappears before the shear response, presumably because the long-time chain mechanisms (e.g. reptation) available to the shear response are not available to the bulk response, as tested in star polymers.[219] Consequently, the bulk response can often be modeled by a single KWW function while the shear response requires a double KWW function.[215,220] Transformations to and from the other moduli are not as simple as in the elastic case and will be discussed in the next section.

7.3.3 Working with Viscoelastic Functions

In linear viscoelastic materials, the stress at a given time depends on the entire strain history. If the material is linear, stress added at one time causes a strain response

that adds linearly to all other strain responses from stresses added at any other time. The statements above and below are also true with stress as the control parameter and strain as the response. This is known as the Boltzmann superposition principle and can be expressed with Boltzmann superposition integrals:

$$\sigma(t) = \int_0^t E(t-u)\frac{d\varepsilon(u)}{du}du = \int_0^t E(t-u)d\varepsilon. \tag{7.11}$$

The first part of Eq. 7.11 is a convolution integral and it should be noted that care must be taken to properly deal with the $t = 0$ terms in the various forms of Eq. 7.11.[214] The Boltzmann superposition principle is based on the idea that all strains are additive, and in a linear material, so are the responding stresses. The form of these integrals is derived from taking a series of step strains in the continuous limit. This method is relatively simple to implement if the applied strain (stress) is known and the appropriate viscoelastic property ($E(t)$, $G(t)$, etc.) is known. However, the relevant viscoelastic property may not be known. If we only have shear, $G(t)$, and bulk, $K(t)$, moduli for a material, it is incorrect to use the relations of Table 7.1 to write $E(t) = [9K(t)G(t)] / [3K(t) + G(t)]$ and substitute it into Eq. 7.4 or 7.5. The relations among the elastic constants in Table 7.1 cannot be used to directly calculate one viscoelastic property from two others in the time domain.

The viscoelastic material properties can instead be manipulated relatively easily with the help of the Laplace transform.[214] The Laplace transform, $\bar{f}(s)$, of the function $f(t)$ is given by[214]

$$\overline{f}(s) = \mathcal{L}[f(t), t, s] = \int_0^\infty f(t)e^{-st}dt \tag{7.12}$$

where $s = a + i\omega$ is the transform variable. (We will use the overbar notation when referring to a function in the Laplace domain.) Time-dependent viscoelastic responses lie

on the real axis with $\omega = 0$ and frequency-dependent viscoelastic responses are on the positive imaginary axis with $a = 0$ (roughly equivalent to a Fourier transform). The real part a controls how strongly the response is increasing or decreasing with time.

The real power of the Laplace transform is through the *correspondence principle*. The *correspondence principle* states that "if an elastic solution to a stress analysis problem is known, substitution of the appropriate complex-plane transforms for the elastic quantities supplies the viscoelastic solution to the same problem in the transform plane."[214] What is meant by the "appropriate complex plane transforms" is that since we are dealing with time dependent material properties, the material's response depends on the method of excitation. The most common excitation modes are the step function and harmonic excitation. Since any excitation shape can be built from a series of infinitesimal step functions, it is used to derive the response to arbitrary excitations. For a step excitation, the "appropriate complex plane transforms" are the s-multiplied Laplace transforms (i.e. the Carson transforms) of the elastic constants:[214,220]

$$E = \frac{9KG}{3K+G} \rightarrow s\overline{E}(s) = \frac{9s\overline{K}(s)s\overline{G}(s)}{3s\overline{K}(s)+s\overline{G}(s)} \rightarrow \overline{E}(s) = \frac{9\overline{K}(s)s\overline{G}(s)}{3\overline{K}(s)+\overline{G}(s)} \tag{7.13}$$

A significant limitation is found when viscoelasticity and the correspondence principle are applied to Poisson's ratio. In an elastic system, Poisson's ratio has a single clear definition $\nu = -\varepsilon_{11}/\varepsilon_{22}$. However, in a viscoelastic system it is time, stress, and strain history dependent with at least six different definitions depending on the mode of deformation: constant strain, constant stress, sinusoidal, etc.[220–223] This means Poisson's ratio is not a fundamental material constant in viscoelastic systems and that a viscoelastic Poisson's ratio determined in one mode of deformation is not transferrable to calculations involving another mode of deformation, especially in the glass to rubber transition zone

of polymers.[223] Because of this history and mode dependence, the correspondence principle cannot be used with Poisson's ratio except in extremely limited circumstances.[221]

Returning to the application of the correspondence principle, since only the elastic constants are replaced by their Carson transforms, a basic stress equation such as $\sigma = E\varepsilon$ simply becomes $\overline{\sigma}(s) = s\overline{E}(s)\,\overline{\varepsilon}(s)$. It should be apparent that the correspondence principle makes it easy, *in principle*, to convert between various time-dependent moduli or transform a solution to an elastic problem to one for viscoelastic materials. The difficulty lies in performing the Laplace and inverse Laplace transforms on real time-dependent moduli such as the KWW function, which can often not be solved analytically.

7.3.4 Thermoviscoelasticity

We have now separately covered the temperature-dependence and the time-dependence of moduli in real materials. During the quench of a film on either a free-standing frame or supported, both the temperature and applied strain are changing as a function of time. This makes the experiment a non-isothermal viscoelastic (thermoviscoelastic) problem. All of the viscoelastic calculations of the previous section were at constant temperature. If the viscoelastic material properties are temperature dependent and temperature changes during the course of the experiment, it becomes a nonlinear problem and much harder to solve.[224] However, for thermorheologically simple materials it is possible to keep the problem linear by using the time-temperature superposition principle.

Since a change in temperature is the same as a change in time scale, we can write:

$$E_{T_1}(t) = E_{T_{\mathrm{ref}}}\left[\frac{t}{a_{T_{\mathrm{ref}}}(T_1)}\right] \tag{7.14}$$

where $a_{T_{\mathrm{ref}}}(T_1)$ is the time-temperature superposition shift factor for T_1 with T_{ref} as a reference temperature. If $T_1 < T_{\mathrm{ref}}$ then $a_{T_{\mathrm{ref}}}(T_1) > 1$ and Eq. 7.14 can be interpreted such that the $E(t)$ at T_1 is the same as that at T_{ref} except that time passes more slowly by a factor of $1/a_{T_{\mathrm{ref}}}(T_1)$. We can then define a reduced time ξ that is related to the experimental time through[224]

$$d\xi = \frac{dt}{a_{T_{ref}}(T(t))} \tag{7.15}$$

This can be integrated when the temperature is changing as a function of time, giving a functional form for ξ that includes the entire temperature history:[224]

$$\xi(t, T_{ref}) = \int_0^t \frac{dt'}{a_{T_{ref}}(T(t'))} \tag{7.16}$$

If the temperature does not change with time then $\xi(t) = t$.

Now that we have a way to convert a temperature change to a time scale change, we can replace t with ξ in the viscoelastic modulus term of the Boltzmann superposition integral:

$$\sigma(t) = \int_0^t E\{\xi[t, T(0)] - \xi[u, T(0)]\}\frac{d\varepsilon(u)}{du}du \tag{7.17}$$

Because the temperature is changing with time, the thermal expansion of the material must be added as an additional term in the strain ε. Fortunately, we have already included the thermal expansion in the strain definition for this experiment. However, Eq. 7.17 is both explicit and implicit in t and is thus no longer a convolution integral, meaning that we cannot use the Laplace transform methods discussed previously on an equation of this form.[224] Luckily, ξ is monotonically increasing with time and thus can be inverted to obtain $t = g(\xi)$. This makes it possible (in principle) to rewrite the Boltzmann superposition integral entirely using ξ

$$\hat{\sigma}(\xi) = \int_0^{\xi} E(\xi - \xi') \frac{d\hat{\varepsilon}(\xi')}{d\xi'} d\xi' \tag{7.18}$$

but with different stress and strain functions defined using $g(\xi)$ through[224]

$$\sigma(t) = \sigma\big(g(\xi)\big) = \hat{\sigma}(\xi) \text{ and } \varepsilon(t) = \varepsilon\big(g(\xi)\big) = \hat{\varepsilon}(\xi) \tag{7.19}$$

With these new definitions for the stress and strain in terms of the reduced time we should be able to do manipulations in the Laplace domain, but with the reduced time taking the place of the regular time in the Laplace transformations.

7.4 Thermoviscoelastic Solution for Free-Standing and Supported Films

7.4.1 Analytical Solution

If the elastic solution to the problem is given by Eq. 7.4, then the viscoelastic solution from blindly applying the correspondence principle would be

$$\overline{\hat{\sigma}}(s) = \frac{s\overline{E}(s)\overline{\hat{\varepsilon}}(s)}{1 - s\overline{\nu}(s)} \tag{7.20}$$

where the (inverse) Laplace transformation is done with respect to the reduced time ξ. However, there are numerous problems with using this expression. It is inapropriate to use the correspondence principle on Poisson's ratio in this situation as discussed in section 7.3.3 and even if we were to try, there is an almost complete lack of data for the time *and* temperature dependent values of Poisson's ratio $\nu(t, T)$ for PS.[220] There also exist significant discrepancies among various reports [between static (limiting) values reported in handbooks and dynamic measurements, as well as between different dynamic measurements] of Young's relaxation modulus $E(t, T)$.[154,225–228] Given these significant problems, a better formulation of Eq. 7.20 is needed.

Fortuitously, there is good quality data for the bulk relaxation modulus $K(t, T)$[215,217,218] and shear creep compliance $J(t, T)$[215,229] of polystyrene that has already been successfully used for viscoelastic calculations.[215] Stress relaxation is a constant strain experiment whereas creep compliance is a constant stress experiment, essentially inverting Eqs. 7.1-7.3. This leads to the elastic and viscoelastic relations

$$G = {}^{1}/_{J} \rightarrow s\overline{G}(s) = {}^{1}\Big/_{s\overline{J}(s)} \rightarrow \overline{G}(s) = {}^{1}\Big/_{s^2\overline{J}(s)} \tag{7.21}$$

Using Eq. 7.21, Table 7.1, the correspondence principle, and some algebra, we arrive at

$$\overline{\hat{\sigma}}(s) = \frac{18s\overline{K}(s)\overline{\hat{\varepsilon}}(s)}{4+s^2\overline{J}(s)\overline{K}(s)} \tag{7.22}$$

In principle, Eq. 7.22 can be solved for $\sigma(t)$ by calculating the Laplace transform of $J(\xi)$, $K(\xi)$, and $\hat{\varepsilon}(\xi)$ with ξ as the time variable, calculating $\overline{\hat{\sigma}}(s)$ from these using Eq. 7.22, performing the inverse Laplace transform to get $\hat{\sigma}(\xi)$, and reconverting back to $\sigma(t)$ using Eqs. 7.16 and 7.19. This is likely impossible to solve fully analytically and must be done at least in part by numerical techniques. By using interpolating functions for $J(t)$, $K(t)$, $\varepsilon(t)$, $\xi(t)$, $g(\xi)$, and at some intermediate points along the calculation, it should be possible to calculate $\sigma(t)$ numerically. Care must be taken that all modulus data are at the same reference temperature, that this reference temperature is also used in the calculation of ξ, the stress and strain are properly rewritten in terms of ξ, and that the Laplace and inverse Laplace transforms are performed properly with ξ as the time variable.

7.4.2 Sources of Data And Complete Representation in Mathematica

To calculate the strain imposed on the PS as a function of time, we need the thermal expansion of PS and the substrate as well as the cooling rate. Data for the thermal expansion of silicon, $\alpha_{Si}(T)$ were taken from Okada & Tokumaru, *Journal of*

Applied Physics **1984**.[158] Their data from 300 K to 1500 K for single crystal silicon were parameterized as: $\alpha(T) / (10^{-6}\ \mathrm{K}^{-1}) = 3.725 \times \{1 - \exp[-5.88\times10^{-3}\ (T - 124\ \mathrm{K})\ \mathrm{K}^{-1}]\} + 5.548\times10^{-4}\ T\ \mathrm{K}^{-1}$.[230] These values were determined by measuring the lattice parameter at a series of temperatures using an X-ray lattice parameter measurement system on both float-zone and Czochralski-grown [111] wafers. The error in the measurement of the thermal expansion coefficient is approximately $0.2\times10^{-6}\ \mathrm{K}^{-1}$.

The data used for the thermal expansion of PS were calculated from the average of two measurements of 500 nm thick PS supported on silicon at a cooling rate of 1°C/min. These data were converted from a thickness measurement of PS confined to a Si surface to the linear thermal expansion of a stress free unconstrained PS sample as discussed in section 7.2. α_{PS} is calculated using Eq. 7.7 every 5°C and interpolated with Mathematica.

For simplicity, the cooling rate was taken to be a constant 90°C/min with a starting temperature of 120°C:

$$q = 90\frac{℃}{minute} \rightarrow T(t) = 120℃ - t\ 90\frac{℃}{minute} \tag{7.23}$$

A constant 90°C/min cooling rate is a reasonable approximation because it is the cooling rate at and just above T_g, where the dynamics are most sensitive to the cooling rate. Strain was then calculated using the thermal expansions and the constant cooling rate as

$$\varepsilon = \int_{120℃}^{T(t)} \left(\alpha_{\mathrm{PS}}(T) - \alpha_{\mathrm{sup}}(T)\right) dT$$

$$= \int_{120℃}^{120℃ - t\ 90\frac{℃}{minute}} \left(\alpha_{\mathrm{PS}}(T) - \alpha_{\mathrm{sup}}(T)\right) dT \tag{7.24}$$

The bulk modulus data, $K(t)$, were taken from the KWW fit given in Grassia, D'Amore, Simon *J. Rheol.* **2010**[215] to the data collected in Meng & Simon *J. Polym. Sci. Part B Polym. Phys.* **2007**[217] and *Review of Scientific Instruments* **2009**[218] on a

commercial PS (Dylene 8), with M_w = 221 kg/mol and M_n = 92.8 kg/mol. Since our timescales are short, it does not matter that Dylene 8 has a much lower MW or is more disperse than our PS because the viscoelastic respone before and at the beginning of the rubbery plateau regime does not depend on MW.[4] The $K(t)$ data were obtained from pressure relaxation measurements performed at two elevated pressures (42 and 76 MPa) and temperatures from $T_g(p)$ + 14°C to $T_g(p)$ - 28°C by shifting downward to atmospheric pressure using fits to the Tait equation (a PVT equation). For measurements above T_g, the sample was cooled to the test temperature at 0.1 K/min and then held for 4 hours before performing the pressure relaxation measurements. Near and below T_g, Struik's protocol was applied with a waiting time of 7-10 days.[22] The reference temperature used in the paper was the T_g they measured at a cooling rate of 0.1 K/min, 93.8°C. The master curve constructed at T_{ref} = 93.8°C, shown in Figure 7.1, covers the timescale from 10^{-3} to 10^9 seconds. There was a vertical shift employed to construct the master curve, but it is too small to be worth including in the calculation (~3% upwards at $T_g(p)$ - 30°C). I interpolated the KWW equation with their fit parameters from 10^{-20} to 10^{20} seconds using log spaced interpolation points ($\Delta\log(t)$ = 0.1). Shifting to the T_{ref} used for the calculation will be discussed below.

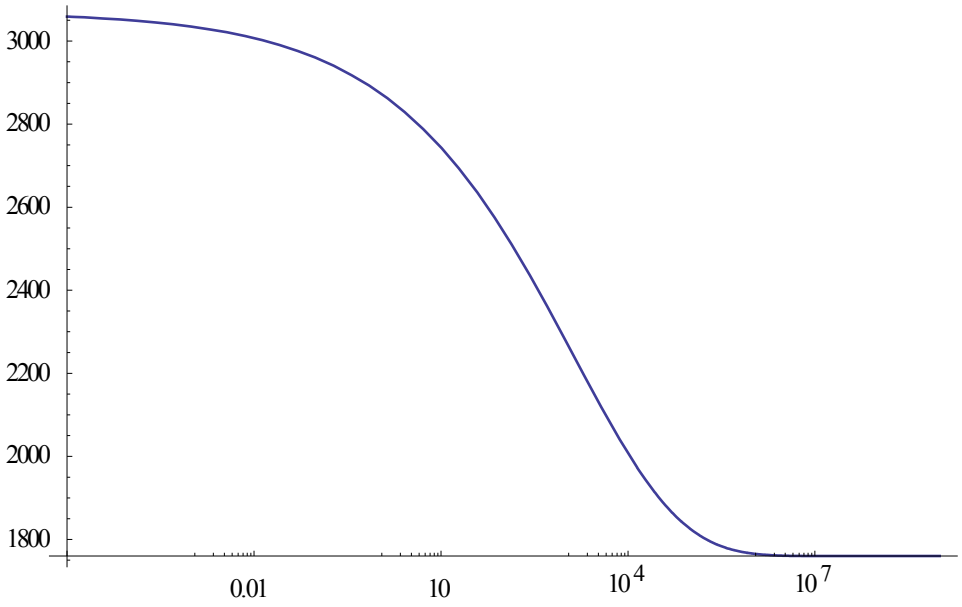

Figure 7.1: Bulk relaxation modulus $K_{93.8C}(t)$ (in MPa) *vs*. time (in seconds) at a reference temperature of 93.8°C calculated from KWW fit in Grassia *et al*.[215] to the data collected by Meng *et al*.[217,218]

The recoverable shear creep compliance data, $J(t)$, were taken from Agarwal's 1975 dissertation while working with Plazek and are shown in Figure 7.2.[229] They used the same Dylene 8 as Simon.[217,218] The creep compliance was collected using a frictionless magnetic bearing torsional apparatus from 97°C to 190°C. Except for lower temperatures where the viscous contribution is negligible, all creep compliance measurements were made of recovery upon removal of torque after steady state flow had been achieved. The cooling rate was not reported, as far as I can find. The reference temperature used for the master curve data is 100°C. Although it may be more technically correct to use the total compliance, and not the recoverable compliance since we are not performing a recovery experiment, the non-recoverable (viscous) part of the compliance does not become significant until after 100 seconds at 125°C; thus, it does not make a noticable difference since our quench starts at 120°C. The data were input

from the tabulated values of the master curve in the Appendix which runs from $10^{-4.4}$ to 10^{16} seconds (although it does not change after $10^{12.8}$ seconds).

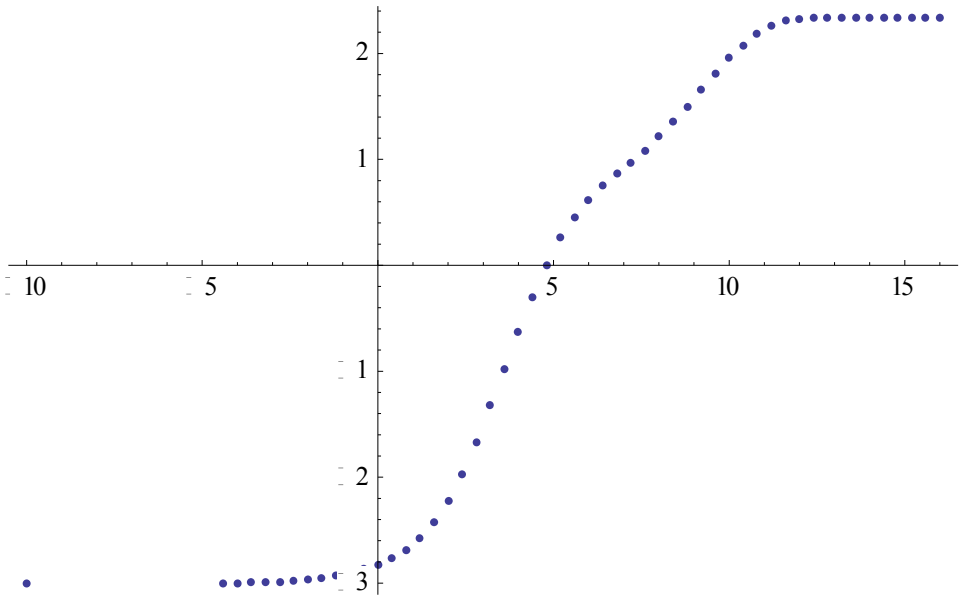

Figure 7.2: Shear creep compliance J_{100C} plotted on a double logarithmic scale. Horizontal axis is log(time) with units of log(seconds) and vertical axis is log(J_{100C}) with units of log(MPa^{-1}). Data from Agarwal's dissertation.[229]

The shift factors, $a_{T_{ref}}(T)$, used for time-temperature superposition and the calculation of ξ were extracted from Meng & Simon *JPSB* **2007**.[217] Above T_g = 93.8°C, the shift factors for both the shear and bulk data are very similar and Simon's WLF fit to Agarwal's data is used:

$$\log\left(a_{93.8°C}(T)\right) = \frac{-16.2(T-93.8°C)}{30.4°C+(T-93.8°C)} \tag{7.25}$$

From T_g = 93.8°C down to T_g - 28°C, only bulk data exist and the data were selected from Figure 8 in Meng & Simon *JPSB* **2007**.[217] These were combined, with extra data points at lower temperatures extending the leveling off of the shift factor due to equilibrium not being reached. Simon *et al*.[217] used long waiting times of 7 days before measuring, thereby reaching equilibrium down to temperatures of T_g - 10°C; whereas we

fall out of equilibrium right at T_g such that it is likely the shift factors should level off faster and sooner. However, this is an insignificant difference as ξ essentially stops changing before T_g as the modulus is effectively stuck at its glassy value. The calculation may be more efficient if the shift factor below T_g is set such that ξ does not asymptote too much. The combined data were interpolated from -6.2°C to 170°C. It was then shifted to T_{ref} = 120°C, i.e. $a_{T_{ref}=120°C}(120°C) = 1$ and is plotted in Figure 7.3:

$$\log(a_{T_{ref}=120°C}(T)) = \log(a_{T_{ref}=93.8°C}(T)) - \log(a_{T_{ref}=93.8}(120°C)) \quad (7.26)$$

In practice, the interpolating function in Mathematica takes the temperature and outputs $\log(a_{T_{ref}=120°C}(T))$.

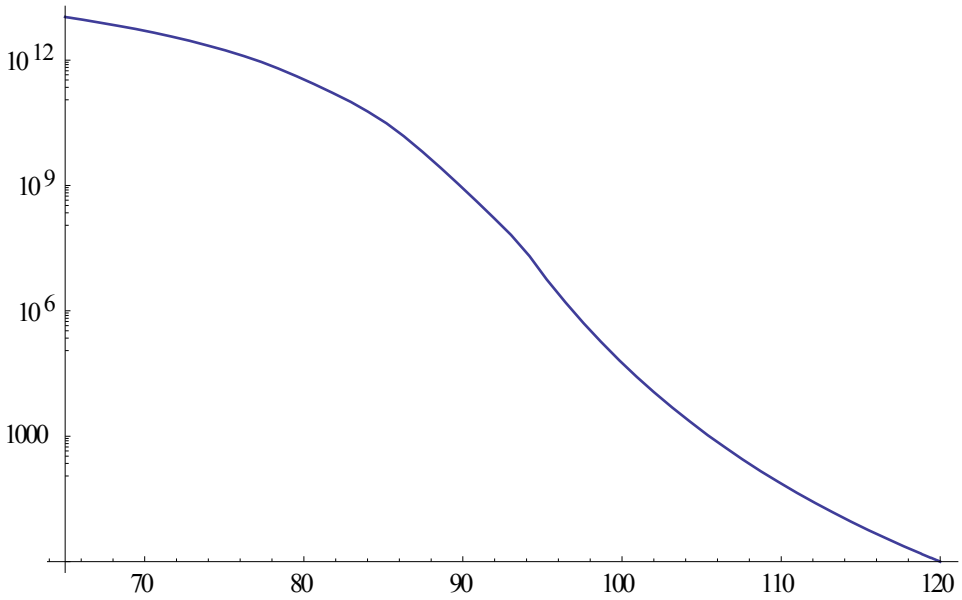

Figure 7.3: Shift factor $a_{T_{ref}=120°C}(T)$ *vs*. temperature (°C) with a reference temperature of 120°C from Meng *et al.*'s WLF fit[217] to Agarwal's data,[229] shifted to T_{ref} = 120°C. Fit and shifting are described in the text.

$K(t)$ and $J(t)$ at T_{ref} = 120°C were generated using time-temperature superposition:

$$K_{120°C}(t) = K_{93.8°C}\left(\frac{t}{10^{\log\left(a_{T_{ref}=93.8°C}(120°C)\right)}}\right) \quad (7.27)$$

$$J_{120°C}(t) = J_{97.9°C}(t\ 10^{\log\left(a_{T_{ref}=93.8°C}(120°C)\right)+\log\left(a_{T_{ref}=93.8°C}(97.9°C)\right)}) \qquad (7.28)$$

where $J(t)$ had to be shifted from its T_g in Agarwal's measurements[229] to the T_g in Simon's measurements[215] before being shifted to 120°C. (The T_g reported by Agarwal is 97.9°C and must be used for the shifting instead of his T_{ref} = 100°C for it to match the $J_{93.8°C}(t)$ data in Figure 6 of Grassia, D'Amore, Simon *J. Rheo.* **2010**.[215]) The $J_{120°C}(t)$ data was interpolated from a $\log(J_{120°C}(t))$ interpolation of Eq. 7.27, using log-spaced interpolation points ($\Delta\log(t) = 0.1$) with t from 10^{-13} to 10^{100}. This needed to be done to ensure a smooth and accurate interpolation as Mathematica's interpolation algorithims do not handle the ~20 orders of magnitude in time and ~5.5 orders of magnitude in values required to represent the complete $J(t)$ response. A comparison of shifted and unshifted $K(t)$ is shown in Figure 7.4 and $J(t)$ is shown in Figure 7.5.

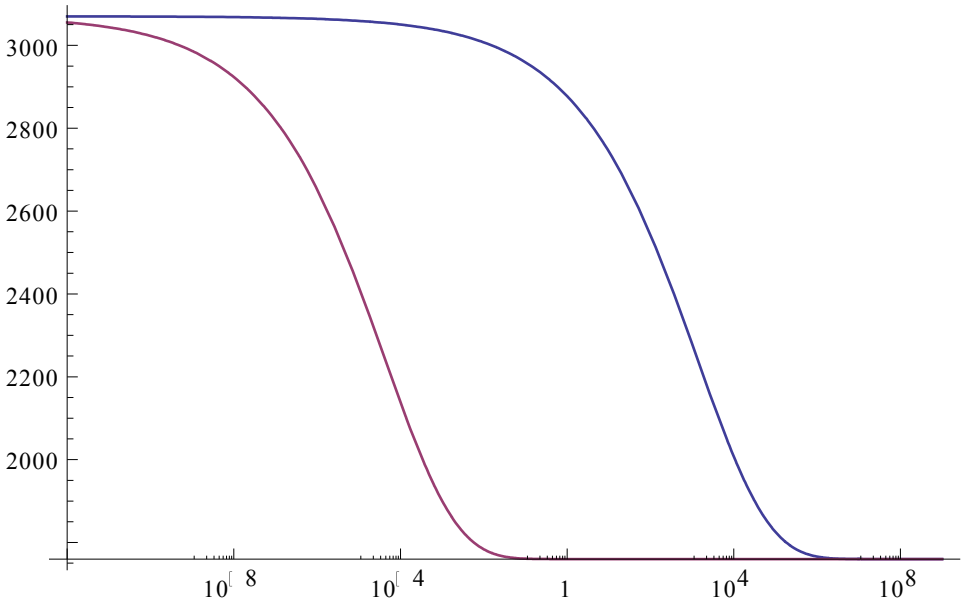

Figure 7.4: Bulk relaxation modulus $K(t)$ (in MPa) *vs*. time (in seconds) for different reference temperatures, calculated from KWW fit in Grassia *et al*.[215] to the data collected by Meng *et al*[217,218] and using the shift factor $a_T(T)$ from Meng *et al*.'s WLF fit[217] to Agarwal's data,[229]. Blue line is calculated with T_{ref} = 93.8°C and maroon line is calculated with T_{ref} = 120°C.

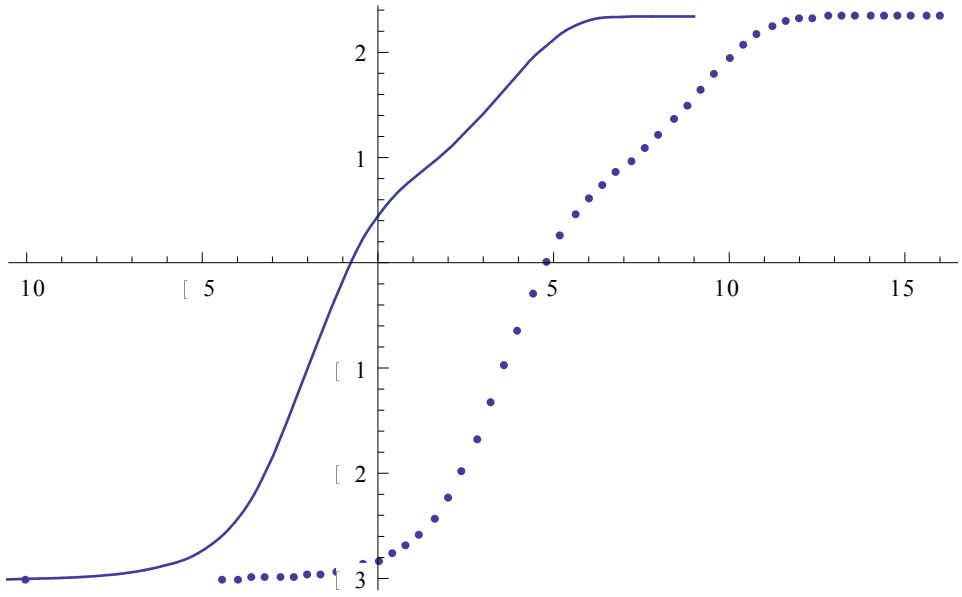

Figure 7.5: Shear creep compliance J plotted on a double logarithmic scale for two different reference temperatures. Horizontal axis is log(time) with units of log(seconds) and vertical axis is log(J) with units of log(MPa^{-1}). Data points from Agarwal's dissertation with T_{ref} = 100°C.[229] Curve is the interpolated data shifted to T_{ref} = 120°C using the shift factor $a_T(T)$ from Meng *et al.*'s WLF fit[217] to Agarwal's data,[229].

The reduced time ξ is now represented by

$$\xi(t) = \int_0^t 1 \Big/ 10\text{^}\log(a_{T_{ref}=120℃}(T(t)))\, dt \tag{7.29}$$

and the temperature history $T(t)$ must be input for $\xi(t)$ to be calculated. With the assumption that the cooling rate is a constant 90°C/min, we can substitute $T(t)$ from Eq. 7.23 into Eq. 7.28:

$$\xi_{90℃/min}(t) = \int_0^t 1 \Big/ 10\text{^}\log\left(a_{T_{ref}=120℃}\left(120℃ - t\ 90\frac{℃}{minute}\right)\right) dt \tag{7.30}$$

Thus, we can now define $g(\xi)$ = t. However, this is analytically very difficult, particularly if we use the actual, time-varying cooling rate. To get around this, we can just calculate $\xi(t)$ for the range of times we are interested in and interpolate the inverse results:

$$g(\xi) = \text{Interpolation}[\{\xi(t), t\}] \tag{7.31}$$

Finally, we now have all the components needed to determine $\sigma(t)$, treating PS as a thermoviscoelastic material, and in principle can do so by calculating

$$\hat{\sigma}(\xi) = \mathcal{L}^{-1}\left[\frac{18s\mathcal{L}[K_{120^{\circ}\mathrm{C}}(\xi),\xi,s]\mathcal{L}[\hat{\varepsilon}(g(\xi)),\xi,s]}{4+s^2\mathcal{L}[J_{120^{\circ}\mathrm{C}}(\xi),\xi,s]\mathcal{L}[K_{120^{\circ}\mathrm{C}}(\xi),\xi,s]}, s, \xi\right] \tag{7.32}$$

In practice, the difficulty lies in making sure that all of these functions are defined and the calculations specified in Mathematica such that the Laplace transforms are properly done with ξ. Mathematica is unable to do the complete calculation in Eq. 7.32 either analytically or via numerical integration of the equivalent convolution integral representation. To do the calculation would likely require much more involved numerical calculations or more intelligent choices of approximate modulus functions so as to allow analytical calculation.

Bibliography

(1) NSF Polymers Workshop. *Interdisciplinary, Globally Leading Polymer Science and Engineering*; 2007; p. 130.

(2) Hunter, D. *Papermaking. The History and Technique of and Ancient Craft*; Dover Publications: New York, 1978.

(3) Riande, E. *Polymer Viscoelasticity Stress and Strain in Practice*; Marcel Dekker: New York, 2000.

(4) Ferry, J. D. *Viscoelastic Properties of Polymers*; 3rd Ed.; Wiley: New York, 1980.

(5) Plazek, D. J. Temperature Dependence of the Viscoelastic Behavior of Polystyrene. *J. Phys. Chem.* **1965**, *69*, 3480–3487.

(6) Kurchan, J.; Langer, J. S.; Witten, T. A.; Wolynes, P. G. Scientific Interview. In *Dynamical Heterogeneities in Glasses, Colloids and Granular Media*; Berthier, L.; Biroli, G.; Bouchaud, J.-P.; Cipelletti, L.; Saarloos, W. van, Eds.; Oxford University Press: New York, 2010; pp. 1–37.

(7) Biroli, G.; Garrahan, J. P. Perspective: The Glass Transition. *J. Chem. Phys.* **2013**, *138*, 12A301.

(8) Berthier, L.; Biroli, G. Theoretical Perspective on the Glass Transition and Amorphous Materials. *Rev. Mod. Phys.* **2011**, *83*, 587–645.

(9) Tarjus, G. An Overview of the Theories of the Glass Transition. In *Dynamical Heterogeneities in Glasses, Colloids and Granular Media*; Berthier, L.; Biroli, G.; Bouchaud, J.-P.; Cipelletti, L.; Saarloos, W. van, Eds.; International Series of Monographs on Physics; Oxford University Press, 2011; pp. 39–62.

(10) Ediger, M. D.; Harrowell, P. Perspective: Supercooled Liquids and Glasses. *J. Chem. Phys.* **2012**, *137*, 080901.

(11) Weeks, E. R.; Crocker, J. C.; Levitt, A. C.; Schofield, A.; Weitz, D. A. Three-Dimensional Direct Imaging of Structural Relaxation Near the Colloidal Glass Transition. *Science* **2000**, *287*, 627–631.

(12) Berthier, L.; Biroli, G.; Bouchaud, J.-P.; Cipelletti, L.; van Saarloos, W. *Dynamical Heterogeneities in Glasses, Colloids, and Granular Media*; Oxford University Press, 2011.

(13) Harrowell, P. The Length Scales of Dynamic Heterogeneity: Results from Molecular Dynamics Simulations. In *Dynamical Heterogeneities in Glasses, Colloids and Granular Media*; Berthier, L.; Biroli, G.; Bouchaud, J.-P.; Cipelletti, L.; Saarloos, W. van, Eds.; International Series of Monographs on Physics; Oxford University Press, 2011; pp. 229–263.

(14) Cipelletti, L.; Weeks, E. R. Glassy Dynamics and Dynamical Heterogeneity in Colloids. In *Dynamical Heterogeneities in Glasses, Colloids and Granular Media*; Berthier, L.; Biroli, G.; Bouchaud, J.-P.; Cipelletti, L.; Saarloos, W. van, Eds.; International Series of Monographs on Physics; Oxford University Press, 2011; pp. 110–151.

(15) Richert, R.; Israeloff, N.; Alba-Simionesco, C.; Ladieu, F.; L'Hote, D. Experimental Approaches to Heterogeneous Dynamics. In *Dynamical Heterogeneities in Glasses, Colloids and Granular Media*; Berthier, L.; Biroli, G.; Bouchaud, J.-P.; Cipelletti, L.; Saarloos, W. van, Eds.; International Series of Monographs on Physics; Oxford University Press, 2011; pp. 152–202.

(16) Tompkins, H. G.; Irene, E. A. *Handbook of Ellipsometry*; William Andrew Pub. ; Springer: Norwich, NY; Heidelberg, Germany, 2005.

(17) Kawana, S.; Jones, R. A. L. Character of the Glass Transition in Thin Supported Polymer Films. *Phys. Rev. E* **2001**, *63*, 021501.

(18) Hutchinson, J. M. Physical Aging of Polymers. *Prog. Polym. Sci.* **1995**, *20*, 703–760.

(19) Greiner, R.; Schwarzl, F. Thermal Contraction and Volume Relaxation of Amorphous Polymers. *Rheol. acta* **1984**, *23*, 378–395.

(20) Priestley, R. D. Physical Aging of Confined Glasses. *Soft Matter* **2009**, *5*, 919–926.

(21) Koh, Y. P.; Simon, S. L. Enthalpy Recovery of Polystyrene: Does a Long-Term Aging Plateau Exist? *Macromolecules* **2013**, *46*, 5815–5821.

(22) Struik, L. C. E. *Physical Aging in Amorphous Polymers and Other Materials*; Elsevier Scientific: Amsterdam; New York, 1978.

(23) Baker, E. A.; Rittigstein, P.; Torkelson, J. M.; Roth, C. B. Streamlined Ellipsometry Procedure for Characterizing Physical Aging Rates of Thin Polymer Films. *J. Polym. Sci. Part B Polym. Phys.* **2009**, *47*, 2509–2519.

(24) Pye, J. E.; Rohald, K. A.; Baker, E. A.; Roth, C. B. Physical Aging in Ultrathin Polystyrene Films: Evidence of a Gradient in Dynamics at the Free Surface and Its Connection to the Glass Transition Temperature Reductions. *Macromolecules* **2010**, *43*, 8296–8303.

(25) Marceau, S.; Tortai, J.-H.; Tillier, J.; Vourdas, N.; Gogolides, E.; Raptis, I.; Beltsios, K.; van Werden, K. Thickness-Dependent Glass Transition Temperature of Thin Resist Films for High Resolution Lithography. *Microelectron. Eng.* **2006**, *83*, 1073–1077.

(26) Lakshman Dissanayake, M. a. K. Nano-Composite Solid Polymer Electrolytes for Solid State Ionic Devices. *Ionics (Kiel).* **2004**, *10*, 221–225.

(27) Liu, R. Y. F.; Jin, Y.; Hiltner, A.; Baer, E. Probing Nanoscale Polymer Interactions by Forced-Assembly. *Macromol. Rapid Commun.* **2003**, *24*, 943–948.

(28) Lang, R. J.; Simmons, D. S. Interfacial Dynamic Length Scales in the Glass Transition of a Model Freestanding Polymer Film and Their Connection to Cooperative Motion. *Macromolecules* **2013**, *46*, 9818–9825.

(29) Jackson, C. L.; McKenna, G. B. The Glass Transition of Organic Liquids Confined to Small Pores. *J. Non. Cryst. Solids* **1991**, *131-133*, 221–224.

(30) Keddie, J. L.; Jones, R. A. L.; Cory, R. A. Size-Dependent Depression of the Glass Transition Temperature in Polymer Films. *Europhys. Lett.* **1994**, *27*, 59–64.

(31) Ediger, M. D. Spatially Heterogeneous Dynamics in Supercooled Liquids. *Annu. Rev. Phys. Chem.* **2000**, *51*, 99–128.

(32) Tsui, O. K. C.; Zhang, H. F. Effects of Chain Ends and Chain Entanglement on the Glass Transition Temperature of Polymer Thin Films. *Macromolecules* **2001**, *34*, 9139–9142.

(33) Ellison, C. J.; Mundra, M. K.; Torkelson, J. M. Impacts of Polystyrene Molecular Weight and Modification to the Repeat Unit Structure on the Glass Transition−Nanoconfinement Effect and the Cooperativity Length Scale. *Macromolecules* **2005**, *38*, 1767–1778.

(34) DeMaggio, G. B.; Frieze, W. E.; Gidley, D. W.; Zhu, M.; Hristov, H. A.; Yee, A. F. Interface and Surface Effects on the Glass Transition in Thin Polystyrene Films. *Phys. Rev. Lett.* **1997**, *78*, 1524–1527.

(35) Forrest, J. A.; Mattsson, J. Reductions of the Glass Transition Temperature in Thin Polymer Films: Probing the Length Scale of Cooperative Dynamics. *Phys. Rev. E* **2000**, *61*, R53–R56.

(36) Mattsson, J.; Forrest, J. A.; Borjesson, L. Quantifying Glass Transition Behavior in Ultrathin Free-Standing Polymer Films. *Phys. Rev. E* **2000**, *62*, 5187–5200.

(37) Lipson, J. E. G.; Milner, S. T. Local and Average Glass Transitions in Polymer Thin Films. *Macromolecules* **2010**, *43*, 9874–9880.

(38) Forrest, J. A.; Dalnoki-Veress, K. When Does a Glass Transition Temperature Not Signify a Glass Transition? *ACS Macro Lett.* **2014**, 310–314.

(39) Ilton, M.; Qi, D.; Forrest, J. A. Using Nanoparticle Embedding to Probe Surface Rheology and the Length Scale of Surface Mobility in Glassy Polymers. *Macromolecules* **2009**, *42*, 6851–6854.

(40) Qi, D.; Ilton, M.; Forrest, J. A. Measuring Surface and Bulk Relaxation in Glassy Polymers. *Eur. Phys. J. E. Soft Matter* **2011**, *34*, 1–7.

(41) Qi, D.; Daley, C. R.; Chai, Y.; Forrest, J. A. Molecular Weight Dependence of near Surface Dynamical Mechanical Properties of Polymers. *Soft Matter* **2013**, *9*, 8958–8964.

(42) Fakhraai, Z.; Forrest, J. A. Measuring the Surface Dynamics of Glassy Polymers. *Science* **2008**, *319*, 600–604.

(43) Yang, Z.; Fujii, Y.; Lee, F. K.; Lam, C.-H. C.-H.; Tsui, O. K. C. Glass Transition Dynamics and Surface Layer Mobility in Unentangled Polystyrene Films. *Science* **2010**, *328*, 1676–1679.

(44) Yang, Z.; Clough, A.; Lam, C.-H.; Tsui, O. K. C. Glass Transition Dynamics and Surface Mobility of Entangled Polystyrene Films at Equilibrium. *Macromolecules* **2011**, *44*, 8294–8300.

(45) Chai, Y.; Salez, T.; McGraw, J. D.; Benzaquen, M.; Dalnoki-Veress, K.; Raphael, E.; Forrest, J. A. A Direct Quantitative Measure of Surface Mobility in a Glassy Polymer. *Science* **2014**, *343*, 994–999.

(46) Paeng, K.; Swallen, S. F.; Ediger, M. D. Direct Measurement of Molecular Motion in Freestanding Polystyrene Thin Films. *J. Am. Chem. Soc.* **2011**, *133*, 8444–8447.

(47) Wallace, W.; van Zanten, J.; Wu, W. Influence of an Impenetrable Interface on a Polymer Glass-Transition Temperature. *Phys. Rev. E* **1995**, *52*, R3329–R3332.

(48) Ellison, C. J.; Torkelson, J. M. The Distribution of Glass-Transition Temperatures in Nanoscopically Confined Glass Formers. *Nat. Mater.* **2003**, *2*, 695–700.

(49) Ellison, C. J.; Kim, S.; Hall, D. B.; Torkelson, J. M. Confinement and Processing Effects on Glass Transition Temperature and Physical Aging in Ultrathin Polymer Films: Novel Fluorescence Measurements. *Eur. Phys. J. E Soft Matter Biol. Phys.* **2002**, *8*, 155–166.

(50) Ellison, C. J.; Torkelson, J. M. Sensing the Glass Transition in Thin and Ultrathin Polymer Films via Fluorescence Probes and Labels. *J. Polym. Sci. B Polym. Phys.* **2002**, *40*, 2745–2758.

(51) Peter, S.; Meyer, H.; Baschnagel, J.; Seemann, R. Slow Dynamics and Glass Transition in Simulated Free-Standing Polymer Films: A Possible Relation between Global and Local Glass Transition Temperatures. *J. Phys. Condens. Matter* **2007**, *19*, 205119.

(52) Riggleman, R. A.; Yoshimoto, K.; Douglas, J.; de Pablo, J. J. Influence of Confinement on the Fragility of Antiplasticized and Pure Polymer Films. *Phys. Rev. Lett.* **2006**, *97*, 045502.

(53) Forrest, J. A.; Dalnoki-Veress, K.; Stevens, J. R.; Dutcher, J. R. Effect of Free Surfaces on the Glass Transition Temperature of Thin Polymer Films. *Phys. Rev. Lett.* **1996**, *77*, 2002–2005.

(54) Forrest, J. A.; Dalnoki-Veress, K.; Dutcher, J. R. Interface and Chain Confinement Effects on the Glass Transition Temperature of Thin Polymer Films. *Phys. Rev. E* **1997**, *56*, 5705–5716.

(55) Dalnoki-Veress, K.; Forrest, J. A.; Murray, C. A.; Gigault, C.; Dutcher, J. R. Molecular Weight Dependence of Reductions in the Glass Transition Temperature of Thin, Freely Standing Polymer Films. *Phys. Rev. E* **2001**, *63*, 031801.

(56) Roth, C. B.; Dutcher, J. R. Glass Transition Temperature of Freely-Standing Films of Atactic Poly(methyl Methacrylate). *Eur. Phys. J. E. Soft Matter* **2003**, *12 Suppl 1*, S103–107.

(57) Roth, C. B.; Pound, A.; Kamp, S. W.; Murray, C. A.; Dutcher, J. R. Molecular-Weight Dependence of the Glass Transition Temperature of Freely-Standing Poly(methyl Methacrylate) Films. *Eur. Phys. J. E Soft Matter Biol. Phys.* **2006**, *20*, 441–448.

(58) Bäumchen, O.; McGraw, J. D.; Forrest, J. A.; Dalnoki-Veress, K. Reduced Glass Transition Temperatures in Thin Polymer Films: Surface Effect or Artifact? *Phys. Rev. Lett.* **2012**, *109*, 055701.

(59) Rotella, C.; Napolitano, S.; Wübbenhorst, M. Segmental Mobility and Glass Transition Temperature of Freely Suspended Ultrathin Polymer Membranes. *Macromolecules* **2009**, *42*, 1415–1417.

(60) Napolitano, S.; Wübbenhorst, M. Structural Relaxation and Dynamic Fragility of Freely Standing Polymer Films. *Polymer* **2010**, *51*, 5309–5312.

(61) Liem, H.; Cabanillas-Gonzalez, J.; Etchegoin, P.; Bradley, D. D. C. Glass Transition Temperatures of Polymer Thin Films Monitored by Raman Scattering. *J. Phys. Condens. Matter* **2004**, *16*, 721–728.

(62) Miyazaki, T.; Inoue, R.; Nishida, K.; Kanaya, T. X-Ray Reflectivity Studies on Glass Transition of Free Standing Polystyrene Thin Films. *Eur. Phys. J. - Spec. Top.* **2007**, *141*, 203–206.

(63) Kim, S.; Roth, C. B.; Torkelson, J. M. Effect of Nanoscale Confinement on the Glass Transition Temperature of Free-Standing Polymer Films: Novel, Self-Referencing Fluorescence Method. *J. Polym. Sci. Part B Polym. Phys.* **2008**, *46*, 2754–2764.

(64) Kim, S.; Torkelson, J. M. Distribution of Glass Transition Temperatures in Free-Standing, Nanoconfined Polystyrene Films: A Test of de Gennes' Sliding Motion Mechanism. *Macromolecules* **2011**, *44*, 4546–4553.

(65) O'Connell, P. A.; Hutcheson, S. A.; McKenna, G. B. Creep Behavior of Ultra-Thin Polymer Films. *J. Polym. Sci. B Polym. Phys.* **2008**, *46*, 1952–1965.

(66) Pye, J. E.; Roth, C. B. Two Simultaneous Mechanisms Causing Glass Transition Temperature Reductions in High Molecular Weight Freestanding Polymer Films as Measured by Transmission Ellipsometry. *Phys. Rev. Lett.* **2011**, *107*, 235701.

(67) Rauscher, P. M.; Pye, J. E.; Baglay, R. R.; Roth, C. B. Effect of Adjacent Rubbery Layers on the Physical Aging of Glassy Polymers. *Macromolecules* **2013**, *46*, 9806–9817.

(68) Forrest, J. A.; Dalnoki-Veress, K. The Glass Transition in Thin Polymer Films. *Adv. Colloid Interface Sci.* **2001**, *94*, 167–196.

(69) Roth, C. B.; Dutcher, J. R. Glass Transition and Chain Mobility in Thin Polymer Films. *J. Electroanal. Chem.* **2005**, *584*, 13–22.

(70) Kim, S.; Hewlett, S. A.; Roth, C. B.; Torkelson, J. M. Confinement Effects on Glass Transition Temperature, Transition Breadth, and Expansivity: Comparison of Ellipsometry and Fluorescence Measurements on Polystyrene Films. *Eur. Phys. J. E Soft Matter Biol. Phys.* **2009**, *30*, 83–92.

(71) Priestley, R. D.; Ellison, C. J.; Broadbelt, L. J.; Torkelson, J. M. Structural Relaxation of Polymer Glasses at Surfaces, Interfaces, and in Between. *Science* **2005**, *309*, 456–459.

(72) Stafford, C. M.; Vogt, B. D.; Harrison, C.; Julthongpiput, D.; Huang, R. Elastic Moduli of Ultrathin Amorphous Polymer Films. *Macromolecules* **2006**, *39*, 5095–5099.

(73) Edmond, K. V.; Nugent, C. R.; Weeks, E. R. Local Influence of Boundary Conditions on a Confined Supercooled Colloidal Liquid. *Eur. Phys. J. Spec. Top.* **2010**, *189*, 83–93.

(74) Alcoutlabi, M.; McKenna, G. B. Effects of Confinement on Material Behaviour at the Nanometre Size Scale. *J. Phys. Condens. Matter* **2005**, *17*, R461–R524.

(75) Richert, R. Dynamics of Nanoconfined Supercooled Liquids. *Annu. Rev. Phys. Chem.* **2011**, *62*, 65–84.

(76) Swallen, S. F.; Kearns, K. L.; Mapes, M. K.; Kim, Y. S.; McMahon, R. J.; Ediger, M. D.; Wu, T.; Yu, L.; Satija, S. Organic Glasses with Exceptional Thermodynamic and Kinetic Stability. *Science* **2007**, *315*, 353–356.

(77) Long, D. R.; Lequeux, F. Heterogeneous Dynamics at the Glass Transition in van Der Waals Liquids, in the Bulk and in Thin Films. *Eur. Phys. J. E Soft Matter Biol. Phys.* **2001**, *4*, 371–387.

(78) Lipson, J. E. G.; Milner, S. T. Percolation Model of Interfacial Effects in Polymeric Glasses. *Eur. Phys. J. B* **2009**, *72*, 133–137.

(79) Kropka, J.; Pryamitsyn, V.; Ganesan, V. Relation between Glass Transition Temperatures in Polymer Nanocomposites and Polymer Thin Films. *Phys. Rev. Lett.* **2008**, *101*, 075702.

(80) De Gennes, P.-G. Glass Transitions of Freely Suspended Polymer Films. *Comptes Rendus l'Académie des Sci. - Ser. IV - Phys.* **2000**, *1*, 1179–1186.

(81) De Gennes, P.-G. Glass Transitions in Thin Polymer Films. *Eur. Phys. J. E Soft Matter Biol. Phys.* **2000**, *2*, 201–205.

(82) Tress, M.; Erber, M.; Mapesa, E. U.; Huth, H.; Müller, J.; Serghei, A.; Schick, C.; Eichhorn, K.-J.; Voit, B.; Kremer, F. Glassy Dynamics and Glass Transition in Nanometric Thin Layers of Polystyrene. *Macromolecules* **2010**, *43*, 9937–9944.

(83) Roth, C. B.; Dutcher, J. Hole Growth in Freely Standing Polystyrene Films Probed Using a Differential Pressure Experiment. *Phys. Rev. E* **2005**, *72*, 021803.

(84) Roth, C. B.; Dutcher, J. R. Hole Growth as a Microrheological Probe to Measure the Viscosity of Polymers Confined to Thin Films. *J. Polym. Sci. Part B Polym. Phys.* **2006**, *44*, 3011–3021.

(85) Svanberg, C. Glass Transition Relaxations in Thin Suspended Polymer Films. *Macromolecules* **2007**, *40*, 312–315.

(86) Paeng, K.; Lee, H.-N. N.; Swallen, S. F.; Ediger, M. D. Temperature-Ramping Measurement of Dye Reorientation to Probe Molecular Motion in Polymer Glasses. *J. Chem. Phys.* **2011**, *134*, 024901.

(87) O'Connell, P. A.; McKenna, G. B. Rheological Measurements of the Thermoviscoelastic Response of Ultrathin Polymer Films. *Science* **2005**, *307*, 1760–1763.

(88) Paeng, K.; Ediger, M. D. Molecular Motion in Free-Standing Thin Films of Poly(methyl Methacrylate), Poly(4- Tert -Butylstyrene), Poly(α-Methylstyrene), and Poly(2-Vinylpyridine). *Macromolecules* **2011**, *44*, 7034–7042.

(89) Baljon, A. R. C.; Williams, S.; Balabaev, N. K.; Paans, F.; Hudzinskyy, D.; Lyulin, A. V. Simulated Glass Transition in Free-Standing Thin Polystyrene Films. *J. Polym. Sci. Part B Polym. Phys.* **2010**, *48*, 1160–1167.

(90) Milner, S. T.; Lipson, J. E. G. Delayed Glassification Model for Free-Surface Suppression of T G in Polymer Glasses. *Macromolecules* **2010**, *43*, 9865–9873.

(91) Baschnagel, J.; Varnik, F. Computer Simulations of Supercooled Polymer Melts in the Bulk and in Confined Geometry. *J. Phys. Condens. Matter* **2005**, *17*, R851–R953.

(92) Tsui, O. K. C. Anomalous Dynamics of Polymer Films. In *Polymer Thin Films*; Tsui, O. K. C.; Russell, T. P., Eds.; 2008; pp. 267–294.

(93) Sharp, J. S.; Forrest, J. A. Free Surfaces Cause Reductions in the Glass Transition Temperature of Thin Polystyrene Films. *Phys. Rev. Lett.* **2003**, *91*, 235701.

(94) Roth, C. B.; McNerny, K. L.; Jager, W. F.; Torkelson, J. M. Eliminating the Enhanced Mobility at the Free Surface of Polystyrene: Fluorescence Studies of the Glass Transition Temperature in Thin Bilayer Films of Immiscible Polymers. *Macromolecules* **2007**, *40*, 2568–2574.

(95) Kim, C.; Facchetti, A.; Marks, T. J. Polymer Gate Dielectric Surface Viscoelasticity Modulates Pentacene Transistor Performance. *Science* **2007**, *318*, 76–80.

(96) Simon, S. L.; Park, J.-Y.; McKenna, G. B. Enthalpy Recovery of a Glass-Forming Liquid Constrained in a Nanoporous Matrix: Negative Pressure Effects. *Eur. Phys. J. E. Soft Matter* **2002**, *8*, 209–216.

(97) Kawana, S.; Jones, R. A. L. Effect of Physical Ageing in Thin Glassy Polymer Films. *Eur. Phys. J. E Soft Matter Biol. Phys.* **2003**, *10*, 223–230.

(98) Priestley, R. D.; Broadbelt, L. J.; Torkelson, J. M. Physical Aging of Ultrathin Polymer Films above and below the Bulk Glass Transition Temperature: Effects of Attractive vs Neutral Polymer−Substrate Interactions Measured by Fluorescence. *Macromolecules* **2005**, *38*, 654–657.

(99) Koh, Y. P.; Simon, S. L. Structural Relaxation of Stacked Ultrathin Polystyrene Films. *J. Polym. Sci. Part B Polym. Phys.* **2008**, *46*, 2741–2753.

(100) Cangialosi, D.; Wübbenhorst, M.; Groenewold, J.; Mendes, E.; Schut, H.; van Veen, A.; Picken, S. J. Physical Aging of Polycarbonate Far below the Glass Transition Temperature: Evidence for the Diffusion Mechanism. *Phys. Rev. B* **2004**, *70*, 224213.

(101) Cangialosi, D.; Wübbenhorst, M.; Groenewold, J.; Mendes, E.; Picken, S. J. Diffusion Mechanism for Physical Aging of Polycarbonate Far below the Glass Transition Temperature Studied by Means of Dielectric Spectroscopy. *J. Non. Cryst. Solids* **2005**, *351*, 2605–2610.

(102) Fukao, K.; Sakamoto, A. Aging Phenomena in Poly(methyl Methacrylate) Thin Films: Memory and Rejuvenation Effects. *Phys. Rev. E. Stat. Nonlin. Soft Matter Phys.* **2005**, *71*, 041803.

(103) Fukao, K.; Koizumi, H. Glassy Dynamics in Thin Films of Polystyrene. *Phys. Rev. E. Stat. Nonlin. Soft Matter Phys.* **2008**, *77*, 021503.

(104) Rowe, B. W.; Freeman, B. D.; Paul, D. R. Physical Aging of Ultrathin Glassy Polymer Films Tracked by Gas Permeability. *Polymer* **2009**, *50*, 5565–5575.

(105) Rowe, B. W.; Pas, S. J.; Hill, A. J.; Suzuki, R.; Freeman, B. D.; Paul, D. R. A Variable Energy Positron Annihilation Lifetime Spectroscopy Study of Physical Aging in Thin Glassy Polymer Films. *Polymer* **2009**, *50*, 6149–6156.

(106) Pfromm, P. H.; Koros, W. J. Accelerated Physical Ageing of Thin Glassy Polymer Films: Evidence from Gas Transport Measurements. *Polymer* **1995**, *36*, 2379–2387.

(107) Dorkenoo, K. D.; Pfromm, P. H. Accelerated Physical Aging of Thin Poly[1-(trimethylsilyl)-1-Propyne] Films. *Macromolecules* **2000**, *33*, 3747–3751.

(108) McCaig, M. S.; Paul, D. R. Effect of Film Thickness on the Changes in Gas Permeability of a Glassy Polyarylate due to Physical Aging Part I. Experimental Observations. *Polymer* **2000**, *41*, 629–637.

(109) Huang, Y.; Paul, D. R. Physical Aging of Thin Glassy Polymer Films Monitored by Gas Permeability. *Polymer* **2004**, *45*, 8377–8393.

(110) Huang, Y.; Paul, D. R. Physical Aging of Thin Glassy Polymer Films Monitored by Optical Properties. *Macromolecules* **2006**, *39*, 1554–1559.

(111) Huang, Y.; Wang, X.; Paul, D. R. Physical Aging of Thin Glassy Polymer Films: Free Volume Interpretation. *J. Memb. Sci.* **2006**, *277*, 219–229.

(112) Pye, J. E.; Roth, C. B. Physical Aging of Polymer Films Quenched and Measured Free-Standing via Ellipsometry: Controlling Stress Imparted by Thermal Expansion Mismatch between Film and Support. *Macromolecules* **2013**, *46*, 9455–9463.

(113) Gray, L. A. G.; Yoon, S. W.; Pahner, W. A.; Davidheiser, J. E.; Roth, C. B. Importance of Quench Conditions on the Subsequent Physical Aging Rate of Glassy Polymer Films. *Macromolecules* **2012**, *45*, 1701–1709.

(114) Keddie, J. L.; Jones, R. A. L.; Cory, R. A. Interface and Surface Effects on the Glass-Transition Temperature in Thin Polymer Films. *Faraday Discuss.* **1994**, *98*, 219.

(115) Tsui, O. K. C.; Russell, T. P.; Hawker, C. J. Effect of Interfacial Interactions on the Glass Transition of Polymer Thin Films. *Macromolecules* **2001**, *34*, 5535–5539.

(116) Priestley, R. D.; Mundra, M. K.; Barnett, N. J.; Broadbelt, L. J.; Torkelson, J. M. Effects of Nanoscale Confinement and Interfaces on the Glass Transition Temperatures of a Series of Poly(n-Methacrylate) Films. *Aust. J. Chem.* **2007**, *60*, 765–771.

(117) Rittigstein, P.; Priestley, R. D.; Broadbelt, L. J.; Torkelson, J. M. Model Polymer Nanocomposites Provide an Understanding of Confinement Effects in Real Nanocomposites. *Nat. Mater.* **2007**, *6*, 278–282.

(118) Kim, J. H.; Jang, J.; Zin, W.-C. Thickness Dependence of the Glass Transition Temperature in Thin Polymer Films. *Langmuir* **2001**, *17*, 2703–2710.

(119) Herminghaus, S.; Jacobs, K.; Seemann, R. The Glass Transition of Thin Polymer Films: Some Questions, and a Possible Answer. *Eur. Phys. J. E Soft Matter Biol. Phys.* **2001**, *5*, 531–538.

(120) Peter, S.; Meyer, H.; Baschnagel, J. Thickness-Dependent Reduction of the Glass-Transition Temperature in Thin Polymer Films with a Free Surface. *J. Polym. Sci. Part B Polym. Phys.* **2006**, *44*, 2951–2967.

(121) Kim, J. H.; Jang, J.; Zin, W.-C. Estimation of the Thickness Dependence of the Glass Transition Temperature in Various Thin Polymer Films. *Langmuir* **2000**, *16*, 4064–4067.

(122) Campbell, C. G.; Vogt, B. D. Examination of the Influence of Cooperative Segmental Dynamics on the Glass Transition and Coefficient of Thermal Expansion in Thin Films Probed Using Poly(n-Alkyl Methacrylate)s. *Polymer* **2007**, *48*, 7169–7175.

(123) Ellison, C. J.; Ruszkowski, R.; Fredin, N.; Torkelson, J. M. Dramatic Reduction of the Effect of Nanoconfinement on the Glass Transition of Polymer Films via Addition of Small-Molecule Diluent. *Phys. Rev. Lett.* **2004**, *92*, 095702.

(124) Kim, S.; Mundra, M. K.; Roth, C. B.; Torkelson, J. M. Suppression of the Tg-Nanoconfinement Effect in Thin Poly(vinyl Acetate) Films by Sorbed Water. *Macromolecules* **2010**, *43*, 5158–5161.

(125) Boucher, V. M.; Cangialosi, D.; Alegría, A.; Colmenero, J. Enthalpy Recovery in Nanometer to Micrometer Thick Polystyrene Films. *Macromolecules* **2012**, *45*, 5296–5306.

(126) Tompkins, H. G. *A User's Guide to Ellipsometry*; Dover Publications: Mineola, N.Y., 2006.

(127) Donth, E. Characteristic Length of the Glass Transition. *J. Polym. Sci. Part B Polym. Phys.* **1996**, *34*, 2881–2892.

(128) Kahle, S.; Korus, J.; Hempel, E.; Unger, R.; Höring, S.; Schröter, K.; Donth, E. Glass-Transition Cooperativity Onset in a Series of Random Copolymers Poly(N -Butyl Methacrylate- Stat -Styrene). *Macromolecules* **1997**, *30*, 7214–7223.

(129) Hempel, E.; Hempel, G.; Hensel, A.; Schick, C.; Donth, E. Characteristic Length of Dynamic Glass Transition near T G for a Wide Assortment of Glass-Forming Substances. *J. Phys. Chem. B* **2000**, *104*, 2460–2466.

(130) Korus, J.; Hempel, E.; Beiner, M.; Kahle, S.; Donth, E. Temperature Dependence of A Glass Transition Cooperativity. *Acta Polym.* **1997**, *48*, 369–378.

(131) Erwin, B. M.; Colby, R. H. Temperature Dependence of Relaxation Times and the Length Scale of Cooperative Motion for Glass-Forming Liquids. *J. Non. Cryst. Solids* **2002**, *307-310*, 225–231.

(132) Wong, C. C.; Qin, Z.; Yang, Z. The Absence of Physical-Aging Effects on the Surface Relaxations of Rubbed Polystyrene. *Eur. Phys. J. E. Soft Matter* **2008**, *25*, 291–298.

(133) Pryamitsyn, V.; Ganesan, V. A Comparison of the Dynamical Relaxations in a Model for Glass Transition in Polymer Nanocomposites and Polymer Thin Films. *Macromolecules* **2010**, *43*, 5851–5862.

(134) Boucher, V. M.; Cangialosi, D.; Yin, H.; Schönhals, A.; Alegría, A.; Colmenero, J. Tg Depression and Invariant Segmental Dynamics in Polystyrene Thin Films. *Soft Matter* **2012**, *8*, 5119–5122.

(135) Frieberg, B.; Glynos, E.; Green, P. F. Structural Relaxations of Thin Polymer Films. *Phys. Rev. Lett.* **2012**, *108*, 268304.

(136) Forrest, J. A. What Can We Learn about a Dynamical Length Scale in Glasses from Measurements of Surface Mobility? *J. Chem. Phys.* **2013**, *139*, 084702.

(137) Ediger, M. D.; Forrest, J. A. Dynamics near Free Surfaces and the Glass Transition in Thin Polymer Films: A View to the Future. *Macromolecules* **2014**, *47*, 471–478.

(138) Daley, C. R.; Fakhraai, Z.; Ediger, M. D.; Forrest, J. A. Comparing Surface and Bulk Flow of a Molecular Glass Former. *Soft Matter* **2012**, *8*, 2206–2212.

(139) Torres, J. M.; Stafford, C. M.; Vogt, B. D. Elastic Modulus of Amorphous Polymer Thin Films: Relationship to the Glass Transition Temperature. *ACS Nano* **2009**, *3*, 2677–2685.

(140) Huang, Y.; Paul, D. R. Effect of Film Thickness on the Gas-Permeation Characteristics of Glassy Polymer Membranes. *Ind. Eng. Chem. Res.* **2007**, *46*, 2342–2347.

(141) Huang, Y.; Paul, D. R. Experimental Methods for Tracking Physical Aging of Thin Glassy Polymer Films by Gas Permeation. *J. Memb. Sci.* **2004**, *244*, 167–178.

(142) McCaig, M. S.; Paul, D. .; Barlow, J. . Effect of Film Thickness on the Changes in Gas Permeability of a Glassy Polyarylate due to Physical Aging Part II. Mathematical Model. *Polymer* **2000**, *41*, 639–648.

(143) Thornton, A. W.; Hill, A. J. Vacancy Diffusion with Time-Dependent Length Scale: An Insightful New Model for Physical Aging in Polymers. *Ind. Eng. Chem. Res.* **2010**, *49*, 12119–12124.

(144) Curro, J. G.; Lagasse, R. R.; Simha, R. Diffusion Model for Volume Recovery in Glasses. *Macromolecules* **1982**, *15*, 1621–1626.

(145) Alfrey, T.; Goldfinger, G.; Mark, H. The Apparent Second-Order Transition Point of Polystyrene. *J. Appl. Phys.* **1943**, *14*, 700–705.

(146) Huang, Y.; Paul, D. R. Effect of Molecular Weight and Temperature on Physical Aging of Thin Glassy poly(2,6-Dimethyl-1,4-Phenylene Oxide) Films. *J. Polym. Sci. Part B Polym. Phys.* **2007**, *45*, 1390–1398.

(147) Boucher, V. M.; Cangialosi, D.; Alegría, A.; Colmenero, J.; González-Irun, J.; Liz-Marzan, L. M. Accelerated Physical Aging in PMMA/silica Nanocomposites. *Soft Matter* **2010**, *6*, 3306–3317.

(148) Cangialosi, D.; Boucher, V. M.; Alegría, A.; Colmenero, J. Free Volume Holes Diffusion to Describe Physical Aging in Poly(mehtyl Methacrylate)/silica Nanocomposites. *J. Chem. Phys.* **2011**, *135*, 014901.

(149) Zhao, J.-H.; Kiene, M.; Hu, C.; Ho, P. S. Thermal Stress and Glass Transition of Ultrathin Polystyrene Films. *Appl. Phys. Lett.* **2000**, *77*, 2843–2845.

(150) Chung, J. Y.; Chastek, T. Q.; Fasolka, M. J.; Ro, H. W.; Stafford, C. M. Quantifying Residual Stress in Nanoscale Thin Polymer Films via Surface Wrinkling. *ACS Nano* **2009**, *3*, 844–852.

(151) Thomas, K. R.; Steiner, U. Direct Stress Measurements in Thin Polymer Films. *Soft Matter* **2011**, *7*, 7839–7842.

(152) Guo, Y.; Zhang, C.; Lai, C.; Priestley, R. D.; D'Acunzi, M.; Fytas, G. Structural Relaxation of Polymer Nanospheres under Soft and Hard Confinement: Isobaric versus Isochoric Conditions. *ACS Nano* **2011**, *5*, 5365–5373.

(153) Benham, P. P.; Crawford, R. J.; Armstrong, C. G. *Mechanics of Engineering Materials*; 2nd ed.; Longman Group: Harlow, Essex, England, 1996.

(154) Brandup, J.; Immergut, E.; Grulke, E. *Polymer Handbook*; Brandup, J.; Immergut, E.; Grulke, E., Eds.; Wiley: New York, 1999.

(155) Seemann, R.; Jacobs, K.; Landfester, K.; Herminghaus, S. Freezing of Polymer Thin Films and Surfaces: The Small Molecular Weight Puzzle. *J. Polym. Sci. Part B Polym. Phys.* **2006**, *44*, 2968–2979.

(156) Miyazaki, T.; Nishida, K.; Kanaya, T. Thermal Expansion Behavior of Ultrathin Polymer Films Supported on Silicon Substrate. *Phys. Rev. E* **2004**, *69*, 061803.

(157) Simon, S. L.; Sobieski, J. W.; Plazek, D. J. Volume and Enthalpy Recovery of Polystyrene. *Polymer* **2001**, *42*, 2555–2567.

(158) Okada, Y.; Tokumaru, Y. Precise Determination of Lattice Parameter and Thermal Expansion Coefficient of Silicon between 300 and 1500 K. *J. Appl. Phys.* **1984**, *56*, 314–320.

(159) Beaucage, G.; Composto, R.; Stein, R. S. Ellipsometric Study of the Glass Transition and Thermal Expansion Coefficients of Thin Polymer Films. *J. Polym. Sci. Part B Polym. Phys.* **1993**, *31*, 319–326.

(160) *Metallic Materials Properties Development and Standardization (MMPDS-05)*; Battelle Memorial Institute: Washington, D.C., 2010; pp. 3–370.

(161) Bogaard, R. H.; Desai, P. D.; Li, H. H.; Ho, C. Y. Thermophysical Properties of Stainless Steels. *Thermochim. Acta* **1993**, *218*, 373–393.

(162) Tschoegl, N.; Knauss, W.; Emri, I. The Effect of Temperature and Pressure on the Mechanical Properties of Thermo-And/or Piezorheologically Simple Polymeric Materials in Thermodynamic Equilibrium - A Critical Review. *Mech. Time-Dependent Mater.* **2002**, 53–99.

(163) Braun, G.; Kovacs, A. Glass Transition in Powdered Polystyrene. *Phys. Chem. Glas.* **1963**, *4*, 152–160.

(164) Murphy, T. M.; Freeman, B. D.; Paul, D. R. Physical Aging of Polystyrene Films Tracked by Gas Permeability. *Polymer* **2013**, *54*, 873–880.

(165) Boucher, V. M.; Cangialosi, D.; Alegría, A.; Colmenero, J. Enthalpy Recovery of PMMA/Silica Nanocomposites. *Macromolecules* **2010**, *43*, 7594–7603.

(166) Boucher, V. M.; Cangialosi, D.; Alegría, A.; Colmenero, J.; Pastoriza-Santos, I.; Liz-Marzan, L. M.; Liz-Marzán, L. M. Physical Aging of Polystyrene/gold Nanocomposites and Its Relation to the Calorimetric Tg Depression. *Soft Matter* **2011**, *7*, 3607–3620.

(167) Zhang, C.; Guo, Y.; Priestley, R. D. Confined Glassy Properties of Polymer Nanoparticles. *J. Polym. Sci. Part B Polym. Phys.* **2013**, *51*, 574–586.

(168) Tito, N. B.; Lipson, J. E. G.; Milner, S. T. Lattice Model of Dynamic Heterogeneity and Kinetic Arrest in Glass-Forming Liquids. *Soft Matter* **2013**, *9*, 3173–3180.

(169) Tito, N. B.; Lipson, J. E. G.; Milner, S. T. Lattice Model of Mobility at Interfaces: Free Surfaces, Substrates, and Bilayers. *Soft Matter* **2013**, *9*, 9403–9413.

(170) Roth, C. B. Mobility and Stability of Glasses. *J. Polym. Sci. Part B Polym. Phys.* **2010**, *48*, 2558–2560.

(171) Chen, K.; Schweizer, K. S. Stress-Enhanced Mobility and Dynamic Yielding in Polymer Glasses. *Europhys. Lett.* **2007**, *79*, 26006.

(172) Chen, K.; Schweizer, K. S. Theory of Yielding, Strain Softening, and Steady Plastic Flow in Polymer Glasses under Constant Strain Rate Deformation. *Macromolecules* **2011**, *44*, 3988–4000.

(173) Lacks, D.; Osborne, M. Energy Landscape Picture of Overaging and Rejuvenation in a Sheared Glass. *Phys. Rev. Lett.* **2004**, *93*, 255501.

(174) Chung, Y. G.; Lacks, D. J. Atomic Mobility in a Polymer Glass after Shear and Thermal Cycles. *J. Phys. Chem. B* **2012**, *116*, 14201–14205.

(175) Eyring, H. Viscosity, Plasticity, and Diffusion as Examples of Absolute Reaction Rates. *J. Chem. Phys.* **1936**, *4*, 283–291.

(176) Riggleman, R. A.; Lee, H.-N.; Ediger, M. D.; de Pablo, J. J. Free Volume and Finite-Size Effects in a Polymer Glass under Stress. *Phys. Rev. Lett.* **2007**, *99*, 215501.

(177) Colucci, D. M.; O'Connell, P. A.; McKenna, G. B. Stress Relaxation Experiments in Polycarbonate: A Comparison of Volume Changes for Two Commercial Grades. *Polym. Eng. Sci.* **1997**, *37*, 1469–1474.

(178) Smith, T. L.; Levita, G.; Moonan, W. K. Reversal and Activation of Physical Aging by Applied Deformations in Simple Compression and Extension. *J. Polym. Sci. Part B Polym. Phys.* **1988**, *26*, 875–881.

(179) Riggleman, R. A.; Schweizer, K. S.; de Pablo, J. J. Nonlinear Creep in a Polymer Glass. *Macromolecules* **2008**, *41*, 4969–4977.

(180) Stevenson, J. D.; Wolynes, P. G. On the Surface of Glasses. *J. Chem. Phys.* **2008**, *129*, 234514.

(181) McKenna, G. B. Ten (or More) Years of Dynamics in Confinement: Perspectives for 2010. *Eur. Phys. J. Spec. Top.* **2010**, *189*, 285–302.

(182) Merabia, S.; Sotta, P.; Long, D. R. A Microscopic Model for the Reinforcement and the Nonlinear Behavior of Filled Elastomers and Thermoplastic Elastomers (Payne and Mullins Effects). *Macromolecules* **2008**, *41*, 8252–8266.

(183) Evans, C. M.; Deng, H.; Jager, W. F.; Torkelson, J. M. Fragility Is a Key Parameter in Determining the Magnitude of T G -Confinement Effects in Polymer Films. *Macromolecules* **2013**, *46*, 6091–6103.

(184) Zhang, C.; Priestley, R. D. Fragility and Glass Transition Temperature of Polymer Confined under Isobaric and Isochoric Conditions. *Soft Matter* **2013**, *9*, 7076–7085.

(185) Starr, F. W.; Douglas, J. Modifying Fragility and Collective Motion in Polymer Melts with Nanoparticles. *Phys. Rev. Lett.* **2011**, *106*, 115702.

(186) Evans, C. M.; Torkelson, J. M. Major Roles of Blend Partner Fragility and Dye Placement on Component Glass Transition Temperatures: Fluorescence Study of Near-Infinitely Dilute Species in Binary Blends. *Macromolecules* **2012**, *45*, 8319–8327.

(187) Fakhraai, Z.; Forrest, J. A. Probing Slow Dynamics in Supported Thin Polymer Films. *Phys. Rev. Lett.* **2005**, *95*, 025701.

(188) Gao, S.; Koh, Y. P.; Simon, S. L. Calorimetric Glass Transition of Single Polystyrene Ultrathin Films. *Macromolecules* **2013**, *46*, 562–570.

(189) Xu, S.; O'Connell, P. a.; McKenna, G. B.; Castagnet, S. Nanomechanical Properties in Ultrathin Polymer Films: Measurement on Rectangular versus Circular Bubbles. *J. Polym. Sci. Part B Polym. Phys.* **2012**, *50*, 466–476.

(190) Wang, J.; McKenna, G. B. Viscoelastic and Glass Transition Properties of Ultrathin Polystyrene Films by Dewetting from Liquid Glycerol. *Macromolecules* **2013**, *46*, 2485–2495.

(191) Langhe, D. S.; Murphy, T. M.; Shaver, A.; LaPorte, C.; Freeman, B. D.; Paul, D. R.; Baer, E. Structural Relaxation of Polystyrene in Nanolayer Confinement. *Polymer* **2012**, *53*, 1925–1931.

(192) Fukao, K.; Terasawa, T.; Oda, Y.; Nakamura, K.; Tahara, D. Glass Transition Dynamics of Stacked Thin Polymer Films. *Phys. Rev. E* **2011**, *84*.

(193) Dalal, S. S.; Fakhraai, Z.; Ediger, M. D. High-Throughput Ellipsometric Characterization of Vapor-Deposited Indomethacin Glasses. *J. Phys. Chem. B* **2013**, *117*, 15415–15425.

(194) Sarangapani, P. S.; Schofield, A. B.; Zhu, Y. Relationship between Cooperative Motion and the Confinement Length Scale in Confined Colloidal Liquids. *Soft Matter* **2012**, *8*, 814–818.

(195) Kahle, O.; Wielsch, U.; Metzner, H.; Bauer, J.; Uhlig, C.; Zawatzki, C. Glass Transition Temperature and Thermal Expansion Behaviour of Polymer Films Investigated by Variable Temperature Spectroscopic Ellipsometry. *Thin Solid Films* **1998**, *313-314*, 803–807.

(196) Fukao, K.; Miyamoto, Y. Glass Transitions and Dynamics in Thin Polymer Films: Dielectric Relaxation of Thin Films of Polystyrene. *Phys. Rev. E* **2000**, *61*, 1743–1754.

(197) Miyazaki, T.; Nishida, K.; Kanaya, T. Contraction and Reexpansion of Polymer Thin Films. *Phys. Rev. E* **2004**, *69*, 022801.

(198) Inoue, R.; Kawashima, K.; Matsui, K.; Kanaya, T.; Nishida, K.; Matsuba, G.; Hino, M. Distributions of Glass-Transition Temperature and Thermal Expansivity in Multilayered Polystyrene Thin Films Studied by Neutron Reflectivity. *Phys. Rev. E* **2011**, *83*, 021801.

(199) Yang, C.; Takahashi, I. Broadening, No Broadening and Narrowing of Glass Transition of Supported Polystyrene Ultrathin Films Emerging under Ultraslow Temperature Variations. *Polym. J.* **2011**, *43*, 390–397.

(200) Gray, L. A. G.; Roth, C. B. Stability of Polymer Glasses Vitrified under Stress. *Soft Matter* **2014**, *10*, 1572–1578.

(201) Prevosto, D.; Capaccioli, S.; Ngai, K. L. Origins of the Two Simultaneous Mechanisms Causing Glass Transition Temperature Reductions in High Molecular Weight Freestanding Polymer Films. *J. Chem. Phys.* **2014**, *140*, 074903.

(202) Wu, X.; Liu, C.; Zhu, Z.; Ngai, K. L.; Wang, L. Nature of the Sub-Rouse Modes in the Glass−Rubber Transition Zone of Amorphous Polymers. *Macromolecules* **2011**, *44*, 3605–3610.

(203) Ediger, M. D.; Angell, C. A.; Nagel, S. R. Supercooled Liquids and Glasses. *J. Phys. Chem.* **1996**, *100*, 13200–13212.

(204) Paeng, K.; Richert, R.; Ediger, M. D. Molecular Mobility in Supported Thin Films of Polystyrene, Poly(methyl Methacrylate), and poly(2-Vinyl Pyridine) Probed by Dye Reorientation. *Soft Matter* **2012**, *8*, 819–826.

(205) Torres, J. M.; Stafford, C. M.; Vogt, B. D. Impact of Molecular Mass on the Elastic Modulus of Thin Polystyrene Films. *Polymer* **2010**, *51*, 4211–4217.

(206) Stafford, C. M.; Harrison, C.; Beers, K. L.; Karim, A.; Amis, E. J.; VanLandingham, M. R.; Kim, H.-C.; Volksen, W.; Miller, R. D.; Simonyi, E. E. A Buckling-Based Metrology for Measuring the Elastic Moduli of Polymeric Thin Films. *Nat. Mater.* **2004**, *3*, 545–550.

(207) Deng, H.-Y.; Li, R. N.; Huang, H.; Tsui, O. K. C.; Lam, C.-H. Power Spectral Density of Free-Standing Viscoelastic Films by Adiabatic Approximation. *Langmuir* **2013**, *29*, 4283–4289.

(208) Napolitano, S.; Capponi, S.; Vanroy, B. Glassy Dynamics of Soft Matter under 1D Confinement: How Irreversible Adsorption Affects Molecular Packing, Mobility Gradients and Orientational Polarization in Thin Films. *Eur. Phys. J. E. Soft Matter* **2013**, *36*, 61.

(209) Liu, D.; Osuna Orozco, R.; Wang, T. Deviations of the Glass Transition Temperature in Amorphous Conjugated Polymer Thin Films. *Phys. Rev. E* **2013**, *88*, 022601.

(210) Cangialosi, D. Dynamics and Thermodynamics of Polymer Glasses. *J. Phys. Condens. Matter* **2014**, *26*, 153101.

(211) Cangialosi, D.; Boucher, V. M.; Alegría, A.; Colmenero, J. Direct Evidence of Two Equilibration Mechanisms in Glassy Polymers. *Phys. Rev. Lett.* **2013**, *111*, 095701.

(212) Wang, J.; McKenna, G. B. A Novel Temperature-Step Method to Determine the Glass Transition Temperature of Ultrathin Polymer Films by Liquid Dewetting. *J. Polym. Sci. Part B Polym. Phys.* **2013**, *51*, 1343–1349.

(213) Boucher, V. M.; Cangialosi, D.; Alegría, A.; Colmenero, J. Enthalpy Recovery of Glassy Polymers: Dramatic Deviations from the Extrapolated Liquidlike Behavior. *Macromolecules* **2011**, *44*, 8333–8342.

(214) Tschoegl, N. W. *The Phenomenological Theory of Linear Viscoelastic Behavior*; Springer Berlin Heidelberg: Berlin, Heidelberg, 1989.

(215) Grassia, L.; D'Amore, A.; Simon, S. L. On the Viscoelastic Poisson's Ratio in Amorphous Polymers. *J. Rheol. (N. Y. N. Y).* **2010**, *54*, 1009–1022.

(216) Roland, C. M. *Viscoelastic Behavior of Rubbery Materials*; Oxford University Press, 2011.

(217) Meng, Y.; Simon, S. L. Pressure Relaxation of Polystyrene and Its Comparison to the Shear Response. *J. Polym. Sci. Part B Polym. Phys.* **2007**, *45*, 3375–3385.

(218) Meng, Y.; Bernazzani, P.; O'Connell, P. A.; McKenna, G. B.; Simon, S. L. A New Pressurizable Dilatometer for Measuring the Time-Dependent Bulk Modulus and Pressure-Volume-Temperature Properties of Polymeric Materials. *Rev. Sci. Instrum.* **2009**, *80*, 053903.

(219) Guo, J.; Grassia, L.; Simon, S. L. Bulk and Shear Rheology of a Symmetric Three-Arm Star Polystyrene. *J. Polym. Sci. Part B Polym. Phys.* **2012**, *50*, 1233–1244.

(220) Tschoegl, N.; Knauss, W.; Emri, I. Poisson's Ratio in Linear Viscoelasticity - A Critical Review. *Mech. Time-Dependent Mater.* **2002**, *6*, 3–51.

(221) Hilton, H. H. Clarifications of Certain Ambiguities and Failings of Poisson's Ratios in Linear Viscoelasticity. *J. Elast.* **2011**, *104*, 303–318.

(222) Hilton, H. H. The Elusive and Fickle Viscoelastic Poisson's Ratio and Its Relation to the Elastic-Viscoelastic Correspondence Principle. *J. Mech. Mater. Struct.* **2009**, *4*, 1341–1364.

(223) Lakes, R. S.; Wineman, A. On Poisson's Ratio in Linearly Viscoelastic Solids. *J. Elast.* **2006**, *85*, 45–63.

(224) Christensen, R. M. *Theory of Viscoelasticity*; 2nd ed.; Dover Publications: Mineola, 2003.

(225) Hieber, C. A. Assessment of Compliance and Stress-Relaxation Data for Polystyrene. *J. Rheol. (N. Y. N. Y).* **1999**, *43*, 967–976.

(226) Inoue, T.; Hayashihara, H.; Okamoto, H.; Osaki, K. Birefringence of Amorphous Polymers. II. Dynamic Measurement and Relaxation Measurement. *J. Polym. Sci. Part B Polym. Phys.* **1992**, *30*, 409–414.

(227) Shimo, T.; Nagasawa, M. Stress and Birefringence Relaxations of Noncrystalline Linear Polymer. *Macromolecules* **1992**, *25*, 5026–5029.

(228) Fujita, H.; Ninomiya, K. Dependence of Mechanical Relaxation Spectra of Linear Amorphous Polymers on the Distribution of Molecular Weights. *J. Polym. Sci.* **1957**, *24*, 233–260.

(229) Agarwal, P. K. Creep and Creep Recovery Behavior of Commercial Polystyrenes and Low Density Polyethylenes, University of Pittsburgh, 1975.

(230) Watanabe, H.; Yamada, N.; Okaji, M. Linear Thermal Expansion Coefficient of Silicon from 293 to 1000 K. *Int. J. Thermophys.* **2004**, *25*, 221–236.